Chapter 2

Experimental Techniques

Abstract:

In this chapter we will describe all general experimental procedures, setups and instrumental techniques (FTIR, XRD, ICP, Elemental analyses, TGA, BET, SEM, etc.) as well as electrochemical techniques), including the reagents used and the synthesis approach for each material under study.

2.1. REAGENTS

Aniline and pyrrole used for the synthesis of the hybrids where purchased from Aldrich and were purified by means of a distillation under reduced pressure, keeping them under nitrogen at 4°C. Sulfuric (H_2SO_4 96%), phosphoric (H_3PO_4 85%), hydrocholric (HCl 37%), and perchloric ($HClO_4$ 70%) acids were provided by Panreac and they were used according to product specifications. For the synthesis of vanadium pentoxide gel (which will be explained in detail below) we used a Dowex 50wx2-100 resin and sodium metavanadate (90% purity) purchased from Aldrich, used without further purification.

To elaborate the film cathodes, the reagents where dried according to the following procedures: Kinar-flex (binder agent, also known as PVDF polyvinylidene fluoride) provided by Elfatochem and super-P which is amorphous carbon (BET surface area of 60m^2/gr) provided by MMM Belgium were dried under vacuum for 24 hours at 40°C keeping them in a desiccator; acetone purchased from Panreac was dried using a molecular sieve of 0.5nm provided by Merck; finally, dibutyl phtalate (DBP) provided by Aldrich was used with no additional purification.

In order to elaborate anode films, we used graphite (1-2 microns) and metallic lithium ribbon (99.9%, 0.38mm thick) kept in a glove box under argon, both of them provided by Aldrich. The electrolyte used was Selectipur (Battery electrolyte) from Merck, composed of 1M $LiPF_6$ in EC: DMC = 1:1 (lithium hexafluorophosphate 1M in ethyl carbonate: dimethyl carbonate = 1:1,), which was kept in a dry box. Fiberglass membranes from Whatman GF/D were used as separators. They were dried in an oven at 100 °C for 48 hours before using them for the assembly of cells in the dry box.

Other reagents used according to product specifications were: 99% ammonium iron(II) sulfate hexahydrate from Aldrich (for V_2O_5 gel titration); potassium permanganate $KMnO_4$ and manganese sulfate hydrate $MnSO_4 \cdot H_2O$ from Panreac (for manganese hybrids synthesis), vanadium pentoxide V_2O_5 99.6% (used for $VOPO_4 \cdot 2H_2O$ ultrasound synthesis) from Aldrich, and potassium ferrocyanide (II) $K_3Fe(CN)_6 \cdot 3H_2O$ 99% also from Aldrich. Phosphomolybdic acid (PMo12), silicotungstic acid 99.9% (SiW12), and phosphotungstic acid (PW12) used for electrochemical supercapacitor electrodes, were purchased also from Aldrich.

2.2 SYNTHETIC TECHNIQUES

In order to prepare the different hybrids, we used different synthesis parameters depending on the system: PPy or PAni /MnO_2, PAni/V_2O_5, PAni or PPy triple hybrids ($Fe(CN)_6$-V_2O_5), PPy or PAni /$VOPO_4$, and PAni/ PMo12 (phosphomolybdate anion), PAni/SiW12 (silicotungstic anion) or PAni/PW12 (phosphotungstic anion) The detailed procedures for the synthesis of each particular hybrid will be presented in the corresponding chapters and we will give here only general synthetic approaches.

2.2.1 Chemical Syntheses of Hybrid Materials.

We carried out the chemical syntheses of the hybrid materials taking advantage of the oxidizing character of the inorganic compounds (V_2O_5 gel, $KMnO_4$ or MnO_2, $H_3Fe(CN)_6$, $VOPO_4{\cdot}2H_2O$); which allow to carry out "in situ" oxidative polymerizations of the organic monomers (aniline or pyrrole).

2.2.1.1. PAni/MnO_2 Hybrid synthesis

PAni/MnO_2 hybrid synthesis was carried out using oxidative polymerization of aniline in acidic media, using reaction mixtures with total volumes not larger than 70 ml, and we varied three experimental parameters with two levels each one, leading to four resulting experiments. We used permanganate ($AMnO_4$, A = K, H) as oxidizing agent for the preliminary experiments and also MnO_2. Manganese dioxide was prepared "in-situ", from manganese sulfate monohydrate ($MnSO_4.H_2O$) and potassium permanganate ($KMnO_4$). MnO_2 has a lower oxidizing potential than permanganate ion, which is nevertheless sufficient to induce aniline polymerization to polyaniline. In this case the doping anion is sulphate, which compensates the charge.

As we already mention we varied three parameters, which are: a) sulfuric acid concentration (H_2SO_4), b) amount of manganese permanganate ($KMnO_4$), and c) manganese sulfate monohydrate concentration ($MnSO_4.H_2O$). The remaining parameters were kept constant: 0.005 moles of aniline, 72 hours of reaction time, magnetic stirring at 500 rpm and 0 °C, and the order of addition of the reagents (solution of $KMnO_4$ to aniline-$MnSO_4$-H_2SO_4 mixture).

2.2.1.2. PPy/MnO_2 Hybrid Synthesis

The PPy/MnO_2 hybrid was synthesized using volumes not larger than 50 ml, and we carried out a modified experimental design of L_9 (3^3) from Taguchi's tables (see below)[1]. This design allows us to evaluate the three parameters and their levels (which are three in this case), in a simplified way with the minimum amount of experiments. The PPy/MnO_2 hybrid formation was carried out by means of an oxidative polymerization of pyrrole in acidic media. We used as an oxidant agent $KMnO_4$ that when in contact with pyrrole gets reduced to form the inorganic part of the hybrid (MnO_2); and pyrrole gets oxidized in presence of $KMnO_4$ and $HClO_4$, with the resulting MnO_2 as the inorganic phase and (ClO_4^-) as the doping counterion.

As we previously mention, PPy/MnO_2 hybrid synthesis was carried out by varying three parameters: a) concentration of perchloric acid ($HClO_4$), b)concentration of potassium permanganate ($KMnO_4$), and c) reaction time. We kept constant the amount of pyrrole (0.005moles), the magnetic stirring at 500 rpm, the temperature (0°C), and the order of addition of the reagents ($KMnO_4$ solution to pyrrol+$HClO_4$ solution).

2.2.1.3. PAni/V_2O_5 Hybrid Optimization.

PAni/V_2O_5 hybrids were prepared by the method described previously by Lira-Cantú [2]. The "in-situ" polymerization was carried out by adding aniline to the V_2O_5 gel, previously prepared by soft chemistry techniques (ion exchange and polymerization in acidic media) [2-5].

Once we obtained the V_2O_5 gel aged for at least one month, we proceeded with a potentiometric titration (section 2.4.1) in order to determine the amount of V(V) in the gel. V(V) is the responsible for aniline polymerization, therefore by knowing the concentration of V(V) in the gel it is possible to prepare an aniline solution with the appropriate concentration. In general, the synthesis procedure was carried out as follows: the aniline solution was added slowly and continuously (3 min.) to the $V_2O_5.H_2O$ gel (molar ratio aniline:V_2O_5, 3:1), at 0°C, and in principle with a reaction time of 120 hours. Based on this synthesis route, we carried out a study of the influence of the type and intensity of stirring applied during the synthesis and the reagents mixture upon the materials obtained and their performance in reversible lithium cells.

2.2.1.4. PPy/HCF/V_2O_5 Hybrid Synthesis

The synthesis of PPy/HCF/V_2O_5 hybrid was carried out by means of an "In-situ" oxidative polymerization of pyrrole, in a mixed solution of $H_3Fe(CN)_6$/V_2O_5 gel. We used two different inorganic oxidizing agents ($H_3Fe(CN)_6$ and V_2O_5 gel) that can react with pyrrole, to form the inorganic components of the hybrid ($[Fe(CN)_6]^{4-}$/V_2O_5), being at the same time the doping anions that compensate the positive charge of the conducting polymer.

PPy/HCF/V_2O_5 triple hybrid was synthesized by varying the molar ratio of the two inorganic reagents, keeping constant the amount of pyrrole (0.0144 moles/50ml), the magnetic stirring at 500 rpm, the temperature (0°C), a 30 min reaction time, and the order of addition of the reagents (pyrrole solution to $H_3Fe(CN)_6$/V_2O_5 gel solutions).

The V_2O_5 gel used for the synthesis was aged for at least one month and titrated for V(V) (section 2.4.1) right before the synthesis of the hybrid.

2.2.1.5. PAni/HCF/V_2O_5 Hybrid Synthesis

The synthesis of PAni/HCF/V_2O_5 triple hybrid was carried out by means of an "In-situ" oxidative polymerization of aniline, in the presence of $H_3Fe(CN)_6$ and V_2O_5 gel solutions. As for pyrrole, the two inorganic reagents oxidize aniline and get incorporated to the hybrid ($[Fe(CN)_6]^{4-}$/V_2O_5), compensating at the same time the positive charge of the conducting polyaniline.

The synthesis of PAni/HCF/V_2O_5 triple hybrid was optimized following several successive procedures involving the variation of the following parameters: molar ratio of the inorganic reagents, order of addition of the inorganic reagents, and a delay time between additions. Further details on these procedures will be given in Chapter 6. We kept constant the amount of aniline (1 ml in 50 ml), the magnetic stirring at 500 rpm, the temperature (0°C), and the volume solution of the inorganics (each a 50 ml).

The V_2O_5 gel used for the synthesis was aged for at least one month and titrated for V(V) (section 2.4.1) prior to use.

For the synthesis of triple hybrids (PAni or PPy/HCF/V_2O_5), we used volumes not larger than 150 ml and carried out a series of experiments varying the molar ratio of the reagents and the order of their addition.

2.2.1.6. PPy/$VOPO_4$ Hybrid synthesis

The synthesis of PPy/$VOPO_4$ hybrid was carried out by means of an oxidative polymerization of pyrrole in acidic media. In this case we used vanadyl phosphate ($VOPO_4 \cdot 2H_2O$) as the oxidizing agent, in perchloric acid media.

PPy/$VOPO_4$ hybrid was synthesized following several synthetic options which will be described in detail in Chapter 7. The following factors were studied and optimized: a) reaction time, b) order of addition of the reagents, c) concentration of acid ($HClO_4$), d) concentration of pyrrole.

2.2.1.7. PAni/$VOPO_4$ Hybrid synthesis

The synthesis of PAni/$VOPO_4$ hybrid was carried out by means of an oxidative polymerization of aniline in acidic media. We used vanadyl phosphate ($VOPO_4 \cdot 2H_2O$) as the oxidizing agent, in perchloric acid media

As for the polypyrrole derivative, several synthetic procedures were tested for the synthesis of PAni/$VOPO_4$ and the following experimental parameters optimized: a) order of addition of the reagents, b) concentration of acid ($HClO_4$), and c) concentration of aniline.

For PAni/$VOPO_4$ or PPy/$VOPO_4$ hybrids, the “in-situ” synthesis was carried out using volumes not larger than 100ml and we carried out several optimization procedures based on a few synthesis parameters.

The $VOPO_4 \cdot 2H_2O$ phase was in turn synthesized by a sonochemical technique for both hybrids (PAni or PPy/$VOPO_4$). We used vanadium pentoxide with an excess of H_3PO_4 in water, and let it react in an ultrasound bath for 3 hours.

2.2.2 Electrochemical Syntheses of Hybrid Materials

We carried out electrochemical syntheses of the molecular hybrid materials used as electrodes in electrochemical supercapacitors (PAni/PMo12, PAni/SiW12, PAni/PW12), using a cyclic voltammetry (CV) technique. In every case we used aqueous media (aniline+POMs), different scan rates and number of cycles; depending on the hybrid to synthesize.

We used a three electrode cell as shown in figure 2.2. The PAni/POMs hybrids used as electrodes in electrochemical supercapacitors were synthesized using a rigid graphite plate (99.95%) with a thickness of 0.25 mm as working electrode, and a platinum plate (99.9%) 0.1 mm thick as a counter electrode. Both electrodes were

purchased from Goodfellow. The syntheses were carried out by using an EG&G PAR 273A potensiostat/galvanostat, with an EG&G PAR 270 software, which is described in section 2.4.

On the other hand, when the PAni/POMs hybrids were used in the electrochemical supercapacitors as composite films (the capacitance given in F/g) we collected the synthesized material by scraping off from the working electrode (Pt plate). For these experiments a coil of Pt wire was used as counter electrode, and Ag/AgCl as reference electrode.

2.2.3 V_2O_5 Sol-Gel synthesis.

We have used a cation-exchange technique to synthesize $V_2O_5.nH_2O$ gel [6]. Thus, 5 g of sodium metavanadate ($NaVO_3$) was dissolved in approximately 75 ml of water at 80°C. When the solution cooled down we completed the volume up to 100 ml, and the solution was run through a column of Dowex 50wx2-100 cation-exchange resin. The colorless solution turned yellowish orange (typical color of metavanadic acid formation) when it gets in contact with the resin. Finally, we obtained a yellowish orange solution that was let aging for a minimum of one month, obtaining a dark red gel of $V_2O_5{\cdot}nH_2O$.

2.2.3.1 $V_2O_5{\cdot}nH_2O$ Xerogels

$V_2O_5{\cdot}nH_2O$ Xerogels were obtained from hydrogels prepared as described above except that a dynamic aging procedure was used (consisting of aging under continuous stirring for five days). We dried this gel at 100°C to obtain a dark red solid. We prepared different samples of xerogels applying thermal treatments under different atmospheres (O_2, Ar, Air), using a furnace by Carbolite Furnaces (model CSF 12/3) and a tubular furnace by Chesa.

2.3. CHEMICAL CHARACTERIZATION TECHNIQUES

We carried out different chemical analyses for the hybrid materials as part of their basic characterization. Elemental analysis was used to establish the percentages of carbon, nitrogen, hydrogen and sulfur. With atomic absorption analysis (AA) we determined the amount of manganese of the pre-treated manganese oxide hybrid

samples. Induced coupled plasma technique (ICP) was used to determine the percentage of phosphorus, vanadium, and iron.

2.3.1 Elemental Analysis.

Elemental analyses were carried out to determine the percentages of C, N, S and H in the hybrids (organic part), using an elemental analyzer Carlo Erba CHN EA 1108 at maximum combustion temperature of 1800^{o}C. Just before their analysis, samples were dried under vacuum for 3 days. These analyses were carried out at the Analysis Service of the Universitat Autònoma de Barcelona, and also at the Laboratories of the Scientific Services of the Universitat de Barcelona.

2.3.2 Atomic Absorption analysis (AA).

Atomic absorption analyses of manganese were carried out at the Laboratories of the Scientific Services of the Universitat de Barcelona, with a "Unicam PU 9200X" apparatus, with a deuterium corrector under standard conditions, calibrated with 5 standards prepared with 1% HNO_3. The manganese analyses were carried out for several PPy/MnO_2 hybrid samples, synthesized with different amounts of $KMnO_4$.

We first carried out a TGA analysis (4mg approximately) under air up to 500 ^{o}C for 5 h; in order to remove completely the organic mater in the samples. A certain amount of the residual solid (i.e. 1.4369 mg for 20ppm) was dissolved in $H_2O/H_2O_2/HNO_3$ (50/5/5 % volume), to yield a 20 ppm solution of manganese.

In addition, the weight loss from TGA corresponding to the organic mater can be correlated with the results of chemical analysis.

2.3.3 Analysis by Induced Coupled Plasma (ICP).

The V, P, and Fe analyses were carried out using a Thermo Jarrell-Ash model 61E Polyscan multichannel apparatus, under standard conditions at the Laboratories of the Scientific Services of the Universitat de Barcelona. Determination of Metals in the hybrids was carried out by digesting a known amount of the sample in acid at 220 ^{o}C in a pyrex tube with a condenser, evaporating to yield a volume of 2 ml. For the case of hybrids with P (PAni or PPy/$VOPO_4$), the digestion was carried out in acid using a microwave oven CEM Mars X in a high pressure quartz reactor QXP-1500. The volume, in both cases was completed to 100 ml with the addition of HCl (1%). Five patterns prepared with acid were used for calibration.

2.4 ELECTROCHEMICAL TECHNIQUES

We will describe next the several electrochemical techniques used for a variety of synthetic and characterization experiments, such as potentiometric titrations, electrochemical synthesis of hybrids, cycling experiments for the evaluation of hybrid materials as insertion cathodes in reversible batteries, or in electrochemical supercapacitors.

2.4.1 Potentiometric Titration.

We followed a routine potenciometric titration to analyze the V(V) concentration in $V_2O_5.nH_2O$ gel. The titration of each gel used for PAni/V_2O_5 and triple hybrids syntheses was carried out just before the synthesis, to adjust the desired amount of the corresponding monomers to the amount of V(V) on the aged gel. We dissolved 2 ml of gel in 20 ml of deionized water, and we carried out the titration with a solution of $Fe(NH_4)_2(SO_4)_2 \cdot 6H_2O$ (a precisely know amount of ca. 0.98 g in 100 ml of 0.25 M H_2SO_4). For a better detection of the inflection point, we added 1 ml of H_3PO_4 to the V_2O_5 solution. We used a combination electrode composed of a Pt wire combined with a Ag/AgCl cartridge electrode from Metrohm (used for redox titrations). We registered the potential change (mV), and by means of the derivative of the graph mV vs ml, we determined the inflection point and therefore the corresponding concentration of V(V) present in the gel. The concentrations varied from 0.10 to 0.18 M.

2.4.2 Cyclic Voltammetry Technique

We used an EG&G PAR 273A potensiostat/galvanostat, with an EG&G PAR 270 software as shown in figure 2.1.

The potenciostat/galvanostat is based on the control of the applied potential, Ea, or of the applied intensity, I, by varying the resistance value. In galvanostat mode, the system varies the resistance value in a way that the potential difference between the working electrode and reference electrode will provide the required intensity in the circuit between the working electrode and the counter electrode. In the potenciostat mode the resistance value varies in a way that the potential difference between the working electrode and the reference electrode, Ea, will be the one chosen in the program.

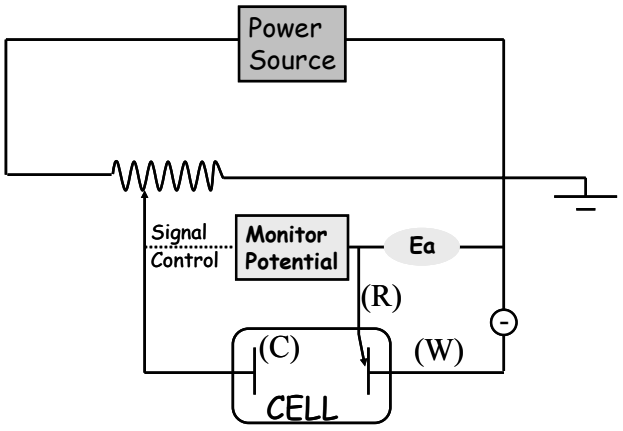

Figure 2.1.- Schematic representation of the Potenciostat/Galvanostate used. R is the reference electrode, C the counter electrode, and W the working electrode.

In figure 2.2 we show the three electrode electrochemical cell used for the synthesis of hybrids applied as electrodes in electrochemical supercapacitors (PAni/PMo12, PAni/SiW12, PAni/PW12). The electrodes that compose this three electrode cell are:

- The Reference electrode (RE) that we used was Ag/AgCl (0.197 vs. NHE) because we work in aqueous media..
- Working electrodes (WE). Active materials for supercapacitors were prepared electrochemically, both as thin film deposits and as thicker deposits for bulk (mass) characterization. For the first case, the Working electrode (WE) used was a rigid graphite plate (0.025 mm thick, 1.3x5 cm). One of the sides was covered and only a surface of 1.3x2.5 cm was exposed, as shown in figure 2.2. For bulk syntheses a a Pt sheet (0.01mm thick, 1.5x5 cm) was used as working electrode and the materials deposited were scrapped off.
- The Counter electrode (CE) used for the experiments dealing with thin film deposits consisted of a Pt sheet (0.01mm thick, 1.5x5 cm) whereas for the synthesis of bulk materials a Pt coil was used

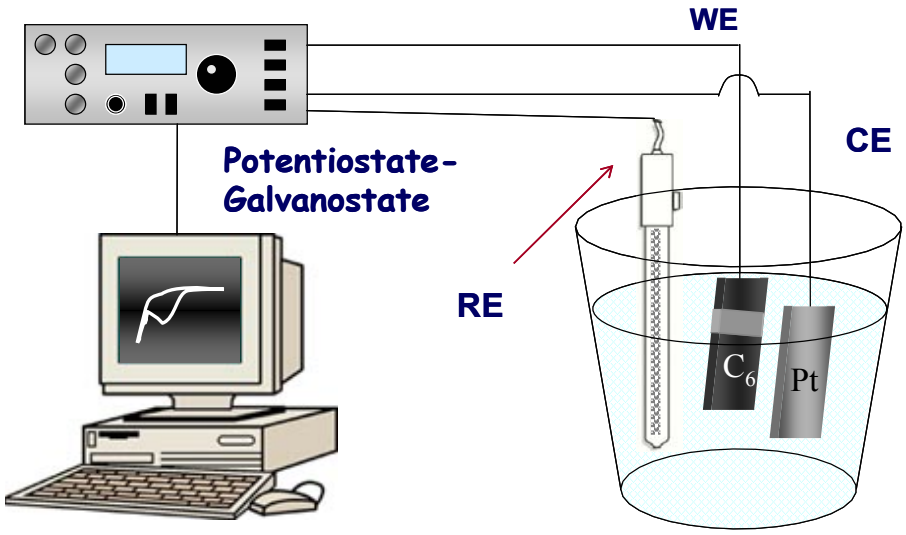

Figure 2.2.- Schematic representation of the three electrode cell setup used for the electrochemical synthesis of polyaniline-polyanions hybrids (electrodes used for the electrochemical capacitors).

We also carried out the electrochemical characterization of these PAni/POMs hybrids using the same three electrode cell setup with a 1M $HClO_4$ electrolyte solution. Using as working electrode the hybrid material deposited as thin film in the surface of the graphite plate, as counter electrode the Pt plate, and Ag/AgCl as the reference.

Finally we should note that, unless indicated otherwise (normally for Arbin output), our cyclic voltammograms are presented as obtained from the indicated potentiostats, following the American criterion for the sign of currents, i.e. positive current for reduction processes

2.4.3 *Rechargeable Lithium Cells and Electrochemical Supercapacitors.*

We carried out tests for the performance of the hybrid materials as cathodes in reversible lithium cells and as electrodes in electrochemical supercapacitors (ESCs) using Swagelok cells [7] presented in figure 2.3. As we describe in this figure, the cell is made of stainless steel when used as a lithium battery, with the inner walls of the cell isolated to avoid short circuits; and the Teflon joints serving as insulators between the current collector and the stainless steal support. Alternatively, Teflon Swagelok cells can be used to ensure electrically isolated cells

For the case of the tests in lithium batteries, we used current collectors of stainless steel for the hybrid and nickel for the lithium electrode; with maximum

working potentials ca. 3.6-3.8V. We used porous fiberglass separators (impregnated with electrolyte solutions) to prevent short circuits between the electrodes in the cell, keeping contact only by the electrolyte [8].

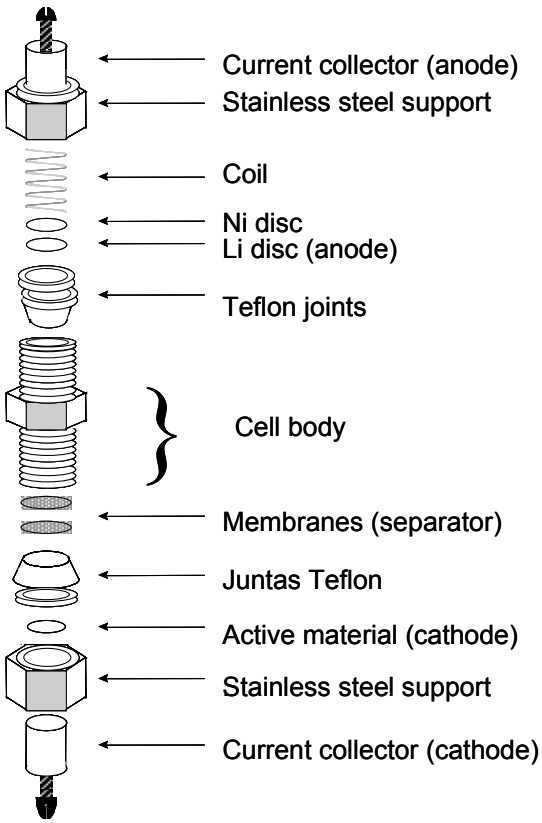

Fig. 2.3.- Swagelok support [8] use for the assembly of rechargeable lithium.

For the case of ESCs, we used stainless steel current collectors; and a polymer electrolyte membrane was used instead of a separator.

The reversible lithium cells and electrochemical supercapacitors analyses were made by means of charge-discharge cycles, using an ARBIN potenciostat-galvanostat model BT2042 with eight exit channels and three selectable current ranges for each individual channel: 1 A (High), 10 mA (Medium) and 100 μA (Low range). The computer-controlled system allows the automatic follow up and recording of the cell voltage, as well as the individual monitoring of anode or cathode potentials with respect to a reference electrode.

Figure 2.4 shows a schematic representation of the ARBIN analyzer. The apparatus is provided with four exit terminals to set up a three-electrode cell allowing the

measurement of potentials vs a given reference electrode. In all cases we just worked with two-electrode cells, thus, terminals 1 and 2 (figure 2.4), were connected to the current collector of the cathode under study and terminals 3 and 4 to the current collector of the anode (metallic lithium). For the electrochemical capacitors we just connected terminals 1 and 2 to one electrode and terminals 3 and 4 to the other electrode. In both cases the assembly only measures the potential difference between the electrodes.

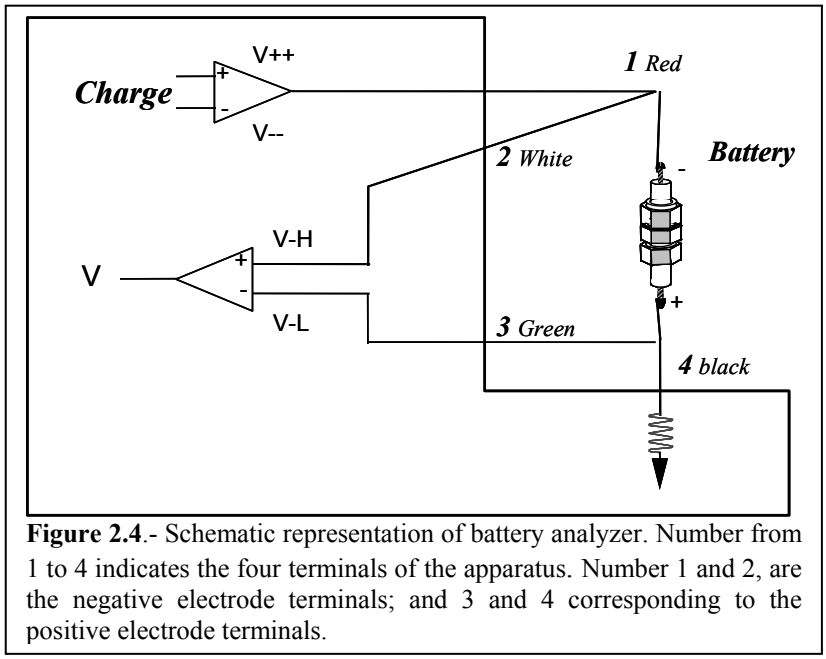

Figure 2.4.- Schematic representation of battery analyzer. Number from 1 to 4 indicates the four terminals of the apparatus. Number 1 and 2, are the negative electrode terminals; and 3 and 4 corresponding to the positive electrode terminals.

This apparatus permits the study of charge-discharge processes of the battery and ESCs by controlling different parameters as the intensity (I), voltage (V), Charge (Q) and the power (W) (figure 2.4). The control variables of the discharge process can be: current (I), voltage (V), time (t), charge (Q), current change (dI/dt), or voltage change (dV/dt). Our experiments were carried out under constant current conditions.

Finally, it should be noted that the ARBIN potentiostat yields data according to the European sign convention (i.e. positive currents for oxidation processes)

2.4.3.1 Electrodes

The anode used in lithium cells was a 13 mm diameter disc of metallic lithium, cut from a lithium ribbon from Aldrich (with a weight approximately to 0.03 g by disc). Cathodes were of two types, either powders or films. In the first case, the hybrid materials obtained were used in powder form to prepare composite electrodes (mixing

the active material with 30% weight of carbon Super-P. On the other hand, film cathodes were made by suspending 52% weight of the active hybrid material, 22% of Kinar flex (PVDF) as binder, and 24% of carbon super-P, and 3 drops of DBP in 2 ml of acetone. This suspension was thoroughly mixed by stirring for 12 hours to yield a homogeneous paste. The films were tape cast onto a glass surface letting the acetone evaporate. After peeling off the film it was washed twice with diethyl ether in order to remove DBP inducing in the film a porous microstructure. Discs of fiberglass membranes (Whatmman GF/D No.1823 070) were used as separators. We used a commercial Selectipur electrolyte from Merck that soaks the membranes. It is important to consider that for a correct operation of these lithium cells the absence of water is essential, therefore they were assembled inside a dry box.

In the case of ESCs all cells were symmetrical devices (i.e. with two identical electrodes). Initially we set up and measure hybrid electrodes prepared for convenience in the form of thin films on graphite substrates by means of cyclic voltammetry. Later on, in order to determine specific capacitance (normalized per unit mass), we devised a parallel CV synthesis on Pt in order to collect the material deposited, weigh it and prepare a composite film electrode with a well-known amount of active material.

For the characterization of thin film electrodes in ESC cells we cut 6x6 mm squares of the film on graphite. On the other hand, the active materials obtained as powders (scrapped off Pt electrodes) were treated as described above for the fabrication of microporous films (1 cm diameter discs) as those used in lithium cells.

A solid electrolyte membrane of commercial Nafion ® 117 (perfluorinated membrane, 12 mm diameter discs, 0.1778 mm thick) was used as separator and electrolyte membrane after impregnation with sulfuric acid. This impregnation was carried out following a standard procedure.[9] We washed the Nafion membrane in a hot solution of 1M sulfuric acid for 2 hours, washed with deionized water, and then treated it in a hot hydrogen peroxide solution (5%) for 1 hour. After treatment the membranes were washed and kept in deionized water until they were used.

2.4.3.2 Data Analysis. Working Conditions

We carried out the complete electrochemical analyses of reversible lithium cells on galvanostatic mode, using a constant current (I) for charge and discharge. The discharge rates used were in some cases calculated based on the expected specific charge for the material to analyze, using the following formula:

$$Q(Ah/Kg) = \{26.806 \cdot n \cdot m(mg)\} / FW \quad (1)$$

where m is the active mass of the material, and n is the number of electrons transferred by formula weight (FW). The constant 26.806Ah/mol, was obtained from Faraday's constant (96480 Coulombs) and transformed to ampere-hour (1C= 1/3600 Ah). From equation (1) we can obtain the theoretical specific charge in Ah/Kg, expected after a complete and ideal discharge of the material.

The speed of the charge/discharge processes is also an important parameter for the performance characterization of a material and a cell. It can be expressed in two main ways. One simply normalizes the current per unit weight (or area) (I=mA/g). This notation was also applied for the analyses of all electrochemical capacitors. The other convention (commonly used by the battery industry) refers to the number of hours needed for the complete discharge of the cell. This later mode relies on the use of the expected specific charge (Q, in equation (1)) which is divided by the number of intended discharge hours to calculate the current intensity to be applied. In this mode, a notation of C/6 rate indicates the discharge of the theoretical charge value over a period of 6 hours. Most of the experiments carried out here were performed with rates between C/6 and C/40.

We carried out calculations to obtain the capacitance of the ESCs, based on the time of discharge and charge of each cycle. The capacitance for each cycle was calculated according to the following formulas:

$$Q = It \quad \text{and} \quad C = Q/\Delta V \quad (2)$$

where I is the current density applied (mA/g or mA/cm^2) and t (seconds) is the time of charging or discharging, obtaining a charge Q (mC/cm^2 or mC/g). This specific charge Q is divided by the applied voltage range (ΔV) obtaining the corresponding capacitance (mF/cm^2 or mF/g). These series of calculations where made for each discharge-charge cycle.

2.5 OTHER PHYSICAL-CHEMICAL CHARACTERIZATION TECHNIQUES.

In this section we will explain the different physical-chemical characterization techniques and the analytical instruments and procedures that we used for the systematic characterization of our materials.

2.5.1 Scanning electron Microscopy (SEM).

We used a Hitachi S-570 microscope to analyze the morphology and microstructure of our materials. To assure a good conductivity samples were covered with gold (or graphite in cases where microanalysis was carried out). The materials were analyzed as powders (with no pressure) in order to measure the particle size, the agglomeration degree, and their effect on the electrode material characteristics.

2.5.2 BET Analyses.

BET method is based on the adsorption of nitrogen by solid materials, providing data in order to calculate the specific surface area, and the pore distribution in our PAni/V_2O_5 hybrids. The BET analyses relate the total volume adsorption at a certain relative pressure with the corresponding monolayer, in order to calculate the surface area. [10]

These analyses was carried out in a “Micrometrics ASAP 2000” BET apparatus over a well known weight of the hybrids. Before the adsorption of nitrogen, it was necessary to de-gas the hybrid samples with a vacuum treatment of 14 hours.

2.5.3 TGA Analyses.

In order to determine the amount of organic mater and hydration water in the hybrids and hydrogel, we used a Perkin Elmer TGA 7 balance; with a maximum sensibility of 0.1 μg under air, argon, or oxygen atmospheres. Before this analysis, the hybrid samples were dried out and washed with diethyl ether.

- Chemical composition study by means of thermogravimetry

A precisely known mass of the sample was heated in a controlled way in a thermobalance, while the change of weight is measured and registered. The traces obtained provide information on the thermal stability of the sample and the temperatures at which several dehydration/decomposition processes take place, whereas the percentage weight lost (or gained), provides useful information on the composition,

regarding organic and inorganic components. So, in our cases it is possible to obtain quantitative information on the amount of water or solvents, as well as the amount of inorganic matter (residue) present in our materials.

2.5.4. Fourier Transform Infrared spectroscopy (FTIR Spectroscopy).

Infrared spectroscopy analyses were carried out on pellets of the samples dispersed in dry KBr, using a Nicolet 710 FTIR spectrophotometer or a Perkin Elmer Spectrum one. The samples were dried under vacuum before making the pellets.

2.5.5 X-Ray Diffraction (XRD).

Two different powder diffractometers were used: a Rigaku with rotating anode, model "Rotaflex" Ru-200B with a secondary graphite monochromator, and a Siemens D500CD with a secondary graphite monochromator. The wavelength in both cases corresponded to Cu Kα (λ=1.5418 Å). The diffraction patterns were recorded between 4 and 60^{o} in 2θ.

2.5.6 Resistivity Measurements

Four probe Van der Pauw method was used to measure the resistivity at ambient temperature and calculate the conductivity of the samples. This method uses four contacts over pellets obtained under pressure, having any geometry, where the following characteristics need to be fulfilled:

- The contacts have to be placed on the sample circumference
- The contacts have to be very small
- The thickness of the sample has to be homogeneous
- The surface of the sample has to be totally interconnected.

The conductivity is calculated from the formula given below. In practice, we carried out numerous measurements, in order to get a correct result, due to the existence of parasitic tensions or possible inhomogeneities.

$$\sigma = 1 / (\pi d / 8\ln 2) \bullet [((R_{ab}-R_{ba})/I_{cd}) + ((R_{ad}-R_{da})/I_{bc}) +((R_{dc}-R_{cd})/I_{ab})+ ((R_{bc}-R_{cb})/I_{ad})] \bullet f [R_{ab,cd}/R_{bc,da}]$$

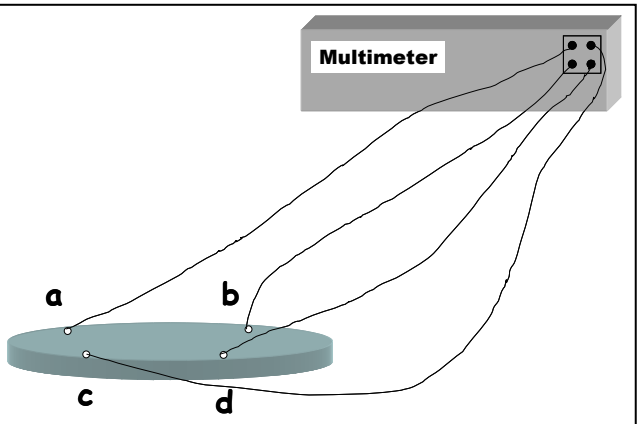

Figure 2.5.- Geometry and contact points, used in the Van de Pauw resistivity measurements.

For every test, two resistivities were measured corresponding to the direct and inverted current. In this way we eliminate the contribution of the thermoelectric potentials due to possible temperature gradients in the sample.

Assigning labels **a, b, c** and **d** to the four contacts**,** the method consists of measuring the resistance between **d** and **c**, when we apply a current between **a** and **b**; the resistance between **a** and **d**, when we apply a current between **b** and **c**; the resistance between **b** and **c**, when the current is applied between **a** and **d**; and finally the resistance between **a** and **b**, when the current is applied between **c** and **d**. Remembering that in each set of points, the current is applied in two directions. [11]

We have only carried out systematic measurements of the resistivities of the optimized $VOPO_4$ hybrids, using graphite paint to fix the contacts to the sample.

2.6 TAGUCHI'S EXPERIMENTAL DESIGN

Dr. Taguchi's method goes back to 1949, where he introduced concepts that allowed the improvement of the conventional experimental design efficiency. He used a series of basic concepts that permits a quicker analysis of the influence of the parameters on the system under study.

When a series of parameters determine the outcome of an experiment, all of which are assumed critical for the result, we can carry out a long series of experiments where each parameter is varied keeping the rest of them constant. However, even for a relative small number of parameters and their possible values, the combination matrix is too large. Taguchi's method approaches this problem by means of a tabulated selection of options (Taguchi's tables) in order to reduce the number of experiments that would result of the combination of all the factors and levels that influences over the system (affecting minimally the capacity to extract conclusions).

REFERENCES

[1] Taguchi, G.; Konichi, S.*; Arreglos Ortogonales y Gráficas Lineales: Herramientas para la Ingeniería de Calidad.*; 1ra. Ed.; ASI International; Monterrey N.L., **1991**.
[2] Lira Cantú, M.; *Materiales Híbridos Orgánico-Inorgánico a Base de Fosfomolibdato o Pentóxido de Vanadio Dispersos en Polímeros Orgánicos Conductores. Aplicación como Electrodos de Inserción en Baterías de Litio*.; Universitat Autònoma de Barcelona, Barcelona, **1997**, pp 244.
[3] Lira-Cantú, M.; Gómez-Romero, P.; *Int. J. of Inorg. Mat*. **1999**(1), 111.
[4] Lira-Cantú, M.; Gómez-Romero, P.; *Solid State Chem*. **1999**(147), 601.
[5] Lira-Cantú, M.; Gómez-Romero, P.; *J. Electrochem. Soc.* **1999**(146), 2029.
[6] Livaje, J., *Chem. Mater*. **1991**(3), 578.
[7] Guyomard, D.; Tarrascon; *J. Electrochem. Soc.* **1991**(139), 937.
[8] Gozdz, A.S.; *Rechargeable Lithium Intercalation battery with hybrid polymeric electrolyte*; Gozdz, A.S. Ed.; Bell Communications Research, Inc.; United States of America, **1994.**
[9] Savinell, R.; Yeager, E.; Tryk, D.; Landau, U.; Wainright, J.; Weng, D.; Lux, K.; Litt, M.; Rogers, C.; *J. Electrochem. Soc.***1994**(141), L46.
[10] Ruiz Paniego, A.; *Anales de Química* **1989**(85), 386.
[11] Van der Pauw, L.J.; Philip Res. Reports **1958**(13), 1.

Chapter 3

MnO_2 Hybrids

Abstract:

This chapter centers on MnO_2 hybrid materials and their possible application as electrodes in rechargeable lithium batteries. We have approached the study of these hybrids as an alternative to crystalline manganese oxides, which capacity is frequently limited by irreversible phase transitions. Furthermore, we have always followed the approach of simultaneous synthesis of the organic and inorganic components in an attempt to get nanocomposite materials. We present here our synthetic results on PAni/MnO_2 and PPy/MnO_2 and chemical, spectroscopic and electrochemical studies of the resulting materials. In the case of PAni derivatives our approach led to the isolation of PAni olygomers with no substantial amounts of MnO_2 . On the other hand, PPy/MnO_2 nanocomposite hybrids (essentially amorphous) were prepared by direct one-pot reaction of pyrrole and potassium permanganate, obtaining hybrids with different amounts of MnO_2. Hybrids with higher MnO_2 contents present greater specific capacities but worse cyclability.

3.1. INTRODUCTION

Manganese oxides are some of the most popular materials in electrodes for primary lithium batteries due to their great abundance, low cost, favorable charge density, high chemical and electrochemical stability, high discharge potential, and a low toxicity; which converts them into attractive materials, from an environmental point of view. Within the family of manganese oxides we can find manganese dioxide (we will refer to this oxide by its ideal formula, MnO_2 notwithstanding its complex chemistry and non-stoichiometry), which is an attractive material for non-aqueous lithium rechargeable cells, where their electrochemical properties strongly depend on the powder morphology and the crystalline structure. [1-5]

Before the 1990's a lot of work was carried out on MnO_2, even though not much was known about the lithium insertion mechanism [4]. According to Pistoia [6], many discrepancies existed regarding the behavior of manganese dioxide as a lithium insertion cathode due to the coexistence of diverse phases that make it a complex material. Probably the research carried out in the past, deals with mixtures of different phases and the materials under study differed from one case to another. Also it has been proven that the Mn_2O_3 phase formation is responsible for the detrimental behavior of these types of materials [6]. In the last 10 years different MnO_2 phases have been isolated and electrochemically characterized. [7-10]

Known phases of MnO_2 include β-MnO_2 (pyrolusite) and ramsdellite (MnO_2), which are relatively pure manganese dioxide; and α-MnO_2 (cryptomelane $KMn^{2.5+}{}_8O_{16}$), δ-MnO_2, γ-MnO_2 among others, which contain significant amounts of other ions as part of the integral structure. The structures can be described in terms of the specific arrangements of MnO_6 octahedra. Joining the octahedra in different ways leads to the different structural variations. In the case of β-MnO_2 (pyrolusite), the octahedra are connected by the corners forming simple chains. Parallel tunnels are present in cryptomelane (α-MnO_2 = $KMn^{2.5+}{}_8O_{16}$) and psilomelane (barium manganese oxide hydroxide), where other species can exist. δ-MnO_2 phase has a lamellar structure with layers of octahedra separated by alkaline ions or water. γ-MnO_2 is more commonly used as a cathode in dry batteries and it is considered a disordered intergrowth structure of ramsdellite and β-MnO_2 (pyrolusite). γ-MnO_2 is the phase that has reached importance in lithium batteries technologies. [11-13]

Electrolytic manganese dioxide (EMD) is a non-stochiometric compound that belongs to the γ-MnO_2 type. Its formula is $MnO_x(OH)_y$, $1.7<x<2$ [14]. One of the most critical characteristics of these non-stochiometric compounds is their oxygen contents. The lower the oxygen contents the more electrocatalytic activity the compound will have. The presence of OH^- has a significant role in the electrochemical behavior; its concentration determines the ionic conductivity; which affects the electrochemical process rate [9-11]. Surprisingly, an analysis of the literature seems to indicate that the manganese dioxides giving best results in lithium reversible cells are the ones that have a mixture of phases. Based on X ray diffraction analyses, it has been suggested that when MnO_2 is discharged, it is reduced to $Mn(III)O_2(Li^+)$ [3,6]. The initial potential of MnO_2 electrodes (which measures their electrochemical activity) depends on the Mn(III)/Mn(IV) ratio , which in turn depends on the synthesis method. The presence of Mn(III) in the same crystallographic position as Mn(IV), can be favored by protonation of the oxide giving way to OH^- ions. The protonation itself depends on the synthesis method. [10]

Frequently, the synthetic methods used to obtain the different MnO_2 phases are based on the decomposition of permanganate precursors ($LiMnO_4$, $NaMnO_4$, and $KMnO_4$). That decomposition has been carried out by different means, from conventional thermal or chemical methods to electrochemical, and, in the last 10 years to sol-gel methods. In this last case, problems arising from the lack of stable Mn(IV) precursors in aqueous solutions have been detected. [5,7,9]

In general, MnO_2 has a low electronic conductivity like most transition metal oxides; however, for good performance as a cathode the presence of a conducting network is necessary. Carbon can be used as a conducting additive, but the problem is reduced only to inter-granular conductivity thereby, and since carbon is not electroactive it results in a certain reduction of the effective energy density. Taking this into account, the introduction of a matrix that could provide enhanced conductivity and electrochemical activity would seem like a good idea. For that reason we approached the design of hybrid materials which could combine the active and inexpensive MnO_2 with electroactive and conducting organic polymers such as polyaniline or polypyrrole.

In this chapter we will describe the synthesis, characterization and the application in reversible Li cells, of hybrid materials based on non-stoichiometric manganese dioxide phases. We used anile and pyrrole as monomers to form

respectively, the polypyrrole-manganese dioxide (PPy/MnO_2) and polyaniline-manganese dioxide ($PAni/MnO_2$) hybrids.

When we began our work there were only few papers related to hybrids based on MnO_2 and polypyrrole as the conducting polymer, and only one patent regarding the use of polyaniline [15]. For the case of the hybrids with polypyrrole: one of them approaches the formation of the hybrid by means of injecting liquid pyrrole in an acidic solution of various crystalline MnO_2 phases previously formed[16]. Other approaches use an electrochemical polymerization of pyrrole in the presence of propylene carbonate, tetraethyl ammonium chloride, and different amounts of β-MnO_2 [17], and a few other papers have reported hybrids based on the spinel $LiMn_2O_4$.[18-20] For the case of Polyaniline hybrids, polyaniline has been used as a binder agent for manganese oxide electrodes. More recently, there have been other publications regarding polypyrrole as the conducting organic polymer. For instance, in one of them the authors use the same electropolymerization procedure of pyrrole in presence of β-MnO_2, as previously mentioned, but in aqueous solutions to show that PPy could be a polaron lattice [21]; and in the last one they prepare electrochemically the PPy/MnO_2 hybrid for its application as electrodes in electrochemical supercapacitors [22].

Our aim was to synthesize PPy/MnO_2 and $PAni/MnO_2$ hybrids by means of the simultaneous chemical synthesis of both components, in order to obtain real nanocomposite hybrid materials where the organic and inorganic parts are dispersed at a molecular level.

For a better comprehension of this chapter, we will divide it into two parts: 1) $PAni/MnO_2$ and 2) PPy/MnO_2.

3.2. $PAni/MnO_2$ HYBRID

The study of this new material is of great importance, because there is no precedent of a similar work. We will explain all the problems that we faced in order to synthesize this material, the corresponding characterization, and the performance as active cathodic material in lithium insertion cells.

3.2.1. PAni/MnO_2 Chemical Synthesis.

The general approach for synthesizing these hybrids made use of a redox reaction between an inorganic oxidizing manganese derivative and a monomer to oxidize (in this case aniline). Through this approach, we intended a simultaneous synthesis of the polyaniline in combination with the inorganic component. Initially, the most obvious choice of an oxidant to use in this reaction was the permanganate ion, which could directly yield MnO_2 when reacting with aniline. However, we faced multiple problems by using potassium permanganate. This is a very powerful oxidizing agent and led to the partial degradation of aniline before polyaniline could be formed. In this section we will explain all the preliminary experiments that we carried out in order to obtain this hybrid.

3.2.1.1. Preliminary Experiments.

We began by using Mn derivatives at their highest oxidation state. The most obvious was potassium permanganate, but we chose to do an ionic exchange of potassium by protons before the reaction, in order to obtain an acidic and oxidant reagent. A simultaneously acidic and oxidizing medium is precisely what is needed to polymerize aniline. The acid derivative of permanganate has been shown to be a very unstable species [5]. However, they have been previously used to obtain Li_xMnO_2 and Li_xMnO_4 phases, but not to synthesize hybrids [23,24]

We prepared an $HMnO_4$ solution by passing 100 ml of 0.41 M solution in deionized water of $KMnO_4$ through an ionic exchange resin (Dowex 50wx2-100). No color change was detected as the permanganate solution was eluted through the column (50 cm long and a 3 cm diameter, packed with 25 cm of resin). We recollected 250 ml of $HMnO_4$ solution. We observed with one day of aging, a color change from violet to the characteristic brown of Mn (IV). Our formed compound in principal is $HMnO_4$. Its known instability [5,24], is the reason why we made it one day before the hybrid synthesis.

The hybrid synthesis was carried out according to the next procedure: we prepared 50 ml of a 0.01M solution of aniline in water and poured them into a 250 ml Erlenmeyer in an ice bath. We added the $HMnO_4$ solution (34 ml of the ion-exchanged solution obtained as described above plus 16 ml of water) dropwise and with magnetic stirring for 20 minutes. After 24 hours of reaction time, we filtered, washed with water

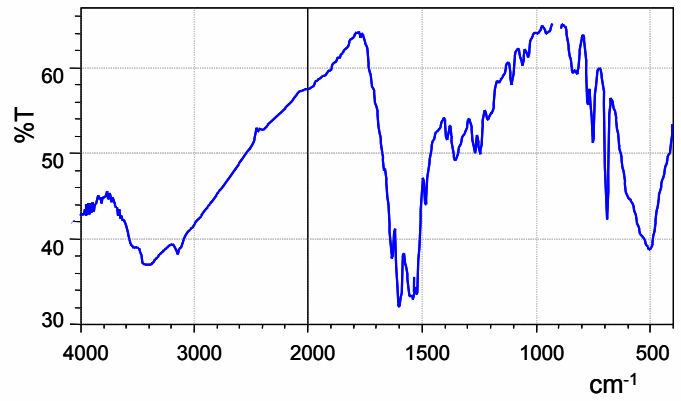

Figure 3.1. FTIR spectrum of PAni/MnO_2 derivatives, synthesized with aniline and $HMnO_4$ (prepared by ionic exchange).

and dried the solid obtained under vacuum at room temperature. In this reaction the nominal aniline:$HMnO_4$ ratio was of 3:1.

We carried out an FTIR spectrum of this solid (figure 3.1). Instead of the typical bands of polyaniline this spectrum shows multiple peaks overlapping between 1500 and 1650cm^{-1}. We cannot rule out the presence of several products, among them unreacted aniline, nitrobenzene (decomposition byproduct), azobenzene (known product when oxidizing aniline with solvent free $KMnO_4$) [25], and/or polyaniline olygomers. On the other hand, this spectrum shows some significant resemblance to spectra reported for aniline olygomers published previously as part of a study on polyaniline and derivatives [26]. Relevant peaks were detected at 700 cm^{-1}, 750 cm^{-1}, and 810 cm^{-1}, and were assigned to olygomers of 2-16 monomer units.[15]

In an attempt to avoid the impurities obtained above, we carried out an alternative synthetic procedure avoiding the ion exchange column and simply using a mild acidic medium. In this conventional synthesis, the oxidative polymerization was carried out using an acid ($HClO_4$) and an oxidant ($KMnO_4$). The parameters that varied were: the amount of $HClO_4$, the amount of $KMnO_4$, and the reaction time. The parameters kept constant were: the amount of aniline (0.05 moles in 25 ml of water), reaction temperature (0^oC ice bath) and the use of magnetic stirring. In order to reduce the number of experiments and estimate the influence of each parameter in the synthesis, we carried out a modified experimental design $L_9(3^3)$ of Taguchi's tables [27].In table III.I we exhibit the resulting nine experiments.

The amounts of $KMnO_4$ were selected based on previous experiments. We used a molar ratio of aniline to permanganate of 1:1. In table III.I, we show the experiments performed.

Table III.I.-Modified Taguchi experimental design $L_9(3^3)$, for the optimal parameter evaluation in the PAni/MnO_2 hybrid synthesis.

Sample	$HClO_4$ in 25ml H_2O	$KMnO_4$ in 20 ml H_2O	Time (h)
MnPa1	0.005 moles	0.0025 moles	1
MnPa2	0.005 moles	0.0015 moles	3
MnPa3	0.005 moles	0.001 moles	5
MnPa4	0.00375 moles	0.0025 moles	3
MnPa5	0.00375 moles	0.0015 moles	5
MnPa6	0.00375 moles	0.001 moles	1
MnPa7	0.0025 moles	0.0025 moles	5
MnPa8	0.0025 moles	0.0015 moles	1
MnPa9	0.0025 moles	0.001 moles	3

FTIR analyses were carried out to detect the possible formation of aniline derivatives. But again, what we generally could detect on the FTIR spectra was the presence of a mixture of olygomers [26]. In figure 3.2, we show the FTIR spectrum of sample MnPa9 which is representative of the rest of the samples differing in the amount of manganese dioxide.

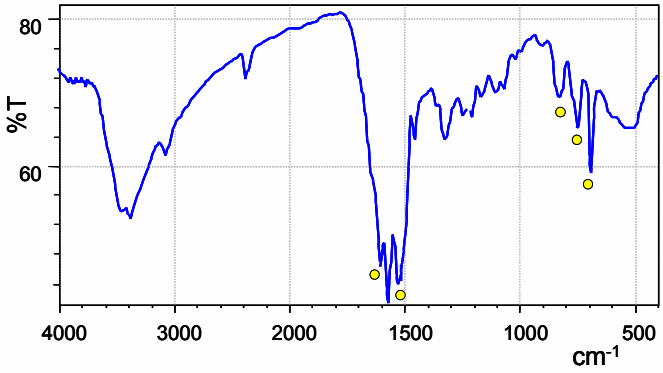

Figure 3.2.- FTIR spectrum of sample MnPa9 synthesized with aniline, $HClO_4$ and $KMnO_4$, which is very representative of the rest of the hybrid samples. The circles mark vibrational modes assigned to polyaniline olygomers.

In order to avoid improductive aniline overoxidation and the formation of olygomers, we considered the use of a reagent less oxidant than permanganate. MnO_2 itself was a good candidate since it contains Mn(IV). In order to maintain our

objectives of an "in-situ" simultaneous formation of the polymer and the oxide MnO_2, we decided to test a reaction where the oxide would be generated "in-situ". The simpler way was to react permanganate with a Mn(II) salt.

We used $MnSO_4 \cdot H_2O$ as Mn (II) source, and instead of using perchloric acid ($HClO_4$) we used sulfuric acid (H_2SO_4) in order to minimize the number of counterions. For the synthesis of the hybrids, we carried out two preliminary experiments to evaluate the convenience of using sulfuric acid. One experiment was done with acid (MPca), and the other one without acid (MPsa). We used the same amount of aniline as before (50 ml of a 0.01M), a temperature of 0^oC, magnetic stirring and a 20 hour reaction time for both experiments. The total amount of Mn(IV), to be generated by means of the reaction shown below [28], was of 0.0025 moles (ratio MnO_2 : aniline 5:1)

$$3Mn^{+2} + 2MnO_4^{-1} + 2H_2O \longrightarrow 5MnO_2 + 4H^+$$

In accordance to the MnO_4^-/Mn^{+2} ratio of 2:3, we used 0.001 moles of $KMnO_4$ gauged up to 20 ml of deionized water, and 0.0015 moles of $MnSO_4 \cdot H_2O$ gauged to 25 ml.

The FTIR spectra of the two materials obtained (figure 3.3) show significant differences. Only the spectrum of the hybrid obtained with acid presents peaks characteristic of aniline polymerization (peaks between 1000 and 1600 cm^{-1}). However, the spectrum is not exactly the one expected for conventional polyaniline with long-chain polymerization but resembles more closely that previously reported for olygomeric units. In this respect, the three peaks between 800-700 cm^{-1} are specially significant and constitute a good fingerprint for polyaniline olygomers [26].The FTIR spectrum for MnO_2 prepared under the same conditions as sample PMca, but without aniline (Fig 3.4) rules out the possibility of this triplet being associated to the MnO_2 phase.

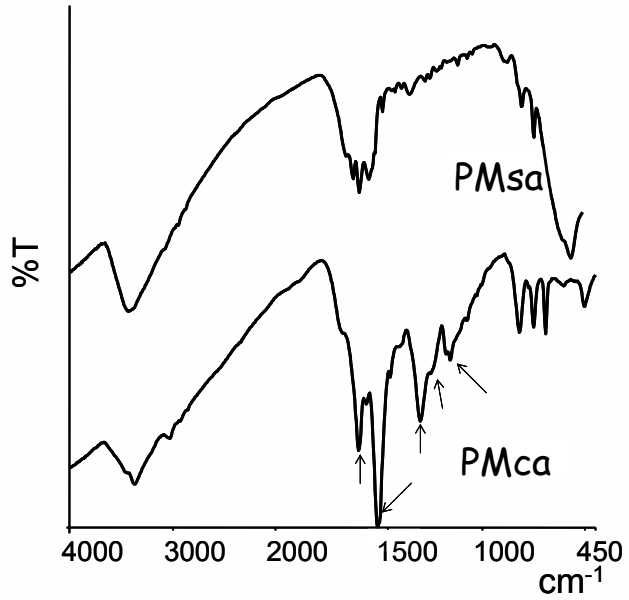

Figure 3.3.- FTIR spectra of samples PMsa and PMca, synthesized by means of aniline reaction with MnO_2, generated in-situ by reaction of permanganate and Mn(II). The arrows indicate the vibrational modes of polyaniline

On the other hand, we can note the great difference of intensity of the peak at 500 cm^{-1}, assigned to MnO_2 on the FTIR spectra of samples PMca and PMsa (figure 3.3). That peak is clearly present when no acid is used, indicating a significant amount of MnO_2 whereas is dubiously present in the material obtained with acid.

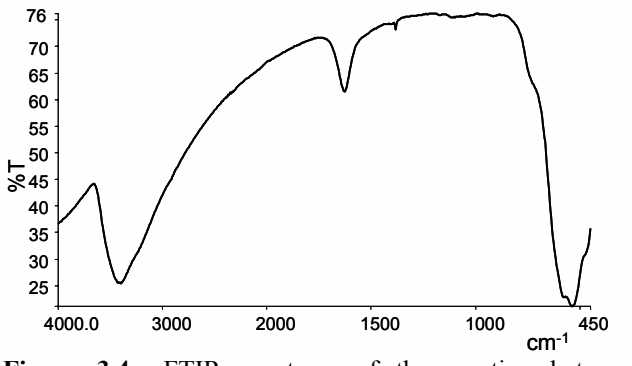

Figure 3.4.- FTIR spectrum of the reaction between $MnSO_4 \cdot H_2O$ and $KMnO_4$, with same conditions as for sample PMca.

3.2.1.2. *Chemical Synthesis*

After the preliminary tests described above, we varied the amount of $KMnO_4$, $MnSO_4 \cdot H_2O$, and of H_2SO_4. The other factors remained constant (T=0°C, t= 72hrs, 0.005 moles of Aniline, the addition of $KMnO_4$ to Ani/$MnSO_4 \cdot H_2O$/H_2SO_4 solution, and magnetic stirring at 500rpm). We modified the reaction time, increasing it in order to attempt to incorporate more manganese dioxide in the final product and to attain longer polyaniline chains. We designed four different experiments, which are indicated on table III.II.

Table III.II.- Design of the four experiments in order to obtain the PAni/MnO_2 hybrid, from a reaction between aniline and in situ MnO_2 (by reaction of permanganate and Mn(II)).

Sample	$KMnO_4$ in 20 ml	$MnSO_4.H_2O$ in 25ml	H_2SO_4
MP1	0.001 moles	0.0015 moles	0.0025 moles
MP2	0.0012 moles	0.0015 moles	0.0025 moles
MP3	0.001 moles	0.0018 moles	0.0025 moles
MP4	0.001 moles	0.0015 moles	0.003 moles

We can detect very minor differences between the FTIR spectra in these four samples (Figure 3.5). In general terms all of them correspond well to the spectrum of olygomeric polyemeraldine [26], and furthermore, somewhat surprising, their spectra show no evidence of MnO_2 (the small peak at ca. 500 cm^{-1} can also be assigned to the olygomers).

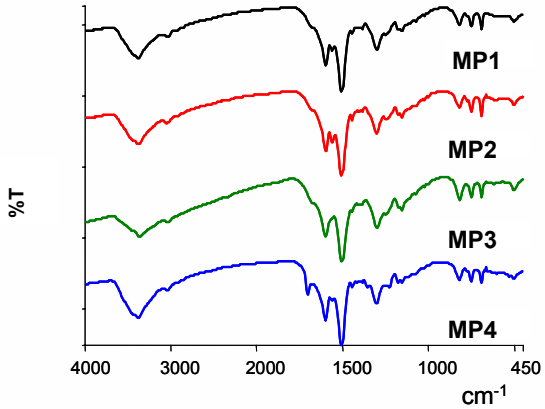

Figure 3.5.- FTIR spectra of samples MP1, MP2, MP3, and MP4 obtain by reaction of aniline with in situ MnO_2

3.2.2. Characterization of Materials from PAni/MnO_2 reactions.

In this section we will discuss the detailed characterization of the four samples of PAni/MnO_2 reaction products (MP1, MP2, MP3, y MP4) by means of several spectroscopic and analytical techniques, in order to determine the final stoichiometry and their formula weight.

But first we will describe a few attempts to extract and separate the possible different components forming these samples. This extraction experiments were decided in view of the olygomeric nature and consequent low molecular weight of the materials obtained, which prompted us to determine their possible solubility.

3.2.2.1. Extraction experiments

The samples obtained in the preceding section were indeed partially soluble in diethyl ether. The portions soluble were always strongly colored with tones ranging from orange to red depending on the concentration of the species extracted. The extraction procedure was as follows: After vacuum-drying the hybrid samples, we washed the solids with ethyl ether until no typical red coloration appeared. We evaporated the solvent at room temperature from this solution, obtaining a dark solid. This solid was analyzed by FTIR diluted in KBr pellets.

In figure 3.6, we present the FTIR spectrum of one of these solids extracted from a solution of MP1 in ethyl ether. In figure 3.7 we show the FTIR spectrum of the insoluble portion of sample MP1 after

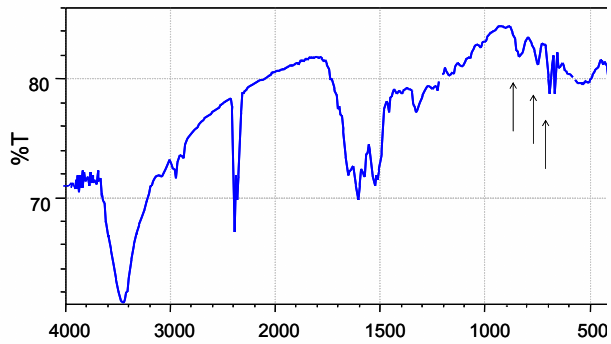

Figure3.6.-FTIR spectrum of the solid extracted from PAni/MnO_2 hybrid of sample MP1. The position of the peaks marked correspond to the characteristic olygomer spectrum

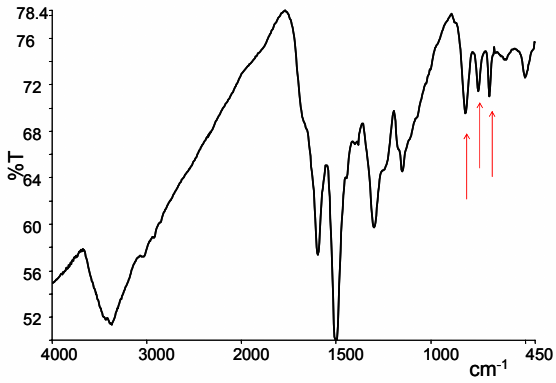

Figure 3.7.- FTIR spectrum of sample MP1 washed with ethylic ether. The intensity and position of the marked triplet of vibrational modes belongs to olygomers of 16 units of aniline.

extraction with ethyl ether. Comparing the spectra from figure 3.6 and 3.7, we can say that the insoluble portion of the hybrid sample is just composed of olygomeric species. Indeed, the whole spectrum in general and the relative intensities of the triplet peaks are identical to those of the 16-mer polyemeraldine olygomer.[26] On the other hand, the spectrum in figure 3.6 also shows a characteristic triplet, indicating the presence of olygomers, most likely of lower molecular weight. However, the complex overlap of peaks in the region between 1400 and 1700 cm-1 indicates the presence of other soluble species probably corresponding to impurities derived from oxidation products of aniline not leading to polymerization.

3.2.2.2. *Stoichiometry and formula weight of PAni/MnO_2 derivatives.*

In order to determine the stoichiometry and formula weight of our materials, we first washed them with ether until no coloration remained in the filtrate (elimination of soluble species) as detailed above. We then proceeded with a TGA analysis of the solid residue to obtain the percentage of inorganic matter (i.e. HSO_4^-, MnO_2), and the percentage of water and organic matter. On the other hand, with elemental analysis we were able to find the composition of the organic part and the doping level with HSO_4^-. Through the combination of the TGA and elemental analysis we obtained the hydration degree, and the inorganic fraction for each sample. With these analyses we determined the stoichiometry and the approximate formula weight of the different derivatives.

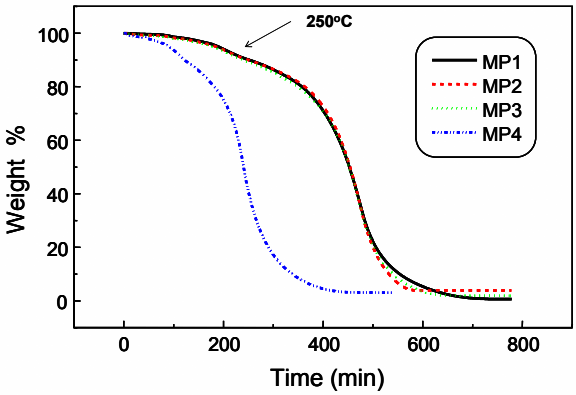

Figure 3.8.- TGA analysis of the four PAni/MnO_2 samples: MP1, MP2, MP3 and MP4. The heating rate used for the first three samples was 1°C/min; and for sample MP4, 2°C/min. We have represented in the abscissa axis the time instead of the temperature, in order to appreciate the 500°C isotherm

3.2.2.2.1. *Thermogravimetric analysis (TGA)*

The samples previously washed with ethyl ether were analyzed by TGA to determine the percentages of organic matter and hydration water, and inorganic matter. The samples were heated in air up to 500°C at a rate of 1°C/min (except sample MP4, where we used a 2°C/min rate).

N.B. We chose this slow

heating rate as a precaution, because, in principle, manganese dioxide could react violently with organic matter. Fortunately, under the described conditions, the reactions remained under control.

Figure 3.8 shows the corresponding traces. There are several features worth discussing. First, the loss of water is barely separated from the main loss of organic matter by a slight inflection point at ca. 250ºC. Most importantly, in all four samples (MP1, MP2, MP3 and MP4) the weight loss is almost complete at the end of the experiment. The residual weights range from 1 to 6% (see Table III.III), which means very minor contents of inorganic matter , a result which is in very good agreement with the FTIR analyses on these compounds. For this reason, we deemed it unnecessary to carry out an atomic absorption analysis, but instead we carried out an FTIR spectrum in dillute KBr pellets. We only detected small bands atributed to the presence of sulphate. This is in good agreement with the low values from S analyses for our materials (see below) and indicates that the 16-mer polyemeraldine olygomer is minimally doped with HSO_4^- anions. In table III.III, we summarize the quantitative data of inorganic matter, and organic matter + water.

Table III.III.- Summarized data obtain from TGA, of the inorganic part and the organic part + water, of PAni/MnO_2 samples.

Sample	% Inorganic matter	% H2O + organic matter
MP1	1	99
MP2	6	94
MP3	4.8	95.2
MP4	4.8	95.2

3.2.2.2.2. Elemental Analysis

The data obtained from elemental analysis helped us to confirm the percentage of organic matter present in the hybrids and the doping level with HSO_4^- anions allowing to establish their composition. The data from these analyses are complementary to TGA analysis in trying to determine the stoichiometry of these compounds. Once we established the polymer composition and calculated the percentage of polyaniline (by difference with the percentage from TGA), we obtained the amount of hydration water and therefore, we could calculate the stoichiometry of each compound.

Table III.IV summarizes the experimental data obtained from elemental analysis of C, H, N, S and compares those values with the ones calculated for the proposed formulas. In view of these and FTIR results, the possible presence of MnO_2 in these samples could only be in the form of traces.

Table III.IV.- Experimental composition from elemental analyses and calculated values for the formula indicated.

	An:Mn^{+2}:Mn^{+7}	%C	%N	%H	%S	Formula
MP1	(5 : 1.5 : 1)					$(C_6H_5N)_{16}[HSO_4^-]_{0.22}11H_2O$
Exp.		68.9	12.0	4.5	0.41	
Calc.		68.74	13.36	1.37	0.42	
MP2	(5 : 1.5 : 1.2)					$(C_6H_5N)_{16}[HSO_4^-]_{0.44}13H_2O$
Exp.		66.5	11.4	4.6	0.81	
Calc.		66.47	12.91	1.55	0.81	
MP3	(5 : 1.8 : 1)					$(C_6H_5N)_{16}[HSO_4^-]_{0.16}14H_2O$
Exp.		66.6	11.3	4.4	0.29	
Calc.		66.82	12.98	1.68	0.29	
MP4	(5 : 1.5 : 1)					$(C_6H_5N)_{16}[HSO_4^-]_{0.25}12H_2O$
Exp.		67.6	11.7	4.6	0.47	
Calc.		67.89	13.19	1.47	0.47	

3.2.3. Study as cathodes in reversible Li cells.

After drying these derivatives under vacuum for three days, we used them as active materials in lithium insertion cathodes. They were mixed with carbon super P at a ratio of 70:30% weight, obtaining a powder composite cathode. The charge-discharge cycles were carried out by using a current density of I = 4 mA/g (slow rate), at a voltage range between 2-3V. In figure 3.9 we present the specific charge of the first cycle of these olygomeric PAni samples. The results were relatively poor; because in general the specific charge was very low compared to hybrid materials [16,17,29]. Sample MP2 is one of the best results along with sample MP1, having specific charges of 32 Ah/g and 30 Ah/g respectively.

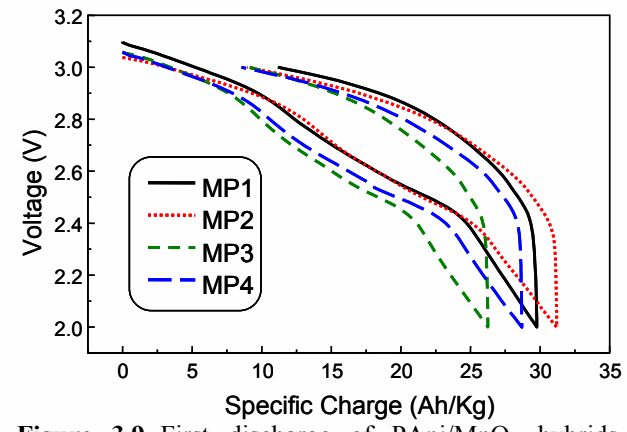

Figure 3.9.-First discharge of PAni/MnO_2 hybrids, using a discharge density current of I = 4mA/g.

3.3. PPy/MnO_2 HYBRIDS

Physical mixtures of polypyrrole and manganese dioxide, as we have previously mentioned, have been used as composite electrodes for rechargeable lithium batteries [16] and supercapacitors [22]. In most cases, these mixtures have been carried out with each of the compounds synthesized separately. Only in a couple of cases, the polymerization of pyrrole was carried out electrochemically in the presence of MnO_2 [16,17], whereas in all cases, MnO_2 itself was previously synthesized as a crystalline phase. The synthesis that we propose here, is an in-situ reaction between pyrrole and a Mn(VII) precursor such as $KMnO_4$, in the presence of acid. The objective is to produce hybrid materials where the organic and inorganic components are truly dispersed at a molecular level.

First we will discuss the chemical synthesis of PPy/MnO_2 hybrid, as well as the corresponding characterization, and finally their performance as a nanocomposite active cathode material in insertion lithium cells.

3.3.1. PPy/MnO_2 hybrid synthesis.

As we have already discussed, the acid derivative of permanganate ion ($HMnO_4$) is too oxidant and unstable. Taking into account that pyrrole monomer is easier to oxidize than aniline, and that it easily can give way to undesirable derivatives (by an oxidative addition process), we decided to use an alternative synthesis method. On this synthesis, the acid and the oxidant were added separately.

We used a constant amount of pyrrole (0.005 moles in 25 ml deionized water), varying the concentration of perchloric acid (always 25ml $HClO_4$), $KMnO_4$ (20ml) and the reaction time; obtaining a modified experiment design $L_9(3^3)$ of the Taguchi tables. The resulting 9 experiments were carried out to evaluate the parameter influence [27]. The parameters that remained unchanged were: reaction in an ice bath with magnetic stirring, and the addition order of the reagents ($KMnO_4$ was added to the mixture of pyrrole+$HClO_4$). The total reaction volume was 70 ml. In the following table (III.V), we summarize the 9 design experiments.

The solutions indicated were mixed dropwise (in ca. three minutes) and left stirring for the time indicated. The solid formed was filtered off, washed with abundant water, and dried under vacuum for three days. The results of this series of synthesis was followed up by means of FTIR spectroscopy (described in detail below), which

showed the simultaneous presence of polypyrrole and MnO_2 in 6 out of the 9 products isolated (hybrids MnPy1 MnPy4, MnPy5, MnPy7, MnPy8, and MnPy9)

Table III.V.- Taguchi's modified experiment design $L_9(3^3)$, to evaluate the optimum synthesis parameters of PPy/MnO_2 hybrids.

First series.	$HClO_4$/25 ml	$KMnO_4$/20 ml	Ratio $HClO_4/MnO_4$	Rxn. time (min)
MnPy1	0.005 moles	0.0025 moles	2:1	5
MnPy2	0.005 moles	0.0015 moles	3.33:1	10
MnPy3	0.005 moles	0.001 moles	5:1	30
MnPy4	0.00375 moles	0.0025 moles	1.5:1	10
MnPy5	0.00375 moles	0.0015 moles	2.5:1	30
MnPy6	0.00375 moles	0.001 moles	3.75:1	5
MnPy7	0.0025 moles	0.0025 moles	1:1	30
MnPy8	0.0025 moles	0.0015 moles	1.66:1	5
MnPy9	0.0025 moles	0.001 moles	2.5:1	10

From Table III.V (first series) we can clearly deduce how the three samples which did not yield the desired hybrids (MnPy2, MnPy3 and MnPy6) are those with a higher $HClO_4/MnO_4^-$ ratio. More specifically we could conclude that a $HClO_4/MnO_4^-$ ratio lower than or equal to 2.5:1 is necessary for obtaining the hybrid.

Taking into account this conclussion, we synthesized four additional samples (MnPy10, MnPy11, MnPy12 and MnPy13) with even lower $HClO_4$:$KMnO_4$ ratios (Table III.VI, second series). In this way, we were using more $KMnO_4$ in the reaction mixture in order to obtain more MnO_2 in the PPy/MnO_2 hybrid.

Table III.VI.-Experiments with more amount of initial $KMnO_4$.

Second series	$HClO_4$/25 ml	$KMnO_4$/20 ml	RATIO $HClO_4/Mn$	rxn Time (min)
MnPy10	0.0025 moles	0.00375 moles	0.66:1	30
MnPy11	0.0025 moles	0.005 moles	0.50:1	30
MnPy12	0.0025 moles	0.00625 moles	0.40:1	30
MnPy13	0.0025 moles	0.0075 moles	0.33:1	30

3.3.2. PPy/MnO_2 characterization.

In this section, we describe how different characterization methods have helped us to determine the PPy/MnO_2 hybrid formation, the stoichiometry of the organic and inorganic part, and thus to calculate the formula weights.

The characterization methods used were FTIR, TGA, elemental analysis, and atomic absorption techniques. In figure 3.10, we show the powder XRD of sample MnPy4 (representative of all samples) which features very broad weak peaks as it could be expected for an almost amorphous phase.

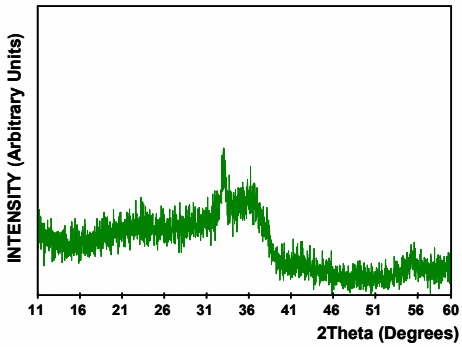

Figure 3.10.- Powder XRD of sample MnPy4, which is amourphous representative of all PPy/MnO_2 hybrid samples

3.3.2.1. FTIR

We have used this technique to check if the polypyrrole in the hybrid materials of table III.V (first series) and III.VI (second series) were formed. In figure 3.11 we show the infrared spectra of the samples synthesized following the experimental design of table III.V (first series), and in figure 3.12 the ones corresponding to the second series, synthesized with larger amounts of $KMnO_4$ (table III.VI). We can observe peaks that correspond to MnO_2 and polypyrrole, thus confirming the formation of the hybrid PPy/MnO_2 in most cases.

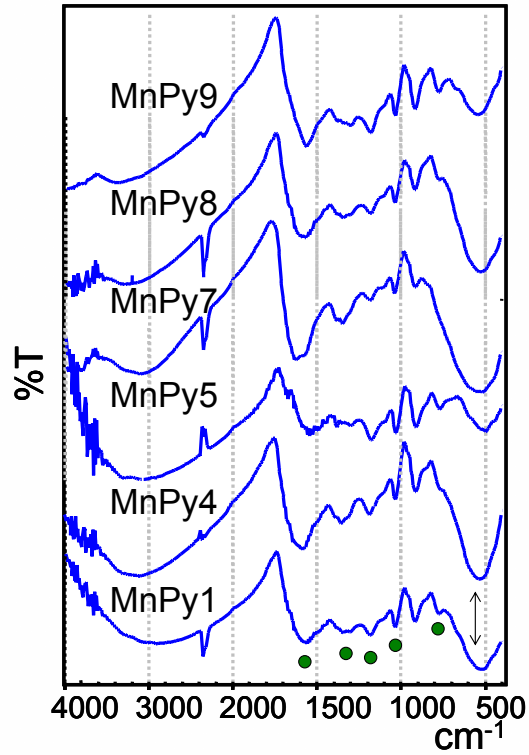

Figure 3.11.- FTIR spectra of synthesized PPy/MnO_2 hybrid samples from table III.VI. where the dots represent the vibrational modes of polypyrrole and the arrow Mn-O.

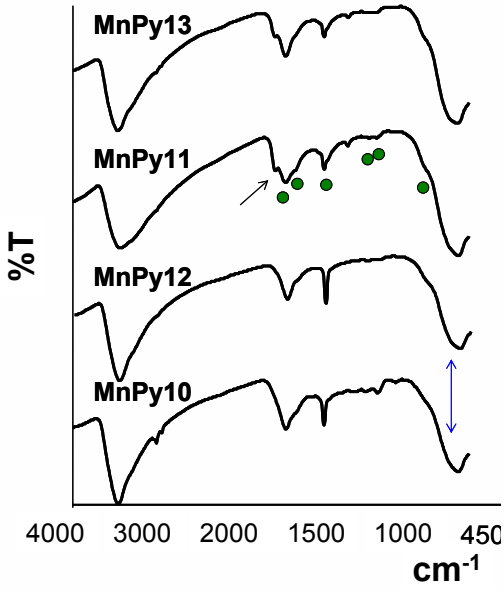

Figure 3.12.- FTIR analysis of PPy/MnO_2,hybrids of table III.VII, where the dots represent the vibrational modes of polypyrrole and the arrow Mn-O.

In table III.VII we summarize all data from the FTIR analysis, including a comparison with data and assignments from previous publications on polypyrrole [28,30,31]. The wide band around 500$cm^{-1}$is characteristic of Mn-O vibrations and allow us an approximate estimate of the relative amount of Mn present in our hybrid samples.

Table III.VII.- Data table of FTIR of all PPy/MnO_2 hybrid samples compared with the bibliographic assign frequencies for polypyrrole.

Assignement [31]	MnPy 1 (cm^{-1})	MnPy 4 (cm^{-1})	MnPY 5 (cm^{-1})	MnPy 7 (cm^{-1})	MnPy 8 (cm^{-1})	MnPy 9 (cm^{-1})	MnPy 10 (cm^{-1})	MnPy 11 (cm^{-1})	MnPy 12 (cm^{-1})	MnPy 13 (cm^{-1})
770-790 cm^{-1} C-H outside plane	766	760	772	790 (sh)	780	777	790 (sh)	790 (sh)	790 (sh)	790 (sh)
1040 cm^{-1} C-H y N-H in plane	1026	1032	1026	1032	1040	1040	1042	1040	1045	1040
1170 cm^{-1}ring vibrations	1190	1184	1166	1178	1178	1178	1140	1120	1150	1120
1300 cm^{-1} C-H in plane	1300	1300	1300	1342	1342	1294		1230		1230
1380 cm^{-1}ring vibr.C=C/C-C & C-N contrib.	1365	1348	1379	1385	Overl ap	1379	1382	1378	1385	1382
1450 cm^{-1}ring vibrations C=C/C-C & C-N contrib.	Over -lap	Over -lap	Over -lap	Over -lap	Over -lap	Over -lap shift	1550 (sh)	1550 (sh)	1550 (sh)	1550 (sh)
1540 cm^{-1} vibrational C=C/C-C	1556	1573	1526	1600	1593	1568	1631	1627	1627	1631
1720 cm^{-1} C=O								1700		1700

Among peaks assigned to polypyrrole, the characteristic bands around 1300 and 1380 cm^{-1} are more or less overlapped in the spectra of all our materials, but they can be distinguished. The bands around 1450 and 1540 cm^{-1} are overlapped and shifted to higher frequencies compared to literature values [30]; but we can distinguish a wide band with a characteristic complex profile where the two peaks should be expected, at least for the samples of the first series (table III.V).

For the samples of the second series, where a greater amount of $KMnO_4$ was used, we can see that the peaks are different. The peaks of polypyrrole at low frequencies are weaker in comparison with the broad Mn-O band, although some polypyrrole is formed. The peak around 1380cm^{-1} is very sharp and different to the normal polypyrrole peak. We found from earlier publications that when polypyrrole is synthesized in acetonitrile you get that type of peak, associated to the formation of COOH groups due to overoxidation; but in our case we used water as solvent. The main PPy peak appears for this series around 1627cm^{-1}, remarkably shifted with respect to the expected literature values (1540). Furthermore, for MnPy11 and MnPy13 we detect an extra peak around 1700cm^{-1}, which has been previously assigned to the formation of C=O groups, indicating the overoxidation of polypyrrole. [32-36]

In figure 3.13, we present the FTIR spectra of the samples of the first series where the hybrid PPy/MnO_2 was not formed. It can be observed that the characteristic vibrational modes of polypyrrole are absent. These samples are: MnPy2, MnPy3, and MnPy6. It is interesting to notice that on the spectra of these samples, we cannot detect the wide band characteristic of manganese dioxide around 500 cm^{-1}.

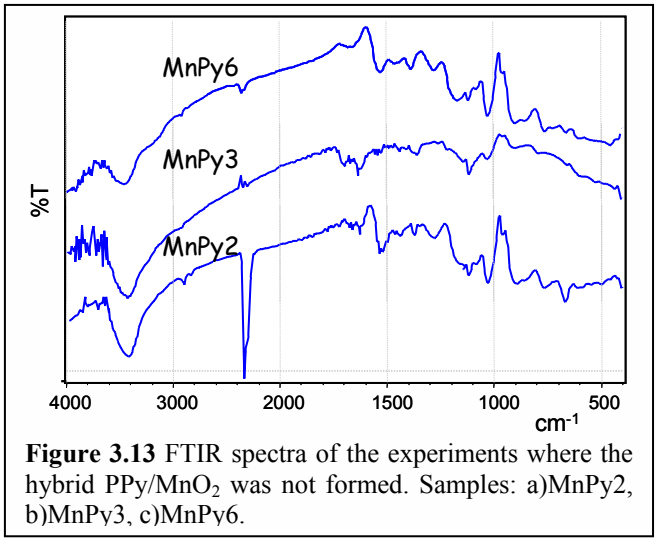

Figure 3.13 FTIR spectra of the experiments where the hybrid PPy/MnO_2 was not formed. Samples: a)MnPy2, b)MnPy3, c)MnPy6.

3.3.2.2. Stoichiometry and formula weight determination.

In order to determine the stoichiometry and the formula weight of our PPy/MnO_2 hybrids, first we dried them under vacuum for 3 days. Then we carried out a TGA analysis to determine the amount of hydration water and organic matter lost and the amount of the residual inorganic matter. We also performed an elemental analysis of our hybrid samples, to determine the percentages of carbon, nitrogen, and hydrogen of the organic mater. For the Mn analysis we used an atomic absorption technique.

3.3.2.2.1. TGA analysis.

We have carried out thermogravimetric analysis under an air atmosphere, heating at a slow rate of 1°C/min up to 500°C and leaving it at this temperature for 5 hours. In figure 3.14 we can observe the results of the TGA analysis of the vacuum-dried samples of PPy/MnO_2. As mentioned before, we chose slow heating conditions as a precautionary measure (N.B. when using a faster heating rate of 5°C/min the sample reacted violently and got spilled over). In figure 3.14 we can appreciate the partial overlap between the dehydration process and the main loss corresponding to decomposition of organic matter, both separated by an inflection point at around 100ºC. The first apparent and most significant fact is that the different PPy/MnO_2 hybrid samples have quite different contents of organic and inorganic matter. The order of the samples arranged from lower to higher inorganic contents is: MnPy5 < MnPy9 < MnPy1 < MnPy8 < MnPy4 < MnPy7 < MnPy10 < MnPy11 < MnPy13 < MnPy12.

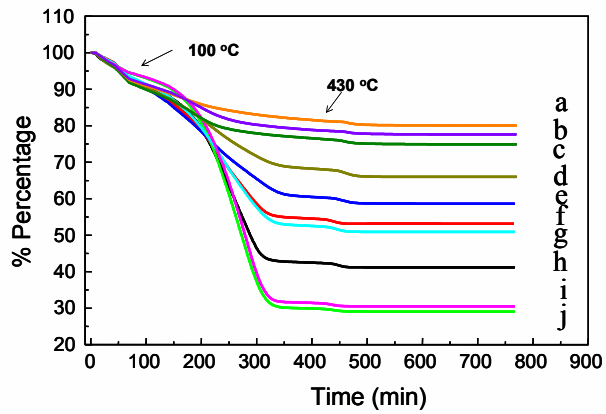

Figure 3.14- Thermogravimetric analysis (TGA) at 1°C/min in air , of the hybrid PPy/MnO_2 samples. (a)MnPy12, (b)MnPyi13, (c)MnPy11, (d)MnPy10, (e)MnPy7, (f)MnPy4,(g)MnPy8, (h)MnPy1, (i)MnPy9, and (j)MnPi5.Py

Finally, we must mention that from the TGA analysis, we have detected a small weight loss around 430°C, associated to oxygen liberation and reduction of Mn (IV →III), a loss which has been assigned in the literature to a phase transition of MnO_2 to Mn_2O_3. [37].

3.3.2.2.2. Analyses of Manganese.

Mn analyses by atomic absorption were carried out for the inorganic residues obtained by TGA analyses, once we eliminated the organic part and the water content of the hybrid samples.

We prepared the respective manganese solutions for each sample, by dissolving a precise weight of the residue in a solution of $H_2O/H_2O_2/HNO_3$ (50/5/5 %volume) to yield a concentration of ca. 20 ppm. This analysis is complementary to TGA and it helped us to determined the stoichiometry of the hybrid samples. In table III.VIII, we present the expected and raw experimental data obtained from the amount of manganese for each of the PPy/MnO_2 hybrid samples.

Table III.VIII.- Comparison between calculated and experimental data of the manganese amount.

Samples	ppm of Mn estimated by TGA	ppm of Mn experimental
MnPy1	19.01	18.65
MnPy4	19.98	19.29
MnPy5	19.85	19.18
MnPy7	15.67	15.35
MnPy8	19.87	19.07
MnPy9	19.90	19.5
MnPy10	19.65	18.45
MnPy11	19.93	17.92
MnPy12	19.54	17.52
MnPy13	19.31	17.52

3.3.2.2.3. Elemental Analysis.

For each of the PPy/MnO_2 hybrid samples we carried out an elemental analysis to find the amounts of carbon, hydrogen and nitrogen. The objective of this analysis was to determine the composition of the organic matter present in the hybrid.

Table III.IX.- Summarized data from chemical analysis and calculated formulas for PPy/MnO_2 hybrids.

	Py:MnO_4^-	%C	%N	%H	%Mn	N/Mn	Formula	Sample
Exp.	2/1	36.12	10.22	2.65	28.25	1.42	$[C_4H_3N]_{1.42}MnO_{1.84}\cdot 0.99H_2O$	**MnPy1**
Calc.		35.05	10.22	3.23	28.23			
Exp.	2/1	23.43	6.68	2.09	35.54	0.74	$[C_4H_3N]_{0.74}MnO_{1.87}\cdot 1.2H_2O$	**MnPy4**
Calc		22.99	6.7	3.01	35.52			
Exp.	10/3	43.25	12.20	2.93	19.5	2.46	$[C_4H_3N]_{2.46}MnO_{1.85}\cdot 2.08H_2O$	**MnPy5**
Calc		41.89	12.21	4.12	17.47			
Exp.	2/1	19.6	5.58	1.93	39.99	0.55	$[C_4H_3N]_{0.55}MnO_{1.77}\cdot 1.02H_2O$	**MnPy7**
Calc		19.22	5.6	2.7	39.97			
Exp.	10/3	26.24	7.39	2.2	36.2	0.85	$[C_4H_3N]_{0.85}MnO_{1.91}\cdot 0.61H_2O$	**MnPy8**
Calc		26.9	7.84	2.5	36.19			
Exp.	5/1	40.7	12.03	2.92	21.27	2.22	$[C_4H_3N]_{2.22}MnO_{1.79}\cdot 1.69H_2O$	**MnPy9**
Calc		41.26	12.03	3.91	21.25			
Exp.	4/3	13.35	4.09	1.20	43.13	0.36	$[C_4H_3N]_{0.36}MnO_{1.96}\cdot 0.94H_2O$	**MnPy10**
Calc		13.65	3.98	2.35	43.37			
Exp.	1/1	6.86	2.28	1.79	46.87	0.19	$[C_4H_3N]_{0.19}Mn_{0.92}O_2\cdot 0.84H_2O$	**MnPy11**
Calc		7.79	2.27	1.93	46.89			
Exp.	4/5	4.03	1.49	1.60	49.95	0.12	$[C_4H_3N]_{0.12}Mn_{0.92}O_2\cdot 0.7H_2O$	**MnPy12**
Calc		5.24	1.53	1.61	49.91			
Exp.	2/3	6.44	2.15	1.74	49.00	0.17	$[C_4H_3N]_{0.17}Mn_{0.95}O_2\cdot 0.7H_2O$	**MnPy13**
Calc		7.29	2.12	1.72	49.02			

Once we calculated the amount of organic matter corresponding to polypyrrole for each sample, we determined by difference (from TGA) the amount of water present in the hybrids. Also, with the data obtained from atomic absorption, we calculated the amount of manganese for each sample. In table III.IX we summarize the calculated and experimental data obtained for each hybrid.

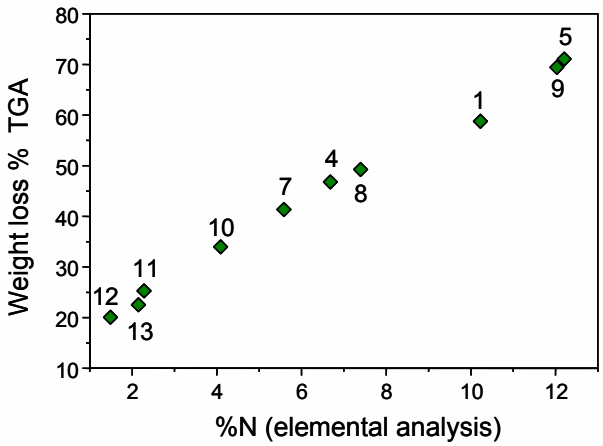

Figure 3.15.-Correlation between the N% of elemental analysis with the weight loss percentage from TGA analysis (%polypyrrole+%water).for all the samples of PPy/MnO_2 hybrid. The numbers in the graph corresponds to the sample number.

The results obatined from chemical analysis and from TGA can be contrasted as

shown in Figure 3.15, where the weight loss obtained from TGA (organic matter + water) are correlated with the % Nitrogen from elemental analyses:

Analyzing the data sumarized in Table III.IX we can extract certain conclussions on the results of the first series of synthesis, concerning especifically the effect of the amount of acid used (for a given pyrrole permanganate ratio) on the amount of polymer in the final hybrid. For samples MnPy1, MnPy4 and MnPy7 with the same Py/MnO_4^{-1} ratio, we can see that with more acid used we incorporate more polypyrrole in the hybrid. Comparing samples MnPy5 and MnPy8 which have the same Py/MnO_4^{-1} ratio, we also see the same direct relationship between the amount of acid used, and the amount of polymer in the hybrid. On the other hand, samples MnPy5 and MnPy9 which have almost the same amount of polymer in the hybrid, are characterized by an identical ratio of acid/$KMnO_4$ in the synthesis.

Concerning the oxidation state of Mn in the residual inorganic phases it can be noted that all the hybrids from the first series of synthesis (table III.V) show a molar ratio O:Mn greater than 2.conforming to formulas of MnO_{2-x} with x>0 (i.e.) Mn(III)-Mn(IV), whereas for hybrids in the second series the molar ratio O:Mn is smaller than 2.

3.3.3. Study as Cathode materials in reversible lithium cells.

In Figure 3.16 we show the first cycle of charge-discharge for each of the PPy/MnO_2 hybrid materials integrated as active cathode materials in the form of powders mixed with carbon Super-P in lithium cells with metallic lithium anodes. The rate of discharge and recharge was in all cases of C/35. The best specific charges found for these hybrids, were for samples with a larger amount of MnO_2 (MnPy12= 115Ah/Kg, MnPy13= 139 Ah/Kg, MnPy11= 150 Ah/Kg, MnPy10= 135Ah/Kg).

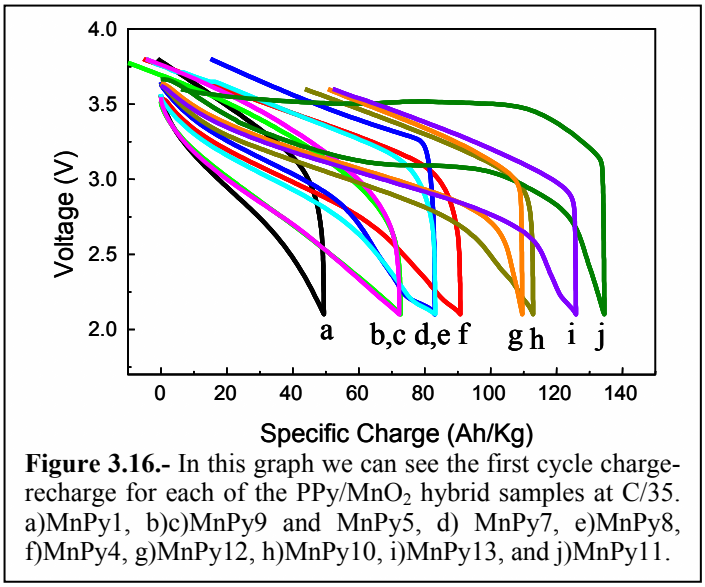

Figure 3.16.- In this graph we can see the first cycle charge-recharge for each of the PPy/MnO_2 hybrid samples at C/35. a)MnPy1, b)c)MnPy9 and MnPy5, d) MnPy7, e)MnPy8, f)MnPy4, g)MnPy12, h)MnPy10, i)MnPy13, and j)MnPy11.

In figure 3.17 we show the relation between the manganese content in the hybrid with the correspondent specific charge of the first discharge cycle. We can confirm that, the higher the manganese content the higher the specific charge will be. However, the reversibility was correspondingly worse for these hybrids in comparison with those containing smaller amounts of inorganic component. Thus, for all the hybrids of the second series mentioned above, wich are the ones with higher contents of Mn, 70% of the initial specific charge is lost after 15 cycles. The explanation for this cycling fading is probably related to the overoxidation and degradation of PPy. For the hybrids with more polypyrrole (first series, Table III.V) the cyclability is better although still substantial, around 45% after 15 cycles.

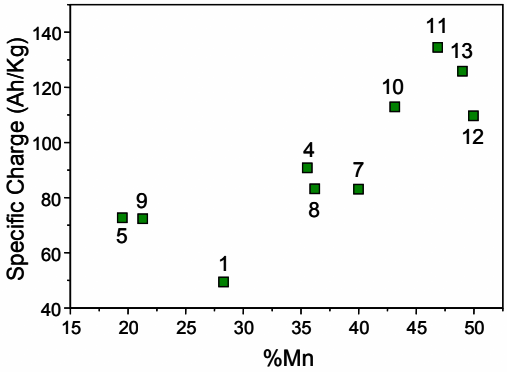

Figure 3.17.- Graphic representation of the relation between the %Mn with the obtain specific charge of the first charge-discharge cycle. The numbers in the graph corresponds to the sample number

Taking into account the complexity and the anion dopants of the conducting polymer, the charge-discharge mechanism of the hybrids is more complex than a system based on an oxide as active material. H. Gemeay and co-workers [16] proposed a mechanism of charge-discharge for their mixtures of PPy and MnO_2 which could also be valid for our PPy/MnO_2 hybrids. It considers the initial superficial charge compensation of MnO_2 by the dopant anions present in the hybrid as well as the incorporation of Li cations during the discharge, followed by a loss of part of the anions associated to the positive charge of the p-doped conducting polymer in the initial state. The proposed mechanism of reference [16] of the charge-discharge process is presented in figure 3.18.

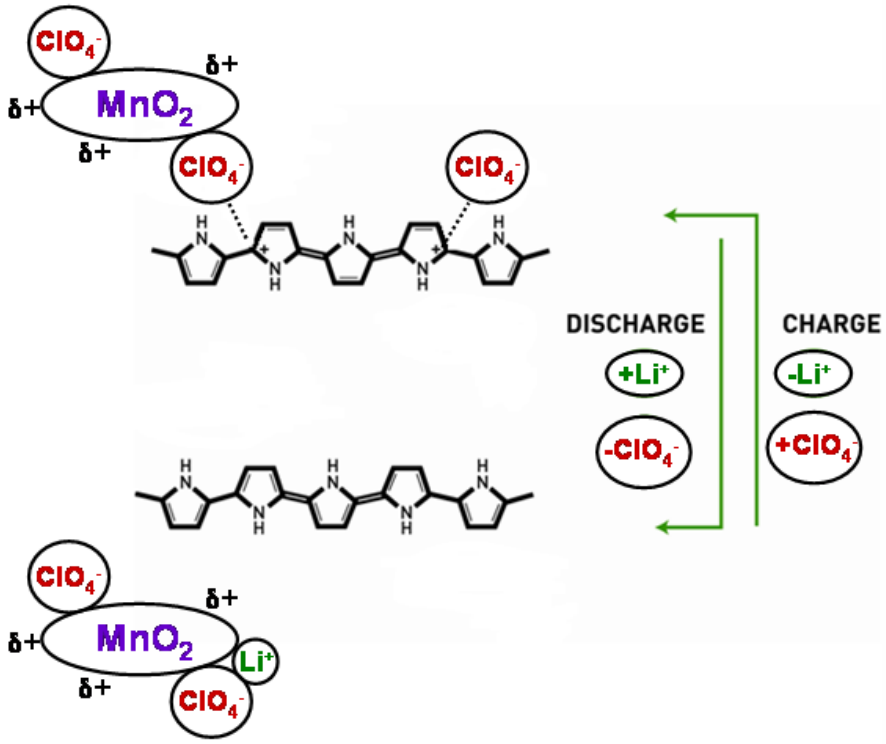

Figure 3.18.-Schematic representation of composition changes in the PPy/MnO2 hybrid, during charge-discharge reactions.

REFERENCES

[1] Bruce, P.G.; *Chem. Commun.* **1997**(19), 1817.
[2] Dampier, F.W.; *J. Electrochem. Soc.* **1974**(121), 656.
[3] Beltowska-Brzezinska, M.; Dutkiewicz, E.; Jolara, S.; *J. Electroanal. Chem.* **1982**(135), 103.
[4] Nardi, C.J.; *J. Electrochem. Soc.* **1985**(132), 1787.
[5] Bach, S.; Henry, M.; Baffier, N.; Livage, J.; *J. of Solid State Chemistry* **1990**(88), 325.
[6] Pistoia, G.; *J. Electrochem. Soc.* **1982**(129), 1861.
[7] Pereira-Ramos, J.P.; Baddour,R.; Bach, S.; Baffier, N.; *Solid State Ionics* **1992**(53-56), 701.
[8] Ohzuku, T.; Kitagawa, M.; Hirai, T.; *J. Electrochem. Soc.* **1990**(137), 769.
[9] Bach, S.; Pereira-Ramos, J.P.; Baffier, N.; Messina, R.; *Electrochimica Acta* **1991**(36), 1595.
[10] Ivanova, N.D.; Kirillov, S.A.; Mishchenki, A.B.; *Electrochim. Acta* **1993**(38), 2305.
[11] Winter, M.; Besenhard, J.O.; Spahr, M.E.; Novak, P.; *Adv. Matter.* **1998**(10), 725.
[12] Hunter, J.; *Solid State Chem.* **1981**(39), 142.
[13] Feng, Q.; Kanoh, H.; Ooi, K.; *J. Mater. Chem.* **1999**(9), 319.
[14] Shen, X.M.; Clearfield, A.; *J. Solid State Chem.* **1986**(64), 270.
[15] Nazri, G.A. (General Motors), Eur. Pat. Appl. (1997) EP 96-203027, US 95-562862.
[16] Gemeay, H.; Nishiyama, H.; Kuwabata, S.; Yoneyama, H.; *J. Electrochem. Soc.* **1995**(142), 4190.
[17] Yoneyama, H.; Kishimoto, A.; Kuwabata, S.; *J. Chem. Soc., Chem. Commun*. **1991**(, 986.
[18] Nishizawa, M.; Mukai, K.; Kuwabata, S.; Martin, C.R.; Yoneyama, H.; *J. Electrochem. Soc.* **1997**(144), 1923.
[19] Kuwabata, S.; Masui, S.; Yoneyama, H.; *Electrochim. Acta* **1999**(44), 4593.
[20] Tran, T.; Truong, N.L.; Nguyen, T.T.; Nguyen, V.T.; *Tap Chi Hoa Hoc* **1999**(37), 95.
[21] Tran, T.; Nguyen, V.T.; *EUROMAT99* Biannual Meeting of the Federation of European Materials Societis, Munich, Germany (2000), editor Grassie, K.; Wiley-VCH Verlang GmbH, Weinhein Germany, 309-315.
[22] Hashmi, S.A.; Upadhyaya, H.M.; *Ionics* **2002**(8), 272.
[23] Chen, R.; Whittingham, S.*; J. Electrochem. Soc* **1997**(144), L64.
[24] Gozdz, A.S.*; Rechargeable Lithium intercalation battery with hybrid polymeric electrolyte*.; Gozdz, A.S., Ed.; Bell Communications Research, Inc.; United States of America., **1994**.
[25] Shaabani, A.; Lee, D.G.; *Tetrahedron Lett.***2001**(42), 5833.
[26] Zhang, W.J.; Feng, J.; MacDiarmid, A.G.; Epstein, A.; *J. Synthetic Metals* **1997**(84), 119.
[27] Taguchi, G.; Konishi, S.*; Arreglos Ortogonales y Gráficas Lineales: Herramientas para la Ingenería de Calidad*.; 1ra. Ed.; ASI International; Monterrey N.L., **1991**.
[28] West, R.C.; Astle, J.M.; *Handbook of Chemistry and Physics*; 60th. Ed.; West, R.C.; Astle, J.M., Ed.; CRC Press; Florida, **1979-1980**, pp D155-D160.
[29] Lira-Cantú, M.; Gómez-Romero, P.; *Int. J. of Inorg. Mat.* **1999**(1), 111.
[30] Lira-Cantú, M.; *Matteriales Híbridos Orgánico-Inorgánico a Base de Fosfomolibdato o Pentóxido de Vanadio Dispersos en Polímeros Orgánicos Conductores. Aplicación como Electrodos de Inserción en Baterías de Litio*.; Lira Cantú, M. Ed.: Universitat Autònoma de Barcelona; Barcelona, **1997**, pp 244.
[31] Lei, J.; Liang, W.; Martin, R.C.; *Synthetic Metals* **1992**(48), 301-312.
[32] Rodriguez,I.; Scharifker, B.R.; Mostany, J.; *J. Electroanal. Chem.* **2000**(491), 117.
[33] Novak, Petr; Rasch, Birgit; Vielstich, Wolf; *J. Electrochem. Soc.* **1991**(138), 3300.
[34] Schlenoff, Joseph B.; Xu, Hong*; J. Electrochem. Soc.* **1992**(139), 2397.
[35] Maia, G.; Ticianelly, E.A.; Nart, F., C.; *Phys. Chem.* **1994**(186), 245.
[36] Christensen, P.A.; Hammett, A.; *Electrochim. Acta* **1991**(36), 1263.
[37] Tsuji, M.; Komarneni, S.; Tamaura, Y.; Abe, M.; *Mat. Res. Bull.* **1992**(27), 741.

Chapter 4

V_2O_5 XEROGELS

Abstract:

It is well known that V_2O_5 has the ability to intercalate large amounts of lithium, when prepared by sol gel techniques or soft chemistry. In this chapter we present a study of a modified synthesis of V_2O_5 gels and evaluate the influence of thermal treatment under different atmospheres on the electrochemical performance of different V_2O_5 xerogels. These materials, which present a greater porosity and surface area as compared with those obtained by solid state reactions, are studied here with a double purpose: characterizing their own performance and providing a system for comparison of the corresponding hybrids described in the next chapter. These xerogels have layered structures made of V_2O_5 slabs and interstitial water. The spacing between the layers varies depending on the amount of water and it can be eliminated in a range of temperatures between 100-360ºC. At higher temperatures these materials crystallize producing the well-known orthorhombic phase. The water contents and the degree of crystallization have been two of the main factors followed to study their influence on specific charge and cyclability in reversible lithium cells.

4.1. INTRODUCTION

Vanadium, chromium, niobium, or molybdenum oxides are characterized by their capacity to electrochemically intercalate large amounts of lithium. Nevertheless, because of their poor cyclability, until now only vanadium oxides have acquired importance as materials for rechargeable electrodes of intermediate voltage ”3V” [1].

Crystalline V_2O_5 has a layered structure, which could also be considered like a 3D network; due to a longer sixth V-O bond. It is formed from VO_5 square base pyramids, which share corners and edges. The axial V-O bond length is shorter than the other four distances, and corresponds to a double bond, which is detected by infrared spectroscopy [2-7]. We can also describe the coordination environment of vanadium on the V_2O_5 structure like VO_6 distorted octahedra, (figure 4.1) a vision that emphasizes the relation with the ReO_3 structure. The longer length of the sixth V-O bond underlines the structural anisotropy of this material, and the capacity to insert ionic or molecular species [1].

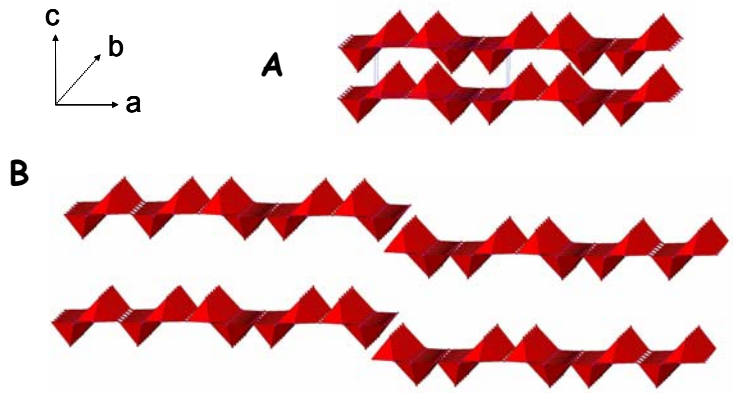

Figure 4.1.-V_2O_5 structures, (A) crystalline phase indicating the unit cell and the long range bond between V-O, and (B) Sketchy structure of the ab plane of the ribbon like corrugated structure of the vanadium pentoxide (V_2O_5) gel and/or xerogel.

Layered materials such as crystalline V_2O_5, commonly present good intercalation properties, providing a good opportunity for the development of lithium insertion materials [8]. Depending on the amount of inserted lithium in crystalline V_2O_5, we can observe various structural modifications (see figure 4.2): when $x<0.01$ the α-phase is formed, if $0.35<x<0.7$ the ε-phase is formed, and around $x=1$, the δ-phase is formed. Up to this point all phase transformations are reversible. However, for values of $x>1$ the δ-phase is irreversibly transformed to the γ-phase. In 1989, it was demonstrated that this γ-phase could be reversibly cycled between the range of $0\leq x\leq 2$ with γ-phase retention. Finally, with a

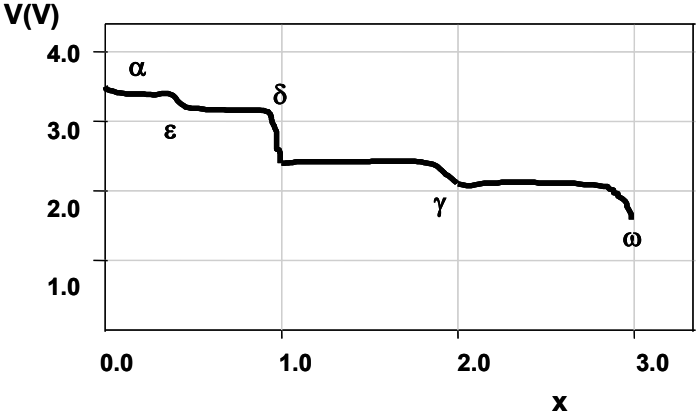

Figure 4.2.- Potential variation during discharge of a cell of crystalline V_2O_5, like active cathodic material (vs. metallic lithium). We indicate the structural changes suffered by the discharge of V_2O_5.

greater insertion of lithium in V_2O_5, an irreversible ω-phase (NaCl type) tends to form [1,9-13].

Besides pure and crystalline V_2O_5, there have been other promising publications concerning partial substitution of vanadium or development of related amorphous systems. For example there have been reports of the substitution of V by other metals to stabilize the irreversible phases [14], V_2O_5 glasses with P_2O_5, V_2O_5 xerogels [15,16], and V_2O_5 aerogels [1,17,18]. In principle these amorphous (or very poorly crystalline) materials offer advantages because they avoid phase transition problems. Furthermore, since they are frequently obtained in a very dispersed form, they benefit from good diffusion coefficients and a low volumetric expansion during lithium insertion; due to a small particle size and a low density. However, long-term cycling stability is still a problem for this type of materials [1].

The synthesis of amorphous V_2O_5 derivatives can be carried out by means of soft chemistry methods [19], in particular by sol-gel methods taking advantage of the hydrolysis of molecular precursors leading to the precipitation of a gel. Two main alternatives are possible in the case of V_2O_5 . In the first method, the vanadate anion is the molecular precursor, which in an acidic medium suffers hydrolysis and condensation reactions that eventually lead to the precipitation of V_2O_5 gel. A second method is carried out by means of the hydrolysis of alkoxide precursors. [20]

We will explain in more detail the hydrolysis and condensation process in acidic media of vanadate anion that we have applied in the present work. V_2O_5 gel is usually synthesized by protonation of vanadate salts by ion exchange. A metavanadate salt solution is run through a column packed with a proton exchange resin, obtaining a light yellowish solution. Under the resulting low pH, and high vanadium concentration, this solution slowly changes with time, turning red as the condensation of vanadate

anion species proceeds through the sol (solid dispersed in liquid) and gel (liquid dispersed in solid) colloidal stages, leading eventually to the formation of a V_2O_5 gel.

The vanadate anion $[VO_4]^{-3}$ is a stable tetrahedral oxoanion at alkaline pH. Any increase in acidity gives way to the condensation processes, which can form a great diversity of polynuclear species, whose nature depends on the pH and the vanadium concentration [21]. For example, on concentrated vanadate (>10^{-1} M) solutions with a pH between 13 and 9, two vanadate anions condense to form $[V_2O_7]^{-4}$ pyrovanadate anion. At lower pH (pH=8) further condensation of tetrahedra takes place forming the metavanadate anion $[V_4O_{12}]^{-4}$, which consists of rings of four tetrahedra sharing corners. At pH lower than 7 (in concentrated vanadium solutions) polynuclear species formed by oxygen-sharing octahedra begin to appear. In this region of the phase diagram dominates the decavanadate anion $[V_{10}O_{28}]^{-6}$ and their protonated forms $[H_nV_{10}O_{28}]^{-(6-n)}$, which are strong acids [21-24]. Finally, under strong acidic media at pH between 0 and 3 the concentrated vanadium solutions give way to precipitation of red V_2O_5 colloidal gels.

These gels are inorganic polymers almost amorphous, whose local structure is similar to the crystalline oxide, but with a long range order not well defined. The gels are composed of ribbon-like particles, which are 10 nm wide (≈ 30 VO_5 polyhedra) and 1μm long (≈300 polyhedrons). These ribbons have a structure as indicated in figure 4.1b. They are extended oxides which result from the acidic condensation of vanadate anion as mentioned above, through a proposed mechanism that involves complex olation/oxolation processes (Figure 4.3).

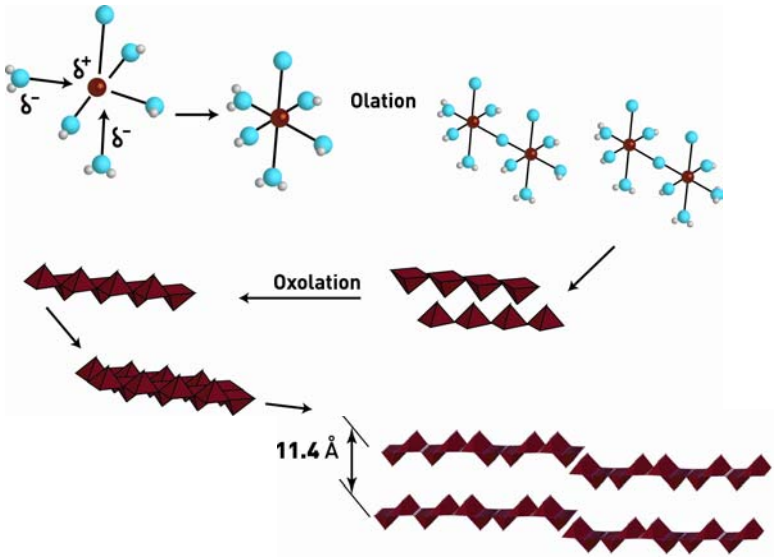

Figure 4.3.- Proposed mechanism for V_2O_5 gel condensation from vanadate anion [22].

$V_2O_5 \cdot nH_2O$ gels are mixed valance oxides, that contain mostly V(V) and some V(IV). The presence of V(IV) is a determining factor for the gel formation. In absence of V(IV) the condensation takes place very slowly, while its presence, even in small amounts, is useful as a catalyst for a quicker formation of the gel. [23]. It has also been proposed that this condensation starts at a rapid pace which decreases with time; but this fact is still under discussion [23]

The gels obtained by the method described above are in fact hydrogels, with a substantial amount of water. From these hydrogels we can obtain V_2O_5 xerogels or aerogels[25]. Aerogels are obtained by means of a solvent exchange (organic solvents like acetone for water) and a CO_2 supercritical drying of the gel, which maintains the microstructure of the gel and leads to a highly microporous solid [17,26-28]. The xerogels are obtained by drying the hydrogel at room temperature, under vacuum or at temperatures under 100^oC [18,20,29-33]. These xerogel materials normally present surface area and porosity which are greater than the ones obtained by solid state synthesis methods though usually not as large as those from aerogels

Xerogels develop layered structures made up of $V_2O_5 \cdot nH_2O$ ribbons and residual intercalated water (figure 4.1b). The spacing between the layers varies depending on the amount of water. This intercalated water can be eliminated by heating at 100-360 ^oC. At higher temperatures the xerogel crystallizes giving way to the formation of the known orthorhombic V_2O_5 crystalline phase [34]. When, in $V_2O_5 \cdot nH_2O$ xerogels $n<0.5$, the structure is similar to the crystalline phase, if $n=0.5$ the xerogel has one layer of water between vanadium slabs, if $n=1.8$ it has a water bylayer, and when $n \geq 6$ an expansion process is presented in the ribbons or layers giving way to the gel. [21]

As part of our work on hybrids containing V_2O_5 derivates, we have studied in some detail, and present in this chapter, several aspects related to the synthesis, chemical, spectroscopic and electrochemical characterization in reversible lithium cells of V_2O_5 xerogels themselves. In chapter 5 we will discuss hybrid materials where V_2O_5 constitutes the inorganic matrix, but for the moment these xerogels deserve their own detailed study. We will describe first the sol-gel synthesis of $V_2O_5 \cdot nH_2O$ gels, the determination of V(V) in the gel, an aging study of the gel through time, the analysis of water content in the gels, and finally a study of V_2O_5 xerogels with different thermal treatments and their characterization as active cathode materials in rechargeable Li cells.

4.2. SYNTHESIS OF $V_2O_5 \cdot nH_2O$ GEL

For the $V_2O_5 \cdot nH_2O$ gel synthesis we used a cation-exchange method described in the literature [21,23,24,29,31,34,35]. We dissolved 5 g of sodium metavanadate ($NaVO_3$) in boiling water (ca. 70ml) and then raised to 100ml to obtain a 0.41M solution. This colorless solution was run through a column packed with a proton-exchange DOWEX 50-wx2 resin. We collected approximately 200 ml of a yellow-orange solution; where the change of color is attributed to the formation of condensed species (decavanadate $[V_{10}O_{28}]^{-6}$) induced by the lowering of pH. After 24 hours we could observe an evolution of the yellow-orange solution to a dark red $V_2O_5 \cdot nH_2O$ gel. Nevertheless, the growth of the $V_2O_5 \cdot nH_2O$ inorganic polymer (with a fiber ribbon like microstructure) can continue evolving for longer periods of time [10-13]. For this reason we made a study of the aging process, monitoring the concentration of V(V) through time.

We synthesized three different batches of the gel following the same procedure described above. Batch (1) consisted of 200 ml and was used for the aging study (see section 4.3 below), batch (2) (1600 ml) was used for the synthesis of all the hybrid PAni/ V_2O_5 materials that will be described in next chapter, as well as for determining water contents in V_2O_5 gels (section 4.4). Finally, batch (3) (200 ml) was used for the study of xerogels, including different thermal treatments and their effect on electrochemical performance (section 4.5). The only difference between these three batches is that in (1) and (2) aging took place on solutions standing still (static aging) whereas in batch (3) aging was performed with magnetic stirring (dynamic aging) in a process that will be described later on.

4.3. DETERMINATION OF V(V) IN $V_2O_5 \cdot nH_2O$ GELS

$V_2O_5 \cdot nH_2O$ is a mixed-valence oxide gel where mostly V(V), but also V(IV) are present. When we synthesize the polyaniline/V_2O_5 hybrid, V(V) is responsible for the oxidation of aniline to polyaniline. This is why it is crucial to know the amount of V(V) in the gel in order to make the hybrid in a controlled manner. From here it follows the importance of knowing exactly the amount of V(V) as a function of time, in other words, the aging study of the gel through time.

Following the method in reference [36], we determined the amount of V(V) in the $V_2O_5 \cdot nH_2O$ gel with an $Fe(NH_4)_2(SO_4)_2 \cdot 6H_2O$ solution. In detail the procedure is as follows: 2 ml of $V_2O_5 \cdot nH_2O$ gel is dissolved in 15 ml of deionized water and 1ml of phosphoric acid (H_3PO_4). We carried out a potentiometric titration of the solution with a combined electrode (platinum wire combined with a Ag/AgCl compartment), using a solution of $Fe(NH_4)_2(SO_4)_2 \cdot 6H_2O$ 0.025 M in 0.02M sulfuric acid (H_2SO_4), obtaining the final point of the titration from the derivative of the titration curve (fig. 4.4). We calculated the concentration of V(V) from the formula:

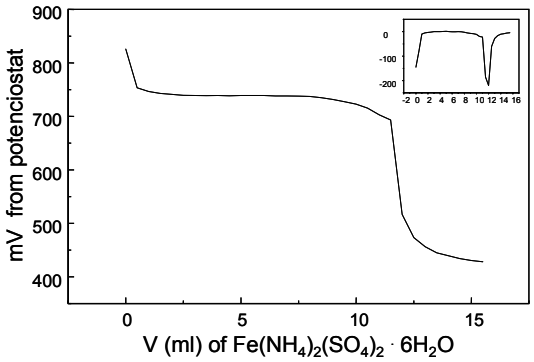

Figure. 4.4.- Typical titration curve for the determination of V(V). In the inset we show the derivative graph,

$$C(V_{(V)}) = C_{Fe}(0.025\ M) \times V_{Fe}(\text{final point}) / V_{gel}(2\ ml)$$

We carried out these potentiometric titrations a few minutes before the synthesis of PAni/V_2O_5 hybrid material. We also used this method to study the aging of the gel through time and to determine V(V) in the gel used to obtain the V_2O_5 xerogels.

4.4. AGING STUDY OF THE GEL

The aging study of the $V_2O_5 \cdot nH_2O$ gel has been carried out over a one year period. The gel has been kept in a sealed 500 ml bottle in presence of air. We systematically titrated the gel every 15 days. The titrations were carried out as described above. In figure 4.5 we can follow the evolution of V(V) in the gel over one year. First we can observe that the V(V) concentration is not stable, but it shows a

tendency to increase stability through time. On the other hand, we can see that the greatest increase takes place at the beginning of the aging process. With this data we can acknowledge the importance of titrating the gel immediately prior to use, in the PAni/V_2O_5.hybrid synthesis.

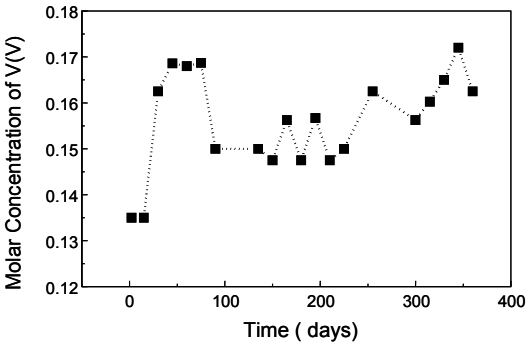

Figure 4.5.- Aging study of V_2O_5 nH_2O gel over a period of one year.

4.5. WATER CONTENT OF GELS USED FOR THE SYNTHESIS OF PAni/V_2O_5 HYBRIDS.

In the $V_2O_5.nH_2O$ xerogels the amount of water is variable, and they can reach up to n=2.2. We can classify these water molecules into three types. The first type of water is weakly bonded and it can be reversibly lost; the quantity is variable but it is around 1.1 molecules of water per V_2O_5 (denoted *a* in the scheme and Figure below); part of this labile water can be lost even by a simple vacuum treatment at room temperature, whereas the remaining water can be eliminated with a light heating at 100-120^oC. The second type of water, which corresponds to 0.4 molecules of water per V_2O_5 (b) is more strongly bounded and more difficult to eliminate, by heating at higher temperatures (ca. 250^oC). Finally the third type of water is chemically bonded (c) and it corresponds to a small amount of water (0.1 molecules per V_2O_5). This water can only be eliminated by heating at a temperature above 320^oC where a structure transformation takes place from the layered V_2O_5 xerogel to crystalline V_2O_5. These successive stages are shown in the following scheme:

$$V_2O_5 \cdot 1.6H_2O \xleftrightarrow{\text{(a) } 120^oC} V_2O_5 \cdot 0.5H_2O \xrightarrow{\text{(b) } 250^oC} V_2O_5\ 0.1H_2O \xrightarrow{\text{(c) } 320^oC} V_2O_5 \text{ crystalline}$$

Taking into account the importance of the amount of water on the electrochemical properties of vanadium pentoxide, we carried out a study of the amount of water in our xerogel to compare to previous results. The gel that we used for this study was made by applying static (see section 4.2) aging for three months, and was the same gel used for the synthesis of PAni/V_2O_5 hybrids. We first performed a preliminary experiment to determine the amount of water lost to form the xerogel from the gel. For this, a tare glass flask was used with a vacuum exit and a frosted glass sealed stopper for vacuum. A precisely weighted amount of gel was placed under vacuum for 48 hours to eliminate water and obtain the xerogel. The percentage of water lost from the conversion of gel to xerogel was 98.25% in weight.

TGA analysis of the remaining red powder (xerogel) was performed in order to determine the hydration water and to compare them to literature results [18]. The TGA analysis was carried out under oxygen atmosphere at a 5 ^oC/min rate up to 500 ^oC and kept for 5 hours. Figure 4.6 shows the results of the analyses.

We detected the existence of four processes of water weight loss. The first one, which also represented the greatest weight loss, took place at temperatures below 100^oC (inflection point at 92 ^oC). This weight loss (a) of 6.76% (equivalent to 0.76 molecules of water by V_2O_5), matches the first type of water previously described. The second weight loss process (b) was observed at 240 ^oC, and the third one (c) at 300^oC. These two processes are very close but can be differentiated under the conditions of our analysis (they can be more clearly detected in the derivative graph of the inset in figure 4.6). Precise quantification of the amount of water of each of the last two processes is difficult; but they represent a 3.25% weight loss (equivalent to 0.37 molecules of water by V_2O_5). Finally, the last dehydration process was detected at 380^oC (d), representing a small 0.5% weight loss (equivalent to 0.06

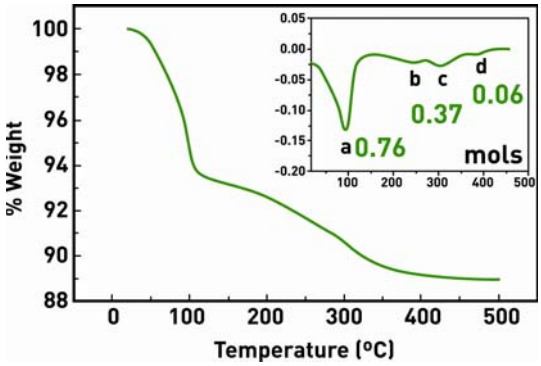

Figure 4.6. TGA analysis of $V_2O_5 \cdot nH_2O$ xerogel. We can see in the small deviation graph (a,b,c,d), the successive weight loss stages of hydration water of V_2O_5 xerogel.

molecules of water by V_2O_5), leading to the formation of the orthorhombic crystalline phase of V_2O_5. The sum of all water weight losses indicates that when our xerogel is dried under vacuum, we get a total 1.19 molecules of water per formula weight (V_2O_5 $1.19H_2O$). The amount of hydration water in these active electrode materials is of great relevance because the presence of water is detrimental to the performance in lithium batteries.

From a general point of view, we can say that these dehydration processes are in good accordance with previous publications. There are some significant differences which suggest the convenience to make a proper characterization of each particular hydrated material. For example, the first three stages that we observed are in good accordance with past publications within a margin of ten degrees; but the amounts of lost water in each step do not coincide. Another difference of our data is the number of stages; in our case we have four stages. The additional stage at 380^{o}C corresponds to a relatively small amount of water.

This suggests that more than two or three well differentiated hydrates can exist with variable amounts of water; not only weakly bonded water but also materials treated at higher temperatures.

4.6. SYNTHESIS OF V_2O_5 XEROGELS.

In order to synthesize the V_2O_5 xerogels, we first dried the gel described in section 4.2 by heating it at 100^{o}C, obtaining a red solid. After the corresponding chemical and structural characterization, we did analyze the electrochemical properties in reversible Li cells in successive charge-discharge cycles. These studies served a double purpose, they allowed to characterize the performance of these inorganic gels but also served as a reference system for comparison with the behavior of PAni/V_2O_5 hybrid.

$V_2O_5{\cdot}nH_2O$ gel was obtained by means of a proton exchange process (section 4.1). After collecting the solution from the column, we stirred for 5 days at 600 rpm and room temperature. At the end of this dynamic aging procedure a dark red gel resulted, in which the amount of V(V) was determined, resulting in a concentration of 0.18M. If we compare this result with the concentration of V(V) obtained by static

aging (figure 4.5), we can notice an accelerated oxidation process associated to the dynamic procedure.

The gel was dried by heating at 100°C for 20 hours. From the resulting red powder material, we separated 13 samples in order to perform different treatments. In table IV.I we detailed the atmosphere and temperature used for each particular sample.

Table IV.I.-Samples of all the obtain xerogels with their given treatment.

Atmosphere treatment	temperature of treatment	sample name (xerogel)
Oxygen	180°C	X1O
	250°C	X2O
	280°C	X3O
	350°C	X4O
Air	100°C	XM
	180°C	X1M
	250°C	X2M
	280°C	X3M
	350°C	X4M
Argon	180°C	X1
	250°C	X2
	280°C	X3
	350°C	X4

4.6.1. X-Ray diffraction.

We carried out powder X-ray diffraction for each of the treated samples (figure 4.7). These series of diffraction patterns show at first glance the structural evolution of the xerogels, which is directly related to the temperature treatment. However, they seemed insensitive to the atmosphere used. The xerogels treated at lower temperatures (180°C), (marked with a • on figure 4.7), present typical diffraction peaks that are in good agreement with previous publications related to this kind of compounds. The low intensity and large peak width indicate a poor crystallinity. Treatments at higher temperatures led to materials in successive stages of evolution, ending with crystalline derivatives of V_2O_5, which are already detected in materials treated at 250°C (marked with a ■ in figure 4.7). But not until 350°C is the formation of the crystalline phase complete (marked with a ▲ in figure 4.7). These phases present narrower peaks implying higher crystallinity. On the other hand, xerogels treated at intermediate temperatures (250°C and 280°C) present some revealing aspects. For example, the additional peak at lower angles (around $2\theta = 10^o$ with a spacing around 8.7 Å) has not been described in previous publications. It seems to be associated to the formation of an intermediate phase coexisting within a short range of temperatures with the known xerogel and the crystalline V_2O_5 derivative.

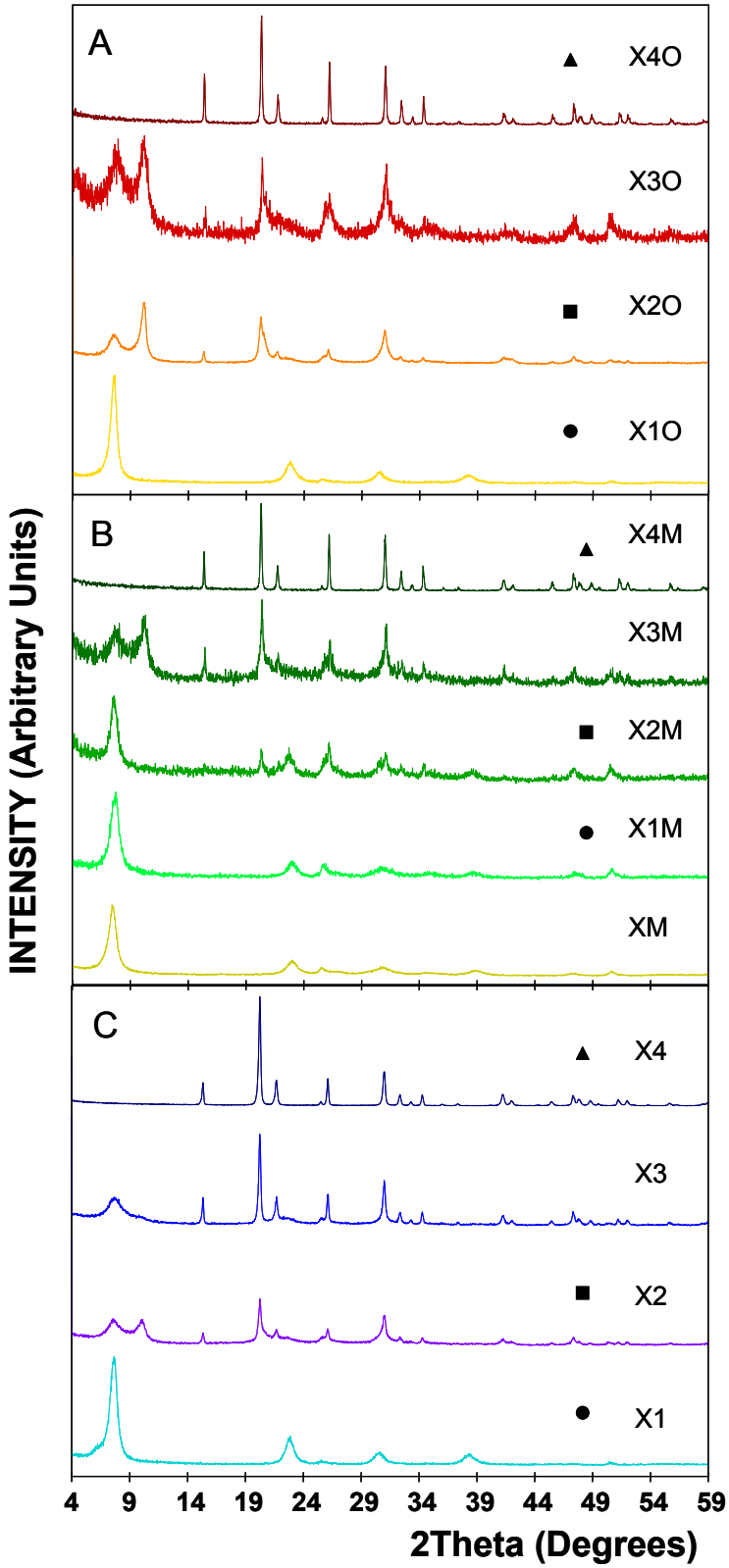

Figure 4.7.- Powder X-Ray diffraction of V_2O_5 xerogels under different treatments: A) set treated under oxygen, B) set treated under air, and C)set under argon. The order of each set of difractograms from top to bottom is the sample treated at 350°C to the lowest temperature treatment of 180°C, excepting the air set which is of 100°C. The (●) indicates samples treated at 180°C. The (■) indicates samples treated at 250°C. The (▲) indicates crystalline samples treated at 350°C.

One of the most significant and informative characteristic of the diffraction patterns from these xerogels, is the peak at lower angles (2θ = 7.5-7.7°) (only absent in crystalline samples, marked with a ▲ of figure 4.7). This peak corresponds to the 001 planes of the layer structure of V_2O_5. In the different samples of xerogels, we have spacings between 11.77 and 11.41Å. This spacing corresponds to the c parameter, where in the case of the crystalline samples, it is between 4.36-4.38Å (figure 4.7, samples marked with ▲), appearing at a higher angle of 20.24-20.34°, indicating the crystalline phase of V_2O_5. This data is in good accordance with previous publications [37-39].

The distance between V_2O_5 layers, as determined from 001 peaks, can vary depending on the temperature and atmosphere of treatment given to the xerogel. There have been different spacings published for V_2O_5 xerogels, for example: 11.36Å (2θ=7.78) [2,6], 11.5Å [40], and 11.4Å [35], differences which could be the result of small differences in treatments. In figure 4.8 we represent the spacing variation of our xerogels vs. temperature and gas used.

We can observe in general, a tendency to decrease the interlayer spacing c as the temperature treatment increases. This behavior is expected, because the 11.5Å spacing corresponds to water between the layers of the xerogel. In treating the xerogels at successively higher temperatures, the water between the layers diminishes until the structure collapses giving way to the crystalline V_2O_5. Our data suggests that we have a continuing series of xerogels, with spacings and intermediate water content between both extremes. This hypothesis is confirmed by the

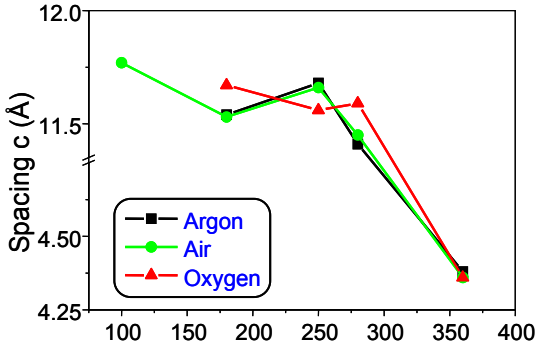

Figure 4.8.- Dependence of temperature and atmosphere treatments of the xerogels vs. the spacings between the layers of V_2O_5.

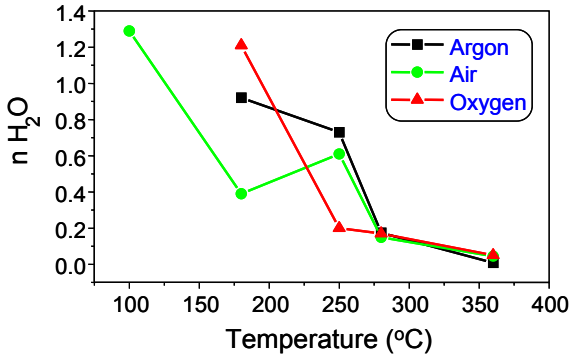

Figure 4.9.- Water mols present in the different xerogels (V_2O_5 ·nH_2O), treated at different temperatures and atmospheres.

data included in figure 4.9, which shows how water content changes with the treatment temperature (water contents of the xerogels were determined by thermogravimetric analyses under oxygen, heating at a rate of 10°C/min up to 550°C for 4 hours).

We can derive some interesting conclusions from this data. First, the higher the treatment temperature raises, the lower the quantity of water between the layers. On the other hand, the atmosphere of treatment has no significant relevance on this aspect. Finally, at 350°C the layer structure collapses giving way to a crystalline form of V_2O_5. At this temperature we almost eliminate all the water from the structure, including chemically bonded water.

4.6.2. Infrared Spectroscopy (FTIR).

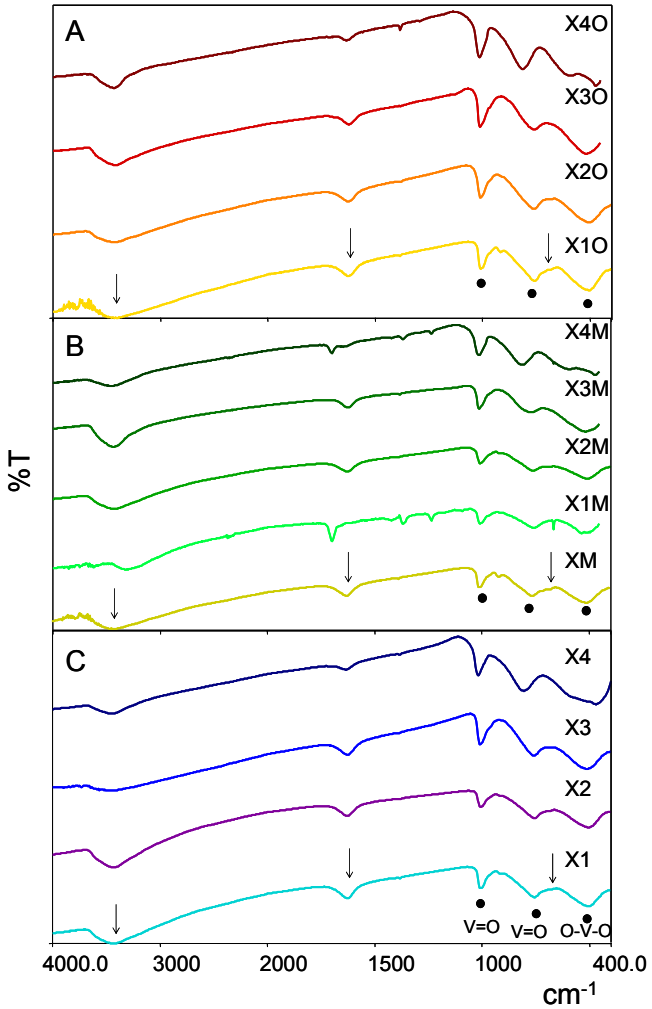

Figure 4.10.- Infrared spectra of the different V_2O_5 xerogels submitted under different treatments. A)set of xerogels treated under oxygen, B) set under air and, C) set under argon. The vibrational modes marked with (•) belong to V_2O_5, and with arrows the hydration water.

As part of the basic characterization of the V_2O_5 xerogels, we report the infrared spectra of the different materials treated under diverse atmospheres and temperatures. In figure 4.10, we present the FTIR analyses for each set of xerogels.

Characteristic vibrational modes from V_2O_5 appear below 1100 cm^{-1}. The band around 1008-1020 cm^{-1} corresponds to V=O stretching vibration [7] and, around 760 cm^{-1} and 510 cm^{-1} to V – O – V stretching mode [41]. All these bands are marked with circles in figure 4.10. Typical hydration water bands are around 3450 cm^{-1} ("vibrational" O-H), 1627 cm^{-1} (bending), and 680 cm^{-1} (marked with arrows in figure 4.10 and 4.11); and they decrease with respect to V_2O_5 bands as the treatment temperature increases. In figure 4.11, we can better appreciate the evolution or disappearance of some hydration water bands in the xerogels.

Around 920 cm^{-1} (marked with an X in figure 4.11) there exists a band that has been described previously [2-7]; but only L. Abelo et al [42] has associated this vibrational mode (922 cm^{-1}) to the presence of H_2O-V bond. This band disappears as the temperature of treatment increases. In comparing these results with X-Ray diffraction, this additional weak band is observed only in the spectra where the xerogels were treated at lower temperatures (180°C) (figure 4.10, samples marked with■, •); which precisely corresponds to the samples with typically less crystalline diffraction patterns (figure 4.7a, b and c). The xerogels where we detect the presence of the crystalline phase (figure 4.7 curves d and further) are precisely the ones where this band is absent. So the results are in good agreement with the association of this vibrational mode.

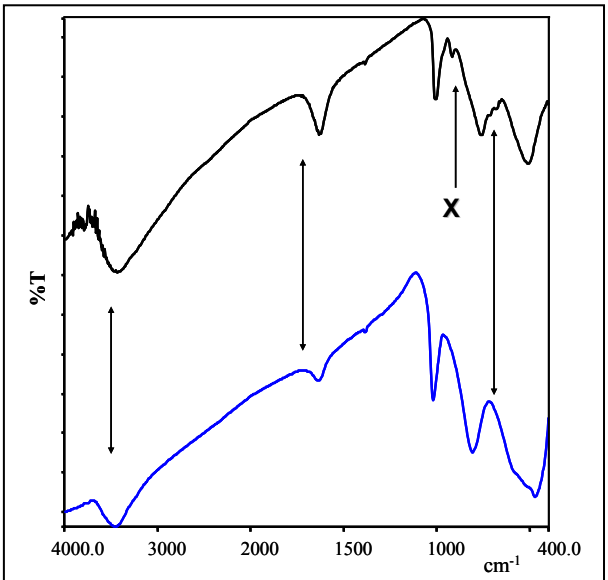

Figure 4.11.- Infrared spectra of sample treated at 180°C under argon(superior) and sample treated at 350°C(inferior), where we show the hydration water bands. X is a small peak that belongs to V_2O_5 amorphous phase.

4.6.3. Rechargeable Lithium Batteries.

Evaluation of the xerogels as cathodes in reversible Li cells was carried out by using the materials in powder form. In order to increase the electrical conductivity, the xerogel samples were crushed into a fine powder and thoroughly mixed with super P carbon (ratio 70:30% weight). In this section we will describe the behavior in reversible cells of diverse materials, analyzing the specific charge, voltage, cyclability, etc; in relation to their chemical and crystal-chemical characteristics, specifically, as a function the different thermal treatments, hydration state of the xerogels and the presence of crystalline phases.

4.6.3.1. Specific Charge

In figure 4.12 we summarize the values of specific charge as a function treatment temperature and atmosphere. These values have been obtained from the first of a series of charge-discharge cycles which will be presented below (under a discharge rate of C/6).

We can extract some interesting conclusions from figure 4.12, first of which is the relationship between the specific charge and the treatment temperature. As the treatment temperature increases, higher specific charges can be obtained. On the other hand, we detected an important influence of the atmosphere of treatment over the final electrochemical properties. Treatments in oxidizing atmospheres gave way to materials with higher specific charge, while the treatments in argon at the same temperatures led to lower values.

The temperature effect is probably due to the fact that at higher treatment temperatures the hydration water content in the xerogels is decreased. On the other hand, the effect of the atmosphere is logical; since an oxidative treatment (oxygen, air) can oxidize the V(IV) to V(V) present in the xerogel, thus, increasing the specific charge .[2,4,6].

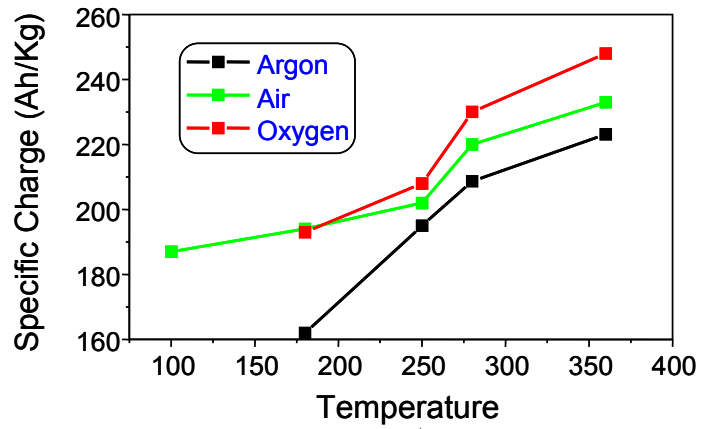

Figure 4.12.-Specific Charge of the 1st discharge of each xerogel, at a cycling velocity of C/6.

4.6.3.2. Effect of the presence of crystalline phase

In this section, our main emphasis will be in identifying the presence of the crystalline phase in some xerogels associated to its characteristic electrochemical behavior. In figure 4.13, we show the first discharge-charge cycle of cells with the treated xerogels as active cathode materials vs. lithium anodes. The cells were cycled in a 3.8-2.1V range, at the current needed to discharge for 6 hours (C/6). Aside from the effect of the treatments on the specific charge (which was summarized in the previous section), in this series of experiments we can appreciate a clear change in the shape of the polarization curves as a function of the treatment temperature of the xerogels. Thus, the materials treated at lower temperatures (180°C) show discharge profiles where the voltage decreases almost linearly. But as the treatment temperature increases, independently of the applied atmosphere of treatment, the charge-discharge curves evolve towards the development of two "plateaus" separated by a characteristic step. These two plateaus are most apparent in the case of crystalline V_2O_5 phase; especially present in the samples treated at 350°C (figure 4.13, X4,X4O,X4M). In accordance with the literature [18,37], these "plateaus" are due to a structural modification giving way to the development of different crystalline phases, when Li ions are intercalated in the original structure.

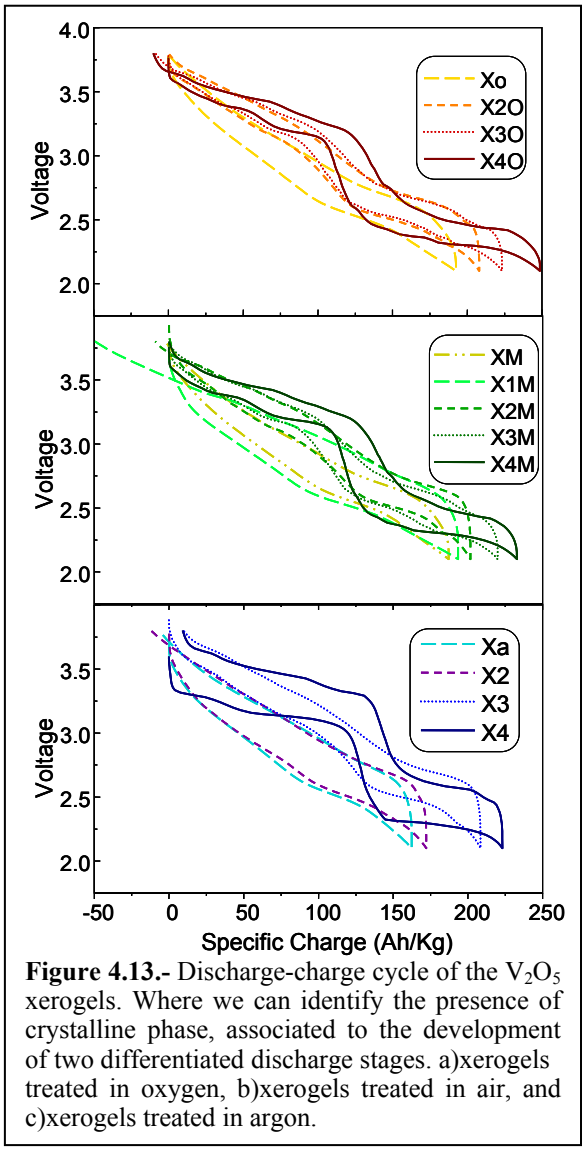

Figure 4.13.- Discharge-charge cycle of the V_2O_5 xerogels. Where we can identify the presence of crystalline phase, associated to the development of two differentiated discharge stages. a)xerogels treated in oxygen, b)xerogels treated in air, and c)xerogels treated in argon.

We have to emphasize that the development of these two plateaus is gradual with temperature treatments and is well correlated with the XRD data. If we check figure 4.7, the XRD patterns

show the presence of crystalline V_2O_5 phase starting from 250°C (figure 4.7 starting from samples ■); and finishing at 350°C with the pure crystalline phase. Correlated with this observations, the samples studied show a stepwise discharge (independently of the atmosphere used) starting from 250°C and leading to a most pronounced step for the samples treated at 350°C. This confirms the relationship between the growth of crystalline V_2O_5 and the presence of two "plateaus" in the discharge-charge curves.

4.6.3.3. Cyclability

Besides the specific charge, we evaluated the performance of rechargeable lithium cells by their capacity to repeat cycles with the least loss of specific charge. These cyclability properties can often be improved by technological developments. In other words, the materials used in the batteries can also be designed or modified to optimize their cyclability properties because they are part of the characteristics of the complete cell design. In our case, we have studied the effect of the several treatments of V_2O_5 xerogels on the cell cyclabilities.

We show in figure 4.14 the relative charge loss of the cell for each of the cathodic xerogels after 15 cycles at a C/6 rate.

We can confirm that a thermal treatment at moderated temperatures seems to influence positively the cyclability. For example: for the oxidizing atmospheres (air and oxygen) the cyclability is better when treated at 250°C or 280°C, than when treated at 180°C and 100°C. For the argon atmosphere the cyclability is better when treated at 180°C and 250°C. The data suggest that the elimination of water is not only beneficial to reach higher values of specific charge, but also to maintain it in successive discharge-charge cycles. The detrimental effect of the presence of water in the cyclability of lithium cells, has been frequently mentioned in the literature for other types of cathodes. Water gives way to undesirable reactions and influences the cyclability of the anode.[43].

The samples treated at higher temperatures (up to 350°C) have the worst cyclability. In this case the amount of water is even lower. However, this cyclability deficiency can be attributed to the presence of the V_2O_5 crystalline phase. This is due to the existence of long range order in V_2O_5 added to the presence of a certain phase change during the intercalation of lithium, (as shown by the stepwise discharge profile) making the reversibility process difficult. It is well known that an ideal redox process for energy storage is the one that takes place with minimum structural change.

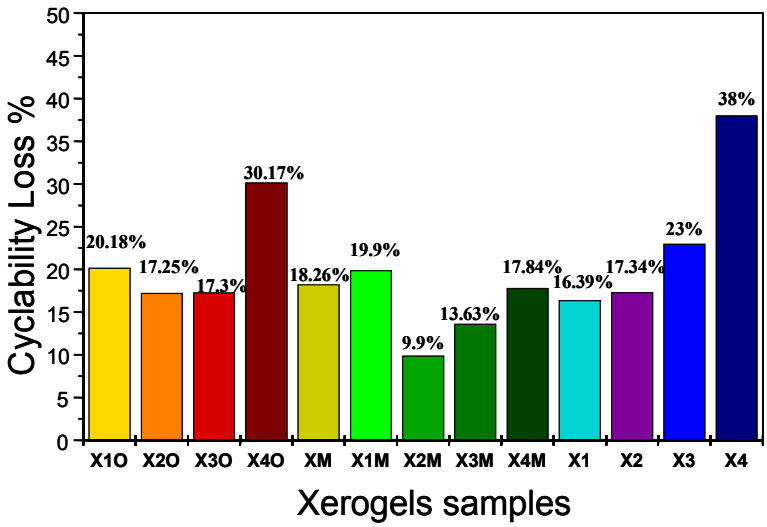

Figure 4.14.- Representation of the cyclability loss (measure as the relative charge loss in 15 cycles) of V_2O_5 xerogels, displayed by atmospheres of treatment. Red range: oxygen, Green range: air, and blue range: argon.

In the case of the xerogels (which are practically amorphous) the structural change is minimum, due to the presence of just short-range order. On the contrary, in the crystalline V_2O_5 the phase change associated to the redox process (extended at long range) renders the process less reversible. [44]

Therefore, we must conclude that concerning cyclability, two opposing factors combine so that materials treated at intermediate temperatures present the best cyclability. That is, the best xerogel materials of our study are those combining a minimum amount of water (temperatures as high as possible) and minimum crystalline phase present.

REFERENCES

[1] Winter,M.; Besenhard, J.O.; Spahr, M.E.; Novak, P.; *Adv. Mater.* **1988**(111), 725.
[2] Lira-Cantu, M.; Gomez-Romero, P.; *Int. J. Inorg. Mat.* **1999**(1), 111.
[3] Kanatzidis, M..; Wu, C.G.*; J. Am. Chem.* **1989**(111), 4139
[4] Lira-Cantu, M.; Gomez-Romero, P.; *Solid State Chem.* **1999**(147), 601.
[5] Leroux, F.; Goward, G.; Power, W.P.; Nazar, L.F.; *J. Electrochem. Soc.* **1997**(144), 3886.
[6] Lira-Cantu, M.; Gomez-Romero, P.; *J. Electrochem. Soc.* **1999**(146), 2029.
[7] Schindler, M.; Hawthorne, F.C.; Baur, W.H.; *Chem. Mater.* **2000**(12), 1248.
[8] Ohzuku, T.; Ueda, A.; Solid State Ionics 1994, 69, 201.
[9] Braithwaite, J.S.; Catlow, C.R.A.; Gale, J.D.; Harding, J.H.; *Chem. Mater.* **1999**(1),1990.
[10] Pecquenard, B.; Gourier, D.; Baffier, N.; *Sol.d State Ion.* **1995**(78), 287.
[11] Dai, J.; Li, S.F.Y.; Gao, Z.; Siow, K.S.; *Chem. Mater.* **1999**(11), 3086-3090.
[12] Delmas, C.; Cognac-Auradou; Cocciantelli, JJ.M.; Menetrier, M.; Doumerc, J.P.; *Solid State Ion.* **1994**(69), 257.
[13] West, K.; Zachau-Christiansen, B.; Jacobsen, T.; Skaarup, S.; *Solid State Ion.* **1995**(76), 15.
[14] García-Alvarado, F.; Tarascon, J.M.; *Solid State Ionics* **1993**(63-65), 401.
[15] Tipton, A.L.; Passerini, S.; Le, D.B.; Owens,B.B.; *Electrochem. Soc.* **1995**(94), 414.
[16] Giogetti, M.; Passerini, S.; Smyrl, W.H.; Mukerjee, S.; Yang, X.Q.; McBreen, J.; *J. Electrochem. Soc.* **1999**(146), 2387.
[17] Passerini, S.; Ressler, J.J.; Le, D.B.; Owens, B.B.; Smyrl, W.H.; *Electrochim. Acta* **1999**(44), 2209.
[18] West,K., Zachau-Christiansen, B.; Jacobsen, T.; Skaarup, S.; *Electrochem. Acta* **1993**(38), 1215.
[19] Morales, J.; *Anal. de Quim.* **1991**(87), 691.
[20] Park, H.K.; Smyrl, W.H.; *J. Electrochem. Soc.* **1994**(141), L25.
[21] Livage, J. *Chem. Mater*. **1991**(3), 578.
[22] Takiyama, K.; **1958**(31), 329.
[23] Lemerle, J.; Nejem, L.; Lefebvre, J.; *J. Inorg. Nucl. Chem.* **1980**(42), 17.
[24] Gharbi, N.: Sanchez, C.; Livage, J.; Lemerle, J.; Nejem, L.; Lefebvre, J.; *J. Inorg. Chem.* **1982**(21), 2758.
[25] Le, D.B.; Passerini, S.; Owens, B.B.; Smyrl, W.H.; *J. Electrochem. Soc.* **1995**(142), L102.
[26] Cousier, F.; Passerini, S.; Smyrl, W.H.; *J. Electrochem. Soc.* **1998**(145),L73.
[27] Le, D.B.; Passerini, S.; Guo, J.; Ressler, J.; Owens, B.B.; Smyrl, W.H.; *J. Electrochem. Soc.* **1996**(143), 2099.
[28] Hirashima, H.; Sudor, K.; *J. Non-Cryst. Sol.* **1992**(145), 51.
[29] Tipton, A.L.; Passerini, S.; Owens, B.B.; Smyrl, W.H.; *J. Electrochem. Soc.* **1996**(143), 3473.
[30] Hirashima, H.; GenGyo, M.; Kojima, C.; Imai, H.; *J. Non-Cryst. Sol.* **1995**(186), 54.
[31] Park, H.K.; Smyrl, W.H.; Ward, M.D.; *J.Electrochem. Soc.* **1995**(142), 1068.
[32] Almeida, E.C.; Abbate, M.; Rosolen, J.M.; *Solid State Ionics* **2002**(140), 241.
[33] Giorgetti, M.; Passerini, S.; Smyrl, W.H.; Mukerjee, S.; Yang, X.Q.; McBreen, J.; *J. Electrochem. Soc.* **1999**(146), 2387.
[34] Yao, T.; Oka, Y.; Yamamoto, N.; *Mat. Res. Bull.* **1992**(27), 669.
[35] Passerini, S.; Chang, D.; Chu, X.; Le, B.L.; Smyrl, W.; *Chem. Mater.* **1995**(7),780.
[36] Kolthoff, I.M.; Sandell, E.B.; Meehan, E.J.; Bruckenstein,S.; *Analisis Quimico Cuantitativo*; 6ta. Ed. Buenos Aires, **1969**.
[37] West,K.; Zachau-Christiansen,B.; Skaarup, S.V.; *Solid State Ion.* **1992**(57), 41.
[38] Shimizu, A.; Tsuma, T.; Inagaki, M.; *Solid State Ion.* **1993**(63-65), 479.
[39] Sayle, D.C.; Gay, D.H.; Rohl, A.L.; Catlow, C.R.A.; Harding, J.H.; Nortier, P.; *J. Mater. Chem.* **1996**(6), 653.
[40] Hibino, M.; Ugaji, M.; Kishimoto, A.; Kudo, T.; *Solid State Ionics* **1995**(79), 239.
[41] Lira-Cantu, M.; *Materiales Hibridos Organico-Inorganico a base de Fosfomolibdato o Pentoxido de Vanadio Dispersos en Polimeros Organicos Conductores. Aplicación como Electrodos de Insercion en Baterias de Litio*.; Ed. Universitat Autonoma de Barcelona: Barcelona, **1997**, pp.244.

[42] Abello, L.; Husson, E.; Repelin, Y.; Lucazeau, G.; *J. Solid State Chem.* **1985**(56), 379.
[43] Glanz, J.; *Science* **1994**(264), 1084.
[44] Shembel, E.; Apostolova, R.; Nagirny, V.; Aurbach, D.; Markovsky, B.; *J. Power Sources* **1999**(80), 90.

Chapter 5

PAni/V_2O_5 Hybrid Materials

Abstract:

We have studied the electrochemical behavior in lithium reversible cells, of hybrids based on an "in situ" oxidative polymerization of aniline with vanadium pentoxide hydrogels by a modified chemical synthesis. We evaluated the effect of synthetic parameters and oxygen treatments on the microstructure and electroactivity of PAni/V_2O_5 hybrids. We carried out the characterization of these materials by XRD, SEM, BET, FTIR, TGA and elemental. The modified synthesis described here leads to highly microporous materials and reduces the need for thermal oxygen treatments to optimize their electrochemical activity. It also induces the incorporation of additional aniline without a great excess of the monomer. We obtained hybrids of PAni/V_2O_5 with high specific charges, up to 280Ah/Kg (at C/6). However this charge slowly fades, stabilizing around 50-60 Ah/Kg after 100 cycles in a typically capacitive behavior. On the other hand, this charge fading is not associated to the destruction or decomposition of the hybrid material as it will be discussed.

5.1. INTRODUCTION

A Nanocomposite organic-inorganic hybrid material involves a new strategy for the preparation of materials with synergic behavior, a complementary behavior between the organic phase and the inorganic phase [1]. Hybrids based on conducting organic polymers (COPs) constitute a small branch of the entire field of hybrid materials. COPs can be grown within van der Waals gaps of layered inorganic phases by polymerization of the corresponding intercalated monomers. In this case this type of hybrid belongs to the category we have labeled as IO (inorganic-organic) hybrid materials [1]. In this line of work, the performance of lamellar inorganic solids as host networks for organic compounds has been applied to obtain materials with polymeric insertion with the desired properties.

One of the most extensively studied and better characterized IO systems is the family of hybrids based on V_2O_5 as the inorganic host. [2-25]. As for any other IO material, the formation of hybrids of COPs inserted in V_2O_5 takes place with the initial intercalation of the corresponding monomer molecules into the inorganic layered structure. The strongly oxidizing character of the oxide induces the redox polymerization of the organic molecules.[8] It is worth remarking that while the inserted polymer is effectively p-doped (partially oxidized) during this process, the V_2O_5 oxide suffers itself a partial reduction that renders it an n-doped (partially reduced) electrically conductive mixed valance (V^{IV}/V^{V}) oxide. Thus, in this process, a mutual doping takes place during redox intercalative polymerization, leading to a material with a double conduction mechanism. [1, 3, 8]

Among CPOs inserted into V_2O_5 we can find reports dealing mostly with polyaniline (PAni) [3,8,12-16,20-23], polypyrrole (PPy) [2,11,17-19], or polythiophene (PTh) [4,11,24]. Specifically; in the last decade, studies on PAni-V_2O_5 hybrids have been centered on their chemistry [4,5,8,13] as well as on their design and synthesis for application as insertion cathodes in rechargeable lithium cells [1,10-12,14-15, 22]. In earlier studies the synthesis included the reaction of anilinum iodide or aniline with preformed films of dry xerogels [3,5-8], or crystalline V_2O_5 particles [12]. More recently, the synthesis procedure has been directed to the simultaneous formation of the organic and inorganic components of the hybrid. [13-15,20]

Figure 5.1 shows an idealized schematic structure of the hybrid synthesized with aniline and V_2O_5.gel.

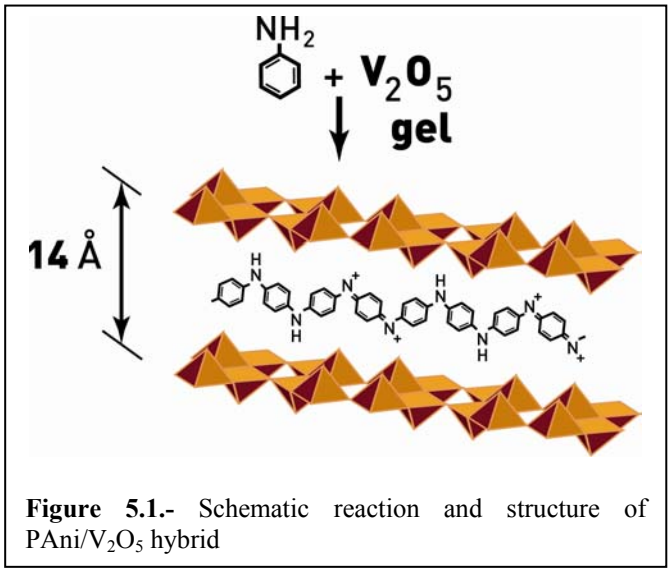

Figure 5.1.- Schematic reaction and structure of PAni/V_2O_5 hybrid

For their application as insertion electrode in rechargeable Li cells, it should be noted that the hybrid materials benefit from the electrochemical activity of both organic and inorganic components and that both contributions effectively correspond to the intercalation of cations, making the material useful within the optimal source-sink reversible cell mechanism [9]. But in addition, there are features like the improved lithium diffusion (Li^+ diffusion coefficients were found to be one order of magnitude better in the hybrids than in the parent V_2O_5 xerogel) [9], or the added capacity of the PAni-V_2O_5 combination that make the performance of the hybrid superior to the sum of its components, in a characteristic synergic behavior [10].

In earlier work carried out in our group, related to PAni/V_2O_5 hybrid materials, [13-15,25], we detected hints of the important influence of certain synthetic parameters on the microstructure and electrochemical properties of these hybrid materials. There were factors such as the stirring procedures during synthesis or oxygen treatments, which were poorly controlled and understood but which were probably affecting the electrochemical activity and final performance of our materials when they were used as cathodes in rechargeable Li cells. These are precisely the aspects that we have studied and will be discussed in this chapter. We will also evaluate the possibility of using these hybrid materials as cathodes in combination with anodes other than lithium (i.e. lithium-inserting graphite's), as well as the behavior of the hybrids during extended periods of charge-discharge (up to 100 cycles). In addition to the electrochemical studies, other techniques like FTIR, powder XRD, SEM, BET, elemental analysis and TGA have been used to further characterize and understand this complex PAni/V_2O_5 system.

5.2. PAni / V_2O_5 SYNTHESIS

For the synthesis of PAni/V_2O_5 hybrids, we carried out an oxidative polymerization of aniline by reacting the monomer "in-situ" directly with V_2O_5 hydrogels, as described by Lira-Cantú [26]. Thus, 1ml aniline was raised to 50ml with deionized water and this solution was added to the corresponding amount of V_2O_5 gel also raised to 50ml with water. The gel had been previously aged for two months and analyzed for V(V) content, in order to determine the amount of V(IV) needed to get an Aniline:V(V) molar ratio of 3:1. The reaction was carried out in an ice bath, with magnetic stirring at 300 rpm, during 120 hours. In previous work by lira-Cantu et al [14,26] and Goward et al. [11] a mild thermal treatment with oxygen at 80^{o}C was found to improve the electrochemical properties (specifically the specific charge) of the resulting hybrids. However, much remained to be studied concerning the performance of these hybrid materials in real lithium cells, in particular their cyclability and the relationship between specific charge/energy density and cyclability with composition and microstructure. In turn, composition and microstructure depend strongly on synthetic conditions, especially when polymeric systems (organic or inorganic) are concerned. With the series of experiments described here we have first tried to show the reproducibility of a complex heterogeneous synthesis of these PAni/V_2O_5 hybrids. Furthermore we have studied the effect of reaction conditions, specifically stirring procedures on the microstructure and electrochemistry of the resulting hybrids.

We carried out a series of syntheses of PAni/V_2O_5 hybrids, beginning with aniline solutions and V_2O_5 gels in the conditions described above; only the stirring procedure was varied. In each case we titrated potentiometrically the amount of V(V) in the V_2O_5 gel (section 4.2) before we proceeded with the synthesis of the hybrid. In all cases (excepting A4 and A5, which are shown further on) we used 50 ml volumes for the solutions of aniline and V_2O_5 gel. The gel was used immediately after the potentiometric titration.

For comparison, in section 5.5 we synthesized two extra samples of PAni/V_2O_5 hybrid, as described by Lira-Cantú [13]. Sample P3 was made with a 3:1 molar ratio, in an ice bath, with magnetic stirring at 300 rpm, during 120 hours; and P14 same as sample P3 changing only the molar ratio to 14:1.

5.2.1. Type of stirring effect.

Through these tests we attempt to explore the possibility of preparing hybrid materials with porous microstructures by means of controlling the stirring procedures during the synthesis, attempting to develop a growth of the hybrids in a liquid-air interface.

We applied five types of stirring procedures, in the order of increasing intensity:

A1) magnetic stirring with air bubbler,

A2) turbine mechanical stirring,

A3) turbo-propeller mechanical stirring,

A4) mechanical mixer, and finally

A5) as in A4, but with successive intervals of resting-stirring.

The diversity of obtained materials was characterized by elemental analysis, TGA, FTIR, XRD, SEM and BET. Notwithstanding, the principal criterion used for the critical evaluation of the results, is the behavior of each material as cathode in rechargeable lithium batteries (at a charge-discharge rate of C/6 as powder cathodes).

- *Magnetic stirring with air bubbler (A1).*

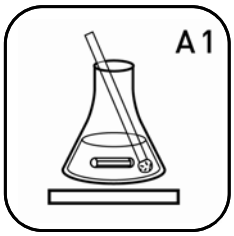

We carried out the synthesis with the conditions mentioned above in a 250 ml erlenmeyer with magnetic stirring (2.5 cm magnetic stirrer) and a gas diffuser used as a bubbler submerged in the reaction mixture of PAni/ V_2O_5, immediately following the addition of aniline to the V_2O_5 gel. After the 5 days reaction, the resulting solid was filtered-off, washed with water, and dried under vacuum. This solid had a powdery texture and spongy aspect. We tried it as a cathode in a rechargeable lithium battery, obtaining a specific charge of 143 Ah/Kg for the first cycle.

- *Turbine Mechanical stirring (A2).*

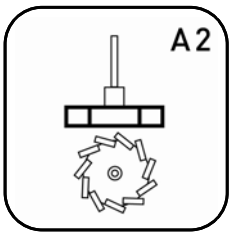

The synthesis was carried out in the same way, but instead of using a magnetic stirrer and a bubbler, we used mechanical stirring with a turbine propeller at 300 rpm. The resulting solid was filtered-off, washed and dried under vacuum. When used as active cathode material in a rechargeable lithium battery, we obtained a specific charge of 173 Ah/Kg for the first cycle.

- *Turbo-propeller Mechanical stirring (A3).*

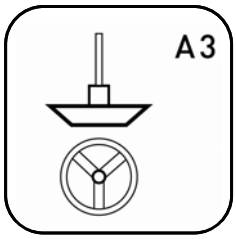

The procedure was similar to the last one, but we used a different propeller design; which produces higher turbulence in the mixture. In this case, we could see higher mobility, so we decided to vary the reaction time to see if it had an influence on the results. We carried out three different syntheses: A35 performed in 120 hours (5 days), A33 in 72 hours (3 days), and the last one A32 in 48 hours (2 days). The resulting solids where filtered-off, washed, and dried under vacuum. We tried them as cathodes in lithium insertion batteries, obtaining different specific charges: for A35 a value of 152 Ah/Kg, for A33 195 Ah/Kg, and finally for A32 a specific charge of 175 Ah/Kg.

This series of experiments tells us that the reaction time is an important parameter to take into account during the synthesis when we apply a different stirring procedure. In other words, the reaction time is correlated with the type of stirring used. So for example, in the synthesis procedure optimized by Lira-Cantu using a conventional magnetic stirring, the optimum reaction time was 120 hours (5 days); while in our case by using a more vigorous stirring procedure, the optimum time was 72 hours (3 days). Although this is not a surprising result, this data shows the need to optimize the synthesis of these complex hybrid materials, which combine the growth of inorganic polymeric gels with the organic polymeric chains.

- *Mechanical mixer (A4).*

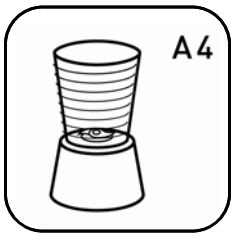

As our previous results show, it is obvious that, by applying a more turbulent type of stirring during the hybrid synthesis, we get better contact between the reagents and the air, and better electrochemical results. That is why our next optimization step was to apply a mechanical mixer where stirring is more turbulent. We carried out the synthesis using the same stoichiometric amounts, but with some modification imposed by the stirring method. For example, we doubled the volume of the reagents because the mechanical mixer used needed more volume to stir properly; and the temperature of synthesis used was room temperature because we could not arrange an ice bath. Finally, we also carried out experiments modifying the reaction time in order to optimize it for this specific stirring procedure.

By applying this type of stirring we can observe the maximum turbulence or mobility reached until now. Permanent foaming is seen, indicating a higher contact with ambient air and between the reagents. We carried out three different syntheses with variable reaction times: 72 hours (3 days) for sample A43, 48 hours (2 days) for sample A42 and 24 hours (1 day) for A41.

In all A4 hybrid samples, foaming is seen during reaction time, and the mixture temperature reached 45 ^{o}C, due to warm up produced by the mechanical stirring. The resulting solids were filtered-off, washed and dried under vacuum. When we analyzed them as cathodic materials in reversible lithium cells, we obtained positive results, confirming the beneficial effect of the most vigorous stirring on the electrochemical charge capacity of these materials The initial specific charge for each sample was: for A43, 196 Ah/Kg, for A42, 199 Ah/Kg, and for A41, 192 Ah/Kg. Some of these results were further improved by a post-treatment in oxygen that will be explained later.

- *Stirring type A4, but with resting-stirring intervals (A5).*

In this case, the hybrid synthesis was performed by using the same method and reaction times (72, 48 and 24 hours) as A4. The only difference is that the stirring was done in time intervals followed by a rest period, in order to keep the synthesis temperature low. The stirring was applied in 10 minute intervals, followed by 1 hour of resting in a cooler at 5^{o}C. We obtained three samples at different reaction times: A5A with a total of 24 hours, A5B with 48 hours total, and A5C with 72 hours. Surprisingly, the results were not as positive as in the case of the A4 procedure. The discharge capacities decreased to 150 Ah/Kg, which indicates that the synthesis temperature of 45^{o}C is not so detrimental to the final electrochemical properties of these hybrid materials. This emphasizes that the stirring procedure is as important as other synthesis parameters such as reaction temperature.

Figure 5.2 presents a comparative analysis of the specific charge of each synthesized hybrid sample for 15 cycles applying a charge-discharge current density of 36.7 mA/g (i.e. a rate of C/7.5, considering 2.5Li intercalation). The line marked as the “reference” corresponds to the best results of Lira-Cantú (not published), with an irregular magnetic stirring (a turbulent agitation that gave way to a spongy substance too hard to reproduce). It should be noted that all these cells were set up using composite powder cathodes, that is, with the hybrid materials mixed with just C super-P (30%) (no binder). From all these data we can see that cyclabilities are relatively

similar for all samples, with a continuous decrease in specific charge, the initial values marking the differences between the different materials.

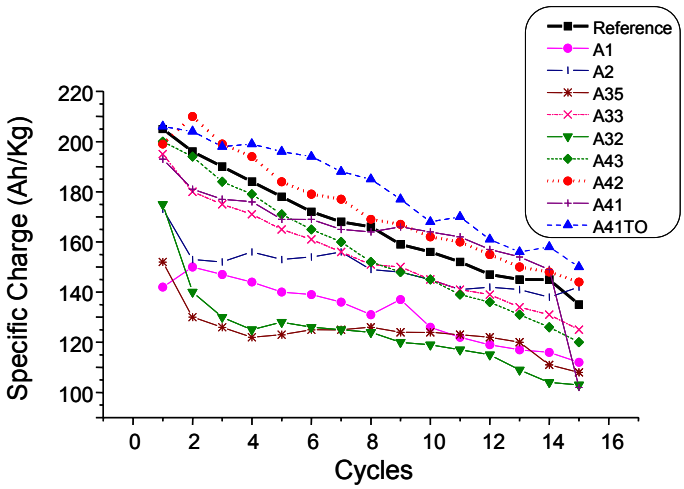

Figure. 5.2.- Graphic representation of the specific charge when applying a I= 36.7 mA/g (C/7.5,2.5Li) rate vs. cycle number for all the different samples of PAni/V_2O_5 hybrids; obtain by different stirring procedures

5.2.2. Oxygen treatments.

Initially, mild thermal treatments at 80°C under oxygen were found to improve the initial specific charge of PAni/V_2O_5 hybrids. This was explained in terms of the reoxidation of V(IV) centers (formed when aniline is polymerized) to V(V) [3].

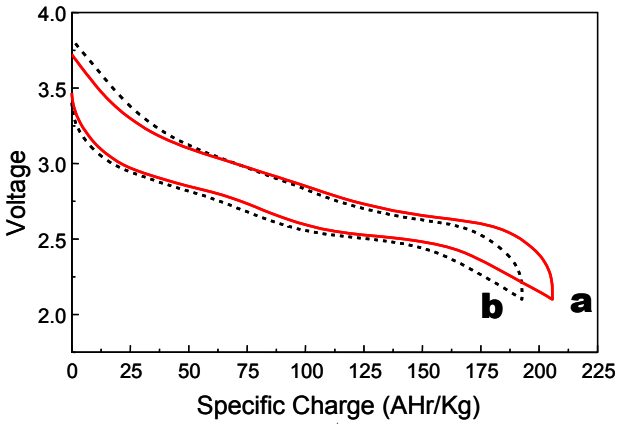

Figure. 5.3.- Comparison of 1st discharge cycle at a rate of C/6, of samples (a) A41TO and (b) A41.

In contrast with those results we have found that for our samples, prepared by the modified stirring procedures described above, that kind of mild treatments in oxygen does not help to achieve better specific charge. On the contrary they experiment losses from their initial specific charge that range from 4.5% to 26%. Only sample A41 was slightly improved (see figure 5.3) from 192 Ah/Kg to 206 Ah/Kg, upon thermal treatment (heating at 5ºC/min up to 80ºC and keeping it for 5h). All other samples got lower values for specific charges after the same treatment.

This could be explained if the enhanced contact between the reacting mixtures and air would facilitate the oxidation of V(IV) without any need for further treatments. In this respect, the modified stirring procedures for synthesis are not only the basis for a more porous microstructure (as will be later confirmed by BET analysis) but also avoid the need for post-synthesis treatments.

Interestingly, the A41 sample, the one exceptionally getting improved upon oxygen treatment, corresponds to the sample with a shorter reaction time and a less porous microstructure as will be presented below.

5.3. PAni/V_2O_5 HYBRID CHARACTERIZATION

In this section we will describe the results of the diverse techniques of chemical, structural, and spectroscopic characterization of our optimized hybrid samples. These samples, which have the best properties, are: A33, A43, A42 and A41TO. We determined the empirical formulas by a combination of elemental and thermogravimetric analyses. We carried out XRD, FTIR and SEM analyses in order to compare with the reference sample. BET analyses were also performed, giving us information about the surface area and the microporous nature of our samples.

5.3.1. XRD (X ray diffraction).

The diffraction patterns of our hybrids are shown in figure 5.4. They present peaks characteristic of V_2O_5 overlapped with broader diffuse scattering peaks associated to the presence of polyaniline. We observe less crystallinity in samples A33 and reference, than in samples A43, A42 and A41TO. As we will discuss later, the morphology detected by SEM in these three samples is similar and different in turn to that of A33.

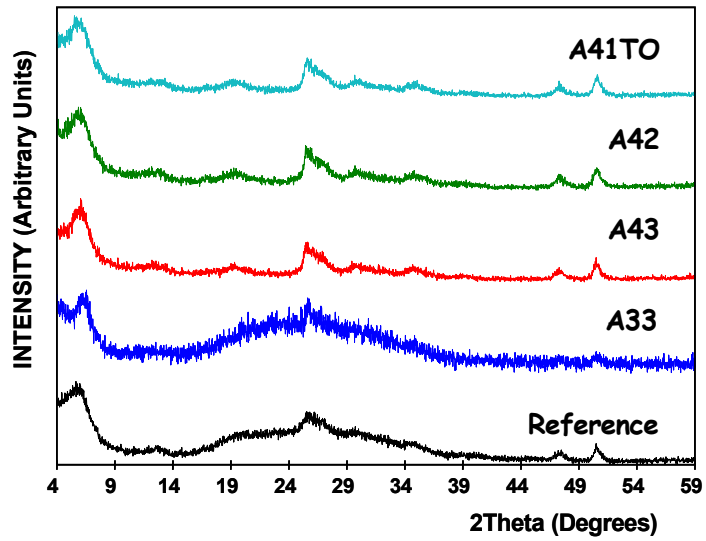

Figure 5.4.- XRD diffraction patterns of PAni/V_2O_5 best hybrid samples.

As in the case of V_2O_5 xerogels, the more intense peak at low angles corresponds to the 001 reflection. Its displacement to lower angles with respect to the xerogel indicates an expansion between the layers of V_2O_5 structure matrix [27]. Indeed, the 001 spacing is larger than in the hydrated xerogel (d=11.4 Å [15], and d=11.5 Å [10]) and somewhat variable depending on the samples, as indicated in table V .I

The net expansion that is summarized in that table represents the expansion associated to the volume occupied by the polymer chain. In order to estimate this expansion we have to take into account the expansion induced by water in the xerogel with 11.4 Å spacing (2.8 Å expansion [3,8])

Table V.I.- X ray powder diffraction data.

Hybrid material	Spacing d(Å)	2θ(°)	Expansion(Å)	Net Expansion(Å)[a]
Reference	14.8	5.96	3.4	6.2
A33	13.6	6.5	2.2	5.0
A43	15.2	5.9	3.8	6.6
A42	14.9	6.0	3.5	6.3
A41TO	14.8	6.0	3.4	6.2

[a] net expansion taking into account the 2.8 A occupied by intercalated water

Finally we can conclude that even though the expansion in some samples is slightly larger, it corresponds to the intercalation of only one layer of polyaniline (estimated as 5.58Å [3,6,8]). These differences can be attributed to the hydration level, or to slight conformational differences of the polymer in the V_2O_5 structure [10].

5.3.2. FTIR analysis.

In this section, we will present the infrared spectroscopy study of our hybrid materials. FTIR spectroscopy has been measured routinely as a convenient way to detect the presence of organic and inorganic components by means of their characteristic vibrational modes.

In figure 5.5, we present the infrared spectra of our best hybrids, where we can appreciate the vibrational modes of polyaniline in the emeraldine form, and the ones that correspond to V_2O_5. The vibrational modes of polyaniline (marked in figure 5.5 with arrows) that are in good accordance with previous publications [8,13-15,26], appeared approximately at 1172 cm^{-1} (C-H ring deformation), 1310 cm^{-1} (C-N arylic secondary amine stretch mode), a 1482 cm^{-1} (C=C aromatic stretch mode), and 1568 cm^{-1} (ring stretch mode between quinone and bencenic groups). The characteristic bands from V_2O_5 appear at 1008 cm^{-1} (stretching V=O), 752 cm^{-1} and 503 cm^{-1} are marked with circles in the figure.

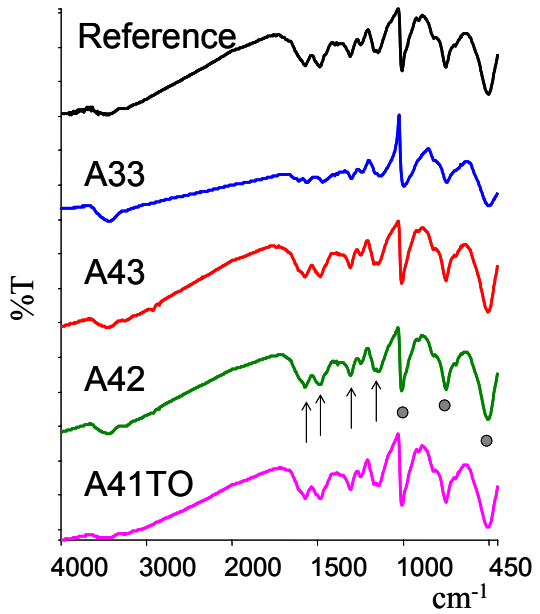

Figure 5.5.- Infrared spectra of the best Pani/V_2O_5 hybrids. The arrows mark the vibrational modes of polyaniline and the circles the ones assigned to V_2O_5.

5.3.3. Scanning electron microscope (SEM).

In figure 5.6, we can observe SEM photographs of the six hybrid samples at a magnifying scale (reference, A33, A43, A42, A41, and A41TO) where we can observe a three micron scale.

We can observe some differences between the samples of the SEM photographs of figure 5.6. Sample A33 has a larger grain size, agglomerated in plates with larger pores. Under higher magnification we did observe a spongy structure for this sample that was not seen in the other hybrid samples. In samples A42, A41 and A41TO, we can detect smaller grain size, agglomerated in plates with smaller pores. Finally, the reference and the A43 samples appear to be similar. They show a more

heterogeneous or polydispersed microstructure, as if they would have an A33 base but with smaller agglomerated grains on the surface as in samples A42, A41 and A41TO. Finally, it could be noted that there is no significant morphology difference between samples A41 and A41TO, showing no influence of the thermal treatment in oxygen.

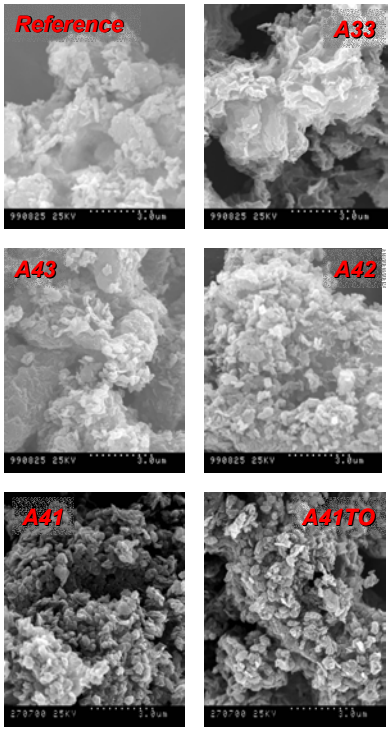

Figure 5.6.- SEM photographs (3μm scale): Reference, A33 (turbo-propeller, 3 days), A42 (2 days), A43 (3 days), A41 (1 day), and A41TO (1day, oxygen treatment). A4 series synthesized with mechanical mixer.

In principle (in the absence of undesired catalytic activity) the materials used as battery cathodes, should preferably present a small particle size in order to increase the active surface area in contact with the electrolyte and improve the ionic diffusion kinetics. We could conclude from SEM analyses, that samples A41, A41TO, A42 and A43 have a larger surface area, because the homogeneity of the small grain size is higher than in the reference and A33 samples.

5.3.4. BET Analyses.

We carried out nitrogen adsorption BET analysis for our samples in order to quantitatively determine their surface area and pore size distribution. [29] The surface area of our samples as determined from BET isotherms fall between 8.4 m^2/g and 99 m^2/g, as detailed in figure 5.7. This figure also tries to correlate surface area with synthetic parameters. Meaningful trends are seen within a particular series of related samples. Thus, we can detect a very significant change within the A4 series of materials. With all other synthetic parameters constant, the surface area of samples A4 increases linearly as the reaction time increases. Alternatively, the effect of post-synthesis oxygen treatment can be established by comparing samples A41 and A41TO (blue), we only detect a small increase of the surface area, when the sample is thermally treated in oxygen falling between the experimental values.

We have also included samples in this figure, data from samples previously prepared in our group (P3 and P14), as well as the already mentioned reference sample. They represent a case opposite to the series A4: Despite the fact that all of them were made in 120 hours reactions, their surface areas are very different due to the different synthetic conditions used (nominal amount of aniline used, stirring routine etc.).

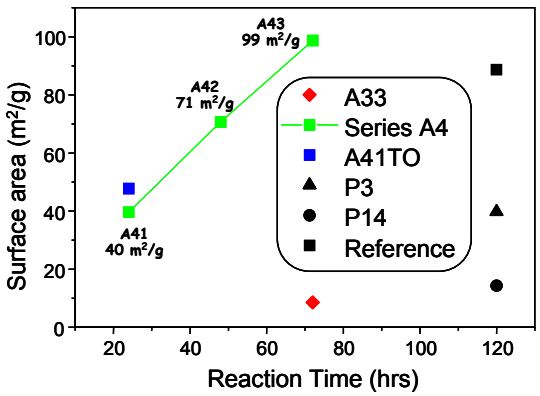

Figure 5.7.- Graph showing the surface area (BET) of samples A4 vs. time. We also include the reference, A33, P3 and P14 for comparison.

On the other hand, we also have determined the pore size distribution by BET analyses that have shown a mesoporosity for all PAni/V_2O_5 hybrid materials.

Finally, we could note the good correspondence between these BET data and the microstructure detected by SEM. Specifically, we can correlate the low surface area of sample A33 with the larger grain size already discussed from SEM images.

5.3.5. Chemical analyses and Stoichiometry determination

After each PAni/V_2O_5 synthesis, the samples were systematically dried under vacuum for three days at room temperature. Before we made the TGA and elemental analysis, we washed them in ethyl ether to eliminate possible soluble fractions that could be present in certain samples. After washing, we dried them again under vacuum for 24 hours at 30°C.

5.3.5.1. TGA Analyses

We carried out thermogravimetric analyses only for our best samples, A43, A42, A41TO, (the ones with better behavior as cathodes). Data are shown in figure 5.10, corresponding to an initial heating rate of 5°C/min up to 500°C under O_2, and then keeping the temperature for 4 hours. All three samples lead to similar weight loss patterns, with a characteristic structure best detected in the derivative curves (inset). The main loss in the TGAs of figure 5.8 corresponds to the decomposition of the polymer, although the last stage at ca. 400ºC could also correspond to the final crystallization process of V_2O_5. These weight losses can therefore be correlated with

the amount of polyaniline per V_2O_5. On the other hand, weight losses below or around 100ºC (assignable to water dehydration) are relatively small for all three samples, indicating an adequate drying procedure prior to TGA analysis. It should also be noted that the minor amounts of weakly bounded water in the hybrids are much smaller than in the corresponding V_2O_5 xerogels (see section 4.5)

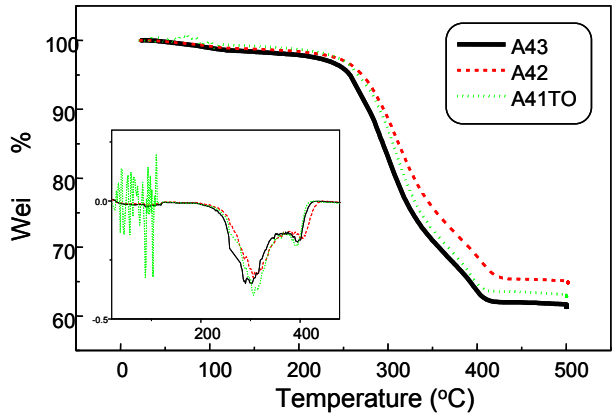

Figure 5.8. –TGA analysis of our optimized hybrids, under oxygen. In the inferior left box, we show the first derivative where we can see clearer the weight losses.

The water molecules of type II and III present in our hybrids (see section 4.4), cannot be quantitatively analyzed by TGA because their weight losses are overlapped with the combustion of the organic part (200ºC-450ºC). What we can clearly appreciate, aside from the thermal stability range, is that all our samples have similar ratios of polyaniline to vanadium pentoxide.

With the help of elemental analysis we can determine more precisely the amount of polyaniline, and, by difference with TGA data, the amount of water present in our hybrids, in order to finally propose an empirical formula for our hybrid materials.

5.3.5.2. Elemental Analyses.

The data from elemental analysis assists us in calculating the percentage of organic matter and composition of our hybrids. This analysis complements the TGA analysis. Once we calculate the stoichiometry, we can compare these experimental results of the amounts of C, H, and N, with the calculated results as indicated in table V.II.

Our results show that our hybrids have similar stoichiometries. The values for Ani:V(V) ratios cluster around one aniline ring per V_2O_5. First of all, it should be noted that this ratio is significantly different from the nominal ratio of 3:1 used in the reactions. The coincidence also seems to hint the formation of a well defined stoichiometric 1:1 adduct between polyaniline and V_2O_5 . Furthermore, it should be noted that earlier work also with 3:1 reaction mixtures had led to a different stoichiometry, specifically to materials with a 0.6:1 Ani:V_2O_5 experimental ratios [26]

Table V.II.- Summarized data from TGA and elemental analysis, in order to determine the stoichiometry and formula weight of the hybrid samples.

	An:V(V)	%C	%N	%H	$\%V_2O_5$ [a]	N/V_2O_5	Formula	Sample
Exp.	3:1	26.81	5.10	1.73	62.84	1.05	$\mathbf{(C_6H_4N)_{1.05}V_2O_5 \cdot 0.6H_2O}$	A41TO
Calc.		26.33	5.11	2.21	63.30		FW= 288.22	
Exp.	3:1	24.75	4.53	1.61	64.8	0.9	$\mathbf{(C_6H_4N)_{0.9}V_2O_5 \cdot 0.8H_2O}$	A42
Calc.		23.38	4.54	1.96	65.56		FW= 277.38	
Exp.	3:1	26.20	4.98	1.85	61.33	1.06	$\mathbf{(C_6H_4N)_{1.06}V_2O_5 \cdot H_2O}$	A43
Calc.		25.85	5.02	2.16	61.56		FW= 295.40	

[a] From residual weights in TGA analyses

On the other hand, as we have presented in section 5.3.1, the 1:1 materials we have studied and reported in this section (with one aniline ring per formula unit), present a XRD spacing consistent with the presence of only a monolayer of polyaniline between the layers of V_2O_5. This was unexpected, because in previous work,[26] a series of materials with an experimental 1:1 $Ani_{ring}:V_2O_5$ ratio featured spacings consistent with a double layer of polymer within V_2O_5 slabs (19.2 Å spacings). In turn, those materials had been obtained with a greater excess of aniline, with much larger Ani:V(V) nominal ratios (11:1 and higher ratios of aniline) [13] . We therefore conclude that the present modified synthesis leads to higher concentrations of polyaniline in the resulting hybrid materials yet with a single layer of polymer intercalated.

The fact that the spacing is maintained consistent with the expansion due to a monolayer leads us to consider the possibility that these materials can arrange a greater concentration of polyaniline without any additional expansion. This aspect, which, without a doubt is of great fundamental interest, deserves future analysis by means of molecular modeling calculations and sophisticated diffraction techniques such as small angle scattering. These methods could give us some clues to the molecular structure, packaging, and crystal-chemical interaction in these systems of challenging chemical and structural complexity.

5.4. ELECTRODE FABRICATION. RECHARGEABLE LITHIUM AND LITHIUM-ION CELLS

So far we have presented the diverse aspects of hybrid materials synthesis and basic characterization. But as we have mentioned, our research is clearly oriented towards a particular application and therefore requires taking the materials two steps forward. First of all, there is the challenge of making electrodes out of electroactive materials. This is not as straightforward as it might seem and it requires the fabrication of composite electrodes. The second step further goes from electrode optimization to reversible lithium cell optimization. Although these steps have more to do with engineering aspects and we have naturally centered on materials science, we cannot renounce to tackle them.

Thus, aside from the intrinsic properties of the electrode active materials and the design and optimization of rechargeable batteries, we must contemplate other factors of vital importance. Some of these factors are, for instance: the form of the materials and fabrication of composite electrodes to enhance the mechanical properties, or the electronic conductivity of the electrodes. In this sense, the addition of binding agents or conductivity enhancers like carbons, are commonly used to elaborate electrodes. On the other hand, it is possible to prepare and apply the composite electrodes in the form of porous films instead of using the material in the form of powders as we have done so far.

In this section we will analyze these electrode design parameters and will try to evaluate their effect on their performance in reversible lithium cells. In addition to the comparative study of film vs. powder electrode performance we have also carried out and present here a comparative study of film electrodes in two different types of battery cells, namely, reversible lithium cells with metallic lithium anodes and reversible lithium cells with lithium-inserting graphite (lithium-ion cells).

As we mentioned in chapter 2, related to experimental techniques the compact electrochemical cells were assembled in Swagelok cells inside a dry box under argon. First we used metallic lithium as negative electrode (anode) vs. our hybrid composite cathodic material. Later, we electrochemically prepared a Li_xC_6 anode to test it in front of a composite hybrid film cathode. These comparative experiments were carried out at a C/7.5 discharge rate.

5.4.1. Electrode preparation.

The composite cathodes were prepared with a variable percent of active material (PAni/V_2O_5 hybrid), depending on their application as either powder or film. The Li_xC_6 anode was electrochemically prepared in a reversible lithium cell, as we will detail later.

5.4.1.1. Powder composite hybrid cathodes.

After we obtained the PAni/V_2O_5 hybrid samples by vacuum drying for three days, we prepared an intimate mixture of 70% weight of the hybrid sample and a 30% of carbon super P (in order to improve the inter-grain electron conductivity of our material). The mixture was directly added in powder form into the Swagelok cell (see set-up details in chapter 2), with a glass fiber separator impregnated with selectipur electrolyte ($LiBF_4$ in 1:1 DME:EC), and metallic lithium as anode.

5.4.1.2. Film composite hybrid cathodes.

Composite microporous films were fabricated by suspending 52% of the active hybrid material (dried under vacuum), 26% of kinar flex (PVDF) as binder [9,14], 22% of super-P carbon, and 3 drops of DBP (dibuthyl phtalate) in 2 ml of acetone. This suspension was thoroughly mixed for 24 hours to yield a homogeneous paste. The films were tape-cast onto a glass surface letting the acetone evaporate. After peeling off the film it was washed twice with diethyl ether in order to remove DBP and some soluble residues (see below), inducing in the film a porous microstructure. We cut the black homogeneous film into circles of 13 mm of diameter.

At this point we need to give a warning on the possible presence of residual species soluble in ether. We observed during the film electrode fabrication, specifically on the final washing with ethyl ether (to eliminate DBP), a variable coloration between yellow and reddish orange depending on the hybrid sample. Our hypothesis is that this soluble residues correspond to small amounts of aniline oxidation by-products or olygomeric polyaniline species in the bulk of our hybrid materials

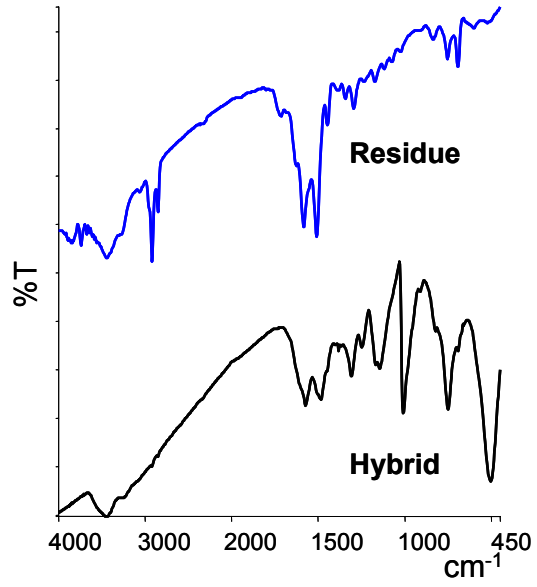

Figure 5.9.- A42 hybrid infrared spectra, and the soluble colored residue.

We carried out an FTIR analysis of one of these samples by evaporating the ether at room temperature under the hood thus obtaining a dark solid. In figure 5.9 we compare two spectra: one from A42 hybrid sample and the other one from the soluble residues extracted from the same sample. The most likely explanation was the presence of additional soluble species such as the already mentioned oxidation byproducts, although the spectrum did not coincide with the more obvious possibilities (hydroquinone, quinones, etc.). On the other hand the residue spectrum presents many features reminiscent of the spectrum of polyaniline dimers [28], although we cannot rule out the presence of other oxidation byproducts.

In an attempt to properly identify these residues, we carried out a proton NMR spectrum of the colored solution in deuterated ether. We obtained a very complex spectrum, preventing any meaningful assignment. We could only conclude that the colored solution of soluble residues was a complex mixture of compounds.

On the other hand, in order to try to establish a correlation between the presence of these soluble species and the synthesis parameters, we carried out extraction tests over different samples. For this, we weighted ca. 2.5mg of each sample (A32, A33, A43, A42, A41, A41TO, P3 and P14), added 2ml of ethyl ether, stirred and let them stand . For samples of series A4 (mechanical mixer) we observed a pale yellow coloration with different intensities depending on the sample: A43>A41>A42. Interestingly, we observed a more intense coloration in sample A41 than in A41TO (the latter practically with no coloration), synthesized with the same parameters, where the only difference was the oxygen treatment for A41TO. This suggests that the oxygen treatment after synthesis gives way probably to a higher polymerization rate in the hybrid preventing the formation of residual byproducts.

Secondly, if we compare samples of series A3(turbo-propeller) with samples of A4 series, we observed that in series A3 no coloration appeared indicating no presence of byproducts. This difference could be due to the different stirring routine but also to the fact that series A4 was synthesized at room temperature (unfeasibility of iced bath).

Finally, for samples P3 (3:1) and P14 (14:1) synthesized with the same parameters, for which the only difference was the amount of nominal aniline [13], we only detected an orange coloration for P14. In this case it is clear that the large excess of aniline is at the origin of soluble species formation. We can therefore conclude that in order to avoid the formation of these species, we need to limit the excess aniline to a 3:1 ratio and carry out the synthesis at low-temperature.

5.4.1.3. Li_xC_6 anodes.

Preparation of Li_xC_6 anodes, as we previously mentioned in chapter 2, was carried out through an electrochemical treatment of graphite vs. an electrode of metallic lithium in a Swagelok cell. First, we prepared a graphite film, then inside the battery support we used it as a cathode vs. a metallic lithium anode, and we finally proceeded to intercalate the lithium into the graphite structure at a C/48 discharge rate, between a voltage range of 2.5-0.03 V. The insertion was carried out by means of two successive discharges (discharge-charge-discharge sequence) in order to avoid the irreversible capacity.

The graphite film is also a composite cathode made of a 74% weight of graphite, 22% of Kinar Flex, and a 4% of super-P carbon to enhance the intergranular conductivity. We added three drops of DBP and stirred the mixture for 24 hours with 2 ml of acetone. We tape cast the suspension onto a plane glass surface, we let it dry, and we cut film disks 13 mm in diameter.

5.4.2. *Battery analyses of composite hybrid cathodes and composite anodes.*

We set up and cycled a whole series of cells based on the different hybrid materials and on the two electrode forming methods (powder and film). We will discuss here only those corresponding to the series A4, because they are qualitatively representative of the behavior of other materials and because for this series we

carried out comparative studies of cells with metallic Li anodes and insertion LiC_6 anodes.

Figure 5.10 shows examples of typical polarization curves for these cells. They correspond to the first discharge-charge cycle for the cells based on sample A42. In terms of initial specific charge, we can obtain a higher value for the cathode in film form (210 Ah/Kg) than in powder form (175 Ah/Kg) due to a better distribution of microporosity (see below). These values can be compared with the expected theoretical value of 236 Ah/Kg calculated for the exchange of 2.5 e^-/Li^+ . Finally in figure 5.11 we can compare the initial specific charge for film cathodes vs. two different Li anodes (metallic lithium and lithium inserted graphite). We observe a lower value for the cell arranged with the Li_xC_6 insertion anode. This is probably due to the formation of a passivation layer (SEI) between the Li_xC_6 anode and electrolyte, giving more resistance for the diffusion of lithium and therefore requiring lower discharge rates (smaller currents) for the display of equivalent charges.

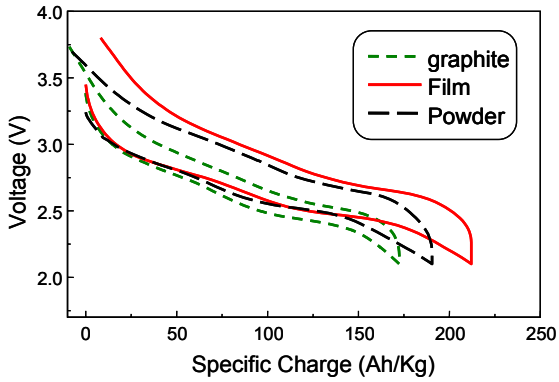

Figure 5.10.- Comparison of the first charge discharge polarization curves for sample A42 as powder and film, vs. Li_xC_6 or Metallic Li anode. I= 36.7 mA/g (C/7.5, for 2.5Li exchange).

In order to summarize the data from different cells and materials we have set the graphs shown in figure 5.11. There we can compare the specific charge of the different cells during the first discharge and the charge loss during the first 15 cycles for each hybrid samples: reference, A33, A43, A42, and A41TO.

First of all we can note that all samples tend to behave in a qualitatively similar way, both concerning their initial values of specific charge and the monotonically decreasing charge with the number of cycles.

On the other hand there is also a general trend for cells built from film electrodes to present an enhanced performance in the form of higher values of specific charge. This is most likely due to differences in the microposority induced by the addition and elimination of DBP in films than to intrinsic differences in the material. This enhanced microporosity allows for a better electrode-electrolyte interface, with a larger contact area and consequently a more efficient use of the active material in films than in powder electrodes at a given current used.

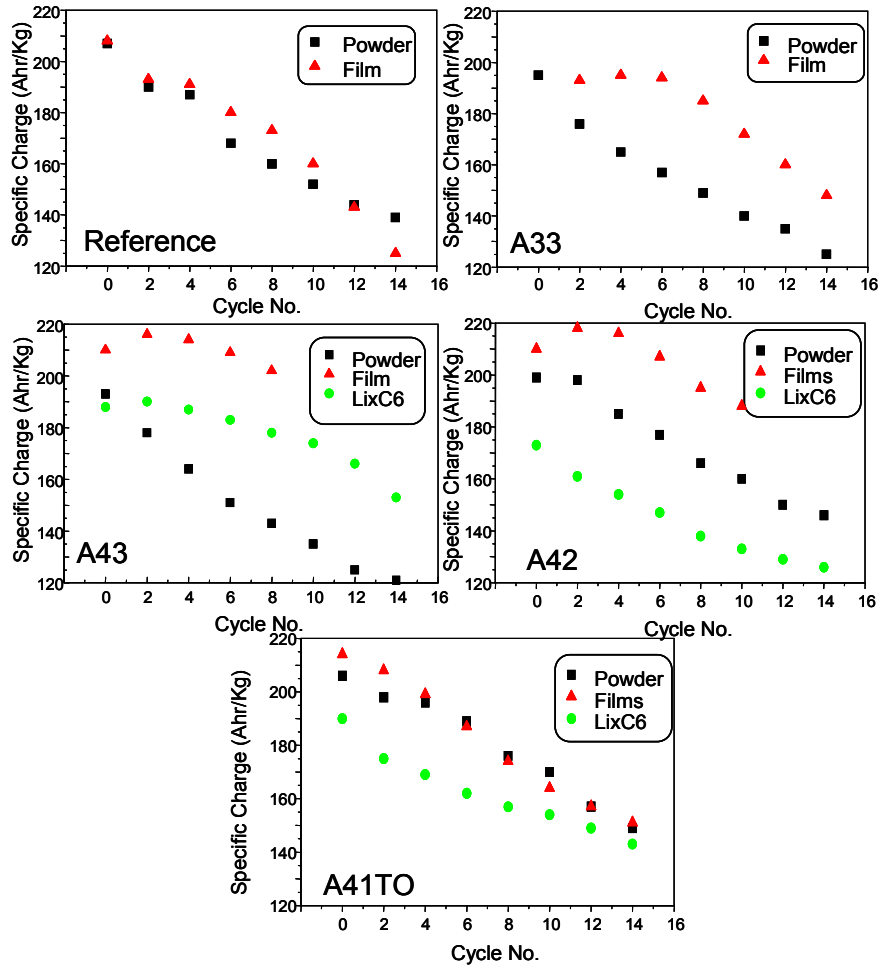

Figure 5.11.- Comparison of composite cathodes on powder, film, and vs. Li_xC_6 anode. In function of the number of cycles, applying a I= 36.7 mA/g (C/7.5,2.5Li) discharge rate.

Finally, we can compare the performance of the cells using metallic lithium anodes and lithium-insertion anodes, both of which were combined with film cathodes; that is we can compare the trends shown by red triangles and green circles in figure 5.11 new respectively. In general, we can observe a better performance in metallic lithium cells. We believe the lower values in lithium insertion cells are due to a SEI film

formation between the carbon negative electrode and the electrolyte during the first cycles. The formation of this SEI layer irreversibly consumes charge, but also contributes to increasing the cell internal resistance, an effect that adds to the already limited transport kinetics of Li^+ in these insertion anodes. [30]

Finally, we can say that the substitution of metallic lithium anodes, by lithium insertion anodes based on graphite (Li_xC_6), does not give way to a systematic improvement on the performance of the cells. For graphite anodes not only the specific charge is equal or smaller than for metallic Li cells but also, the cyclability behavior has not improved. This indicates that the continuous charge drop upon cycling should be attributed to the decay of electrochemical activity of the cathodes or to factors related to cell assembly. We will discuss this aspects further in the following section.

5.5. CYCLABILITY STUDY OF THE OPTIMIZED HYBRIDS.

In this section, we will present the data related to the evolution of specific charge of lithium reversible cells upon repeated cycling. The samples studied were the optimized PAni/V_2O_5 hybrids of series A4 (A43, A42, A41TO).

The electrochemical study was carried out between a voltage range of 3.8-2.1V at C/6 charge-discharge rate (I=36.7 mA/g, 2.5 Li). The data that we show was obtained on cells where film cathodes (prepared as described above and dried under vacuum at 30 ^oC) were combined with metallic lithium anodes.

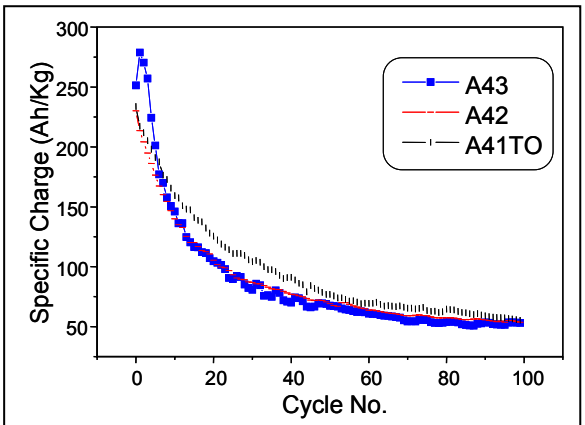

Figure 5.12.- PAni/V_2O_5 cathode comparison of series A4 samples, in successive charge-discharge 100 cycles. C/6 rate.

In figure 5.12, we can compare the evolution of specific charge during the first one hundred cycles of discharge for hybrids from series A4. We can observe that sample A43 has a better initial specific charge compared to sample A42 and A41TO. On the other hand, in spite of the different starting points and falling capacity slopes for the different samples, the final specific charge after 100 cycles tends to stabilize and converge in all cases around values of 50-60 Ah/Kg.

This fading of the electrochemical capacity of these materials was studied by analyzing plots of incremental capacity. Figure 5.13 shows the evolution upon cycling of incremental capacity plots for sample A43, revealing the gradual changes of the several electrochemical processes involved in these cells. In this respect, the different peaks can be assigned to the activity of the different components in the PAni/V_2O_5 hybrids, according to previous reports [13]. Thus, the sharper discharge peak at 2.5 V is assigned to PAni activity (with a minor component from V_2O_5), and this is precisely the activity fading first.

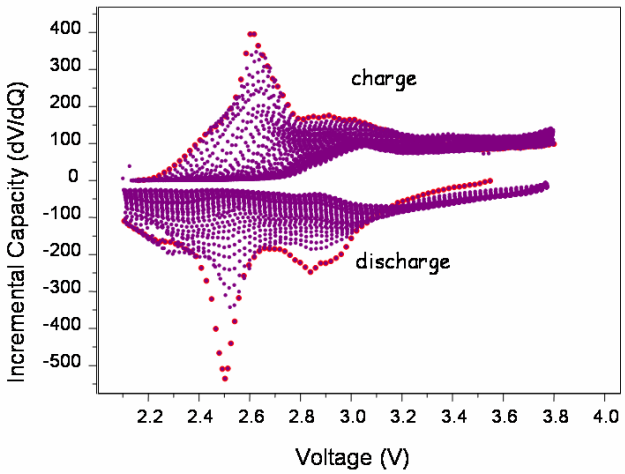

Figure 5.13.- Incremental capacity graph of sample A43, where we can see the degradation through cycling of each part of the PAni/V_2O_5 hybrid

It is interesting to note that the overall evolution of these discharge/charge profiles goes from relatively sharp faradaic peaks characteristic of a battery process to broad non-faradaic capacitive charge profiles like those of the final cycles, more characteristic of a capacitor.

In order to try to understand the reasons for the decline of the specific charge during cycling in these reversible cells, we carried out further comparative electrochemical studies (Li reversible cells, CV) of different PAni/V_2O_5 hybrid samples. Specifically, we compared the performance of our materials with those of other samples prepared according to previously described methods [13]. Table V.III summarizes the characteristics of the samples to be compared in this study: A43, P3 and P14.

Table V.III.- Chemical and Physical characteristics of the different PAni/V_2O_5 hybrids.

Sample	(Ani:V(V)	BET	Intercalation	Formula. FW
P3	(3:1)	39.7 m^2/g	PAni Monolayer	$(PAni)_{0.79}V_2O_5.2.1H_2O$ 289.1 g/mol
P14	(14:1)	14.3 m^2/g	PAni Bilayer	$(PAni)_{1.45}V_2O_5.1.8H_2O$ 344.95g/mol
A43	(3:1)	99.0 m^2/g	PAni Monolayer	$(PAni)_{1.06}V_2O_5.H_2O$ 296.33 g/mol

In figure 5.14 we show the first 100 successive charge-discharge cycles carried out between 3.8-2.1V for each sample with a charge discharge current density of 36 mA/g (C/6 rate). We see how the specific charge values for the first cycles of each materials are correlated with their BET surface area (see inset figure 5.14). But we can also see that, independently of the remarkably different starting points for the initial specific charges, all of them decrease continuously and tend to reach again, a common final value of 50-60Ah/Kg.

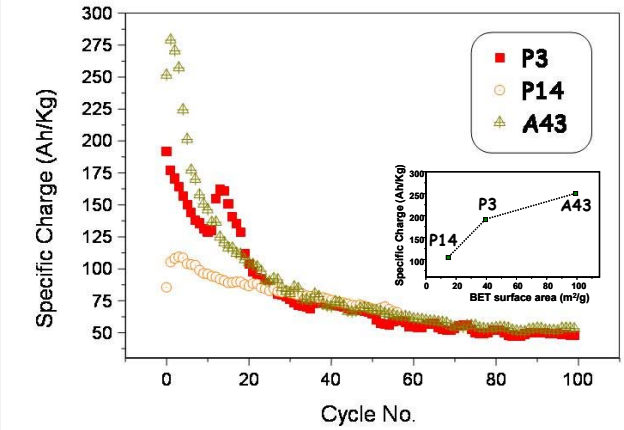

Figure 5.14.- Successive charge-discharge cycles carried out in Li cells at I=36mA/g (C/6 rate at a voltage range of 3.8-2.1V) of the different PAni/V_2O_5 hybrid samples.

This comparative study allows us to conclude that, contrary to what happens for the initial specific charge values, the fading of charge in these cells is independent of the synthesis and microstructure, since it takes place and follows the same general pattern for these three samples, regardless of the very different synthetic conditions used, the chemical compositions, structures and surface areas.

The final series of experiments included in this chapter and which we will describe in the following paragraphs should shed some light on the problem of charge

fading by helping to answer the question of whether this fading is due to our active hybrid material decomposition.

After discharge of the cells used in the previous experimenst (P3, P14 and A43) we observed certain coloration in the residual electrolytes (despite the fact that all the film electrodes had been washed with ether before setting the cells). So we decided to carry out new experiments on the A43 hybrid, with further washings of the hybrid film cathode with fresh electrolyte solution before cycling in Li cells. This pre-cycling washing led indeed to a brownish coloration in the resulting washing solutions before any cycling.

We carried out two series of cyclic voltammograms of this brownish solution (scan rate of 5mV/s, Li reference electrode, Pt working electrode, and Pt counterelectrode) (figure 5.15) thus, detecting the presence of an electroactive species, responsible for the reversible redox process shown. The blue curves correspond to the first two cycles (first program) and the red curve to the following two cycles (2nd. Program). We also noted the increase of intensity of both reduction and oxidation waves with cycling, which could indicate a possible polymerization of the dissolved species, probably olygomeric polyaniline species.

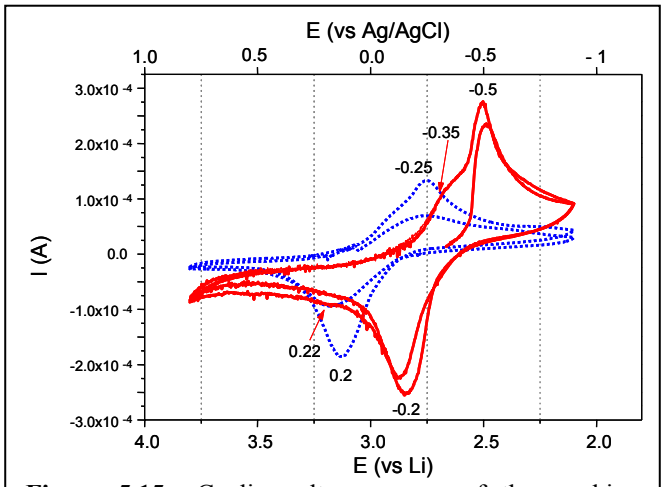

Figure 5.15.- Cyclic voltammogram of the washing electrolyte containing the soluble species extracted from the A43 cathodes. (5mV/seg. CE= Pt, W=Pt, and REF=Li.)

The film electrode washed with electrolyte was then subject to cycling, consecutively, in two different cells. Thus, after performing several cycles 3.8-2.1V (corresponding to the blue squares labeled A43 on Figure 5.16) we opened the first cell in the dry box, washed the cathode again with fresh electrolyte (resulting in just a very light coloration), and set up a second cell by changing the separator membranes, the electrolyte and the anodic lithium disc. Finally we carried out 100 charge-discharge cycles with this new cell (with the old cathode washed) (red circles labeled

A43W in figure 5.16). In this second cell the cycling range was to 3.5-2.1V, since it could not reach 3.8 volts during the first recharge.

We can observe that the value of the specific charge of the washed cathodes after 100 cycles in the second cell decreased further than in previous experiments. This is not so surprising if we take into account that we had removed some electroactive component during the washing with electrolyte.

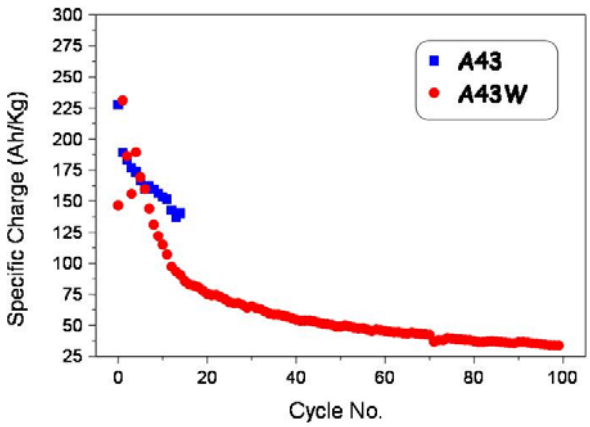

Figure 5.16.- Successive charge-discharge cycles carried out in Li cells of the washed cathodes at a C/7.5 rate (I=30mA/g). A43 is the cathode firstly washed, and A43W the second washing.

Yet, a second and most important observation is the apparent regeneration of the activity of the cathode upon washing and regeneration of the cell. This clearly shows that the active cathode material has not decomposed as it could be inferred from the loss of capacity during the first 15 cycles in the first cell. In going from the first to the second cell, the specific charge goes through some oscillations (from an initial value of ca. 140 to 230 Ah/Kg) but eventually back to high values (i.e. 190 Ah/Kg in the fifth cycle), before suffering again the gradual fading already known by previous experiments. According to these observations, the charge fading of our cells could be due to a process that hinders but does not irreversibly destroy the hybrid material electroactivity. A passivation process gradually hindering the diffusion of lithium through the cathode material could be responsible for this charge lost, however other factors related with cell elements other than the cathode active material cannot be ruled out yet and will require some further work

REFERENCES

[1] Gómez-Romero, P.; *Adv. Mater.* **2001**(13), 163.
[2] Wu, C.G.; Kanatzidis, M.G.; Marcy, H.O.; DeGroot, D.C.; Kannewurf, C.R.; *Polym. Mater. Sci. Eng.* **1989**(61), 969.
[3] Kanatzidis, M.G.; Wu, C.G.; *J. Am. Chem. Soc.* **1989**(111), 4141.
[4] Kanatzidis, M.G.; Wu, C.G.; Marcy, H.O.; DeGroot, D.C.; Kannewurf, C.R.; *Chem. Mater.* **1990**(2), 222.
[5] Ruiz-Hitzky, E.; *Adv. Mater.* **1993**(5), 334.
[6] Liu, Y.J.; DeGroot, D.C.; Schindler, J.L.; Kannewurf, C.R.;. Kanatzidis,M.G.; *J. Chem. Soc. Chem. Commun.* **1993**, 593.
[7] Nakajima, H.; Matsubayashi, G.; *J. Mater. Chem.* **1995**(5), 105.
[8] Wu, C.G.; DeGroot, D.C.; Marcy, H.O.; Schindler, J.L.; Kannewurf, C.R.; Liu, Y.J.; Hirpo, W.; Kanatzidis, M.G.; *Chem. Mater.* **1996**(8), 1992.
[9] Leroux, F.; Koene, B.E.; Nazar, L.F.; *J. Electrochem. Soc.* **1996**(143), L181.
[10] Leroux, F.; Goward, G.; Power, W.P.; Nazar, L.F.; *J. Electrochem. Soc.* **1997**(144), 3886.
[11] Goward, G.R.; Leroux, F.; Nazar, L.F.; *Electrochim. Acta* **1998**(43), 1307.
[12] Kuwabata, S.; Idzu, T.; Martin, C.R.; Yoneyama, H.; *J. Electrochem. Soc.* **1998**(145), 2707.
[13] Lira-Cantú, M.; Gómez-Romero, P.; *J. Solid State Chem.* **1999**(147), 601.
[14] Lira-Cantú, M.; Gómez-Romero, P.; *J. Electrochem. Soc*. **1999**(146),2029.
[15] Lira-Cantú, M.; Gómez-Romero, P.; *Int. J. Inorg. Mat.* **1999**(1), 111.
[16] Pokhodenko, V.D.; Krylov, V.A.; Kurys, Y.I.; Posudievsky, O.Y.; *Phys. Chem. Chem. Phys.* **1999**(1), 905.
[17] Harreld, J.H.; Dunn, B.; Nazar, L.F.; *Int. J. Inorg. Mat.* **1999**(1), 135.
[18] Demets, G.J.F.; Anaissi, F.J.; Toma, H.E.; *Electrochim. Acta* **2000**(46), 547.
[19] Kuwabata, S.; Masui, S.; Tomiyori, H.; Yoneyama, H.; *Electrochim. Acta* **2000**(46), 91.
[20] Oliveira, H.P.; Graeff, C.F.O.; Brunello, C.A.; Guerra, E.M.; *J. Non-Cryst. Solids* **2000**(273), 193.
[21] Sonami, P.; Marimuthu, R.; Mandale, A.B.; *Polym.* **2001**(42), 2991.
[22] Huguenin, F.; Torresi, R.M.; Buttry, D.A.; *J. Electrochem. Soc.* **2002**(149), A546.
[23] Huguenin, F.; Ticianelli, E.A.; Torresi, R.M.; *Electrochim. Acta* **2002**(47), 3139.
[24] Kwon, C.W.; Murugan, A.V.; Campet, G.; Portier, J.; Kale, B.B.; Vijaymohanan, K.; Choy, J.H.; *Electrochem. Commun.* **2002**(4), 384.
[25] Cuentas-Gallegos, A.K.; Palacín, M.R.; Colomer, M.T.; Jurado, J.R.; Gómez-Romero, P.; *Bol. Soc. Esp. Ceram. Vidrio* **2002**(41), 115.
[26] Lira-Cantú, M.; "Materiales Hibridos Organico-Inorganica a Base de Fosfomolibdato o Pentóxido de Vanadio Dispersos en Pol'imeros Organicos Conductores. Aplicación como Electrodos de Insercion en Baterias de Litio."; Ed. *Universitat Autonoma de Barcelona*; Barcelona **1997**, pp 244.
[27] Livage, J.; *Chem. Mater*. **1991**(3), 578.
[28] Zhang, W.J.; Feng, J.; MacDiarmid, A.G.; Epstein, A.; *J. Synthetic Metals* **1997**(84), 119.
[29] Ruiz-Paniego, A.; *Anales de Química* **1989**(85), 386.
[30] Winter, M.; Besenhard, J.O.; Spahr, M.E.; Novák, P.; *Adv. Mater.* **1998**(10), 725